Synthesis and biological evaluation of salicylaldimine complexes based on an alkylated PTA scaffold

University of Cape Town

Irwin Cassells

June 19, 2017

Synthesis and biological evaluation of salicylaldimine complexes based on an alkylated PTA scaffold

Thesis presented for the degree of

Master of Science

by

Irwin Cassells

Department of Chemistry

University of Cape Town

Supervisor: Gregory S. Smith

Co-Supervisors: Alan T. Hutton, Sharon Prince, Tameryn Stringer

2017

Declaration

I declare that "**Synthesis and biological evaluation of salicylaldimine complexes based on an alkylated PTA scaffold**" is my own work and has never been submitted for examination for any degree at any university. All sources are cited and fully reference at the end of each chapter.

Signature removed

Signed by candidate

.....

Irwin Cassells

June 19, 2017

Acknowledgements

I would like to start off expressing my gratitude and thanks to Assoc. Prof. Gregory Smith, Assoc. Prof. Alan Hutton and Prof. Sharon Prince for their advice and guidance throughout the project.

I would also like to acknowledge Mr Pete Roberts for the recording of some NMR spectra and Mr Gianpiero Benincase for microanalytical and electron impact mass spectral analyses. I would like to thank Dr Marietjie Stander (University of Stellenbosch) for the electrospray ionisation mass spectral analyses. A sincere thank you to Ms Sandra Jordaan (IDM, Faculty of Health Science, University of Cape Town) and Dr Serah Kimani (Human and Cell Biology, Faculty of Health Science, University of Cape Town) for their overwhelming patience, guidance and assistance in the cell viability assays.

A special thanks to Dr Tameryn Stringer for her friendship, encouragement, guidance and moulding me into a chemist over the last few years. I would also like to thank Dr Muneebah Adams, Ms Shakeela Sayed, Mrs Deidre van Rooyen, Dr Andrew Burgoyne, Mr Shepherd Siangwata, Mr Dylan Giffard and Dr Preshendren Govender for their encouragement and support throughout the project.

I would like to thank the National Research Foundation (NRF) for their financial support throughout my degree.

Lastly, I would like to thank all my family and friends for their continuous support throughout my studies, especially my parents, siblings, Mr Tavon Petersen and his family.

Abstract

Cancer remains one of the largest pandemics in the world, with millions affected by this disease every year. Since the discovery of the anticancer properties of cisplatin and other platinum-based drugs, metal-based chemotherapies have been extensively researched. Due to the high levels of toxicity of many platinum-based drugs, a rise in research using other metal-based drugs for the treatment of cancer has been observed. Of these, platinum group metals such as ruthenium, rhodium and iridium have shown great promise over the last several decades. RAPTA-type (ruthenium arene 1,3,5-triaza-7-phosphaadamantane) complexes have shown great promise *in vivo* for the treatment of certain cancers. Combining RAPTA with other biologically active groups has often resulted in increased potency and selectivity against various cancer cells *in vitro*. In this study, we investigated the synthesis, characterisation and biological evaluation of salicylaldimine complexes with an alkylated PTA scaffold. All of the metal complexes were screened for their activity against MCF7 breast cancer cells *in vitro*, in addition, the most active complexes were screened against Chinese Hamster Ovarian (CHO) non-cancerous cells to evaluate their selectivity.

A series of salicylaldimine ligands, as well as a benzyl alkylated PTA scaffold were prepared. Complexes of these ligands were synthesised by a reaction with [RuCl(μ-Cl)(*p*-cymene)]$_2$, [RhCl(μ-Cl)(Cp*)]$_2$ or [IrCl(μ-Cl)(Cp*)]$_2$. In addition to this, new PTA containing analogues of these neutral complexes were also prepared by reacting the afore mentioned salicylaldimine complexes with the alkylated PTA scaffold. All the compounds were characterised using an array of techniques including NMR spectroscopy, IR spectroscopy and mass spectrometry. Single crystal X-ray diffraction (XRD) was used to confirm the bidentate coordination mode of the salicylaldimine ligand to the metal centre, as well as the presence of the metal-phosphorus bond for the alkylated PTA complexes.

All of the metal complexes were evaluated against the MCF7 breast cancer cell line. The ruthenium and iridium salicylaldimine complexes showed comparable or greater cytotoxicity than cisplatin at 20 μM against the MCF7 cancer cells, as well as greater

cytotoxicity than their rhodium counterparts. Three of the salicylaldimine complexes exhibited potent activity ($18 < IC_{50} < 21$ μM). Selectivity studies showed that two of these complexes had a greater affinity for cancerous cells than for the CHO non-cancerous cells. All of the alkylated PTA complexes were less cytotoxic than cisplatin against the MCF7 cancer cells. Preliminary mechanistic studies of the most active complexes suggest ruthenium undergoes solvation prior to 5′-GMP binding, whereas iridium was inert to the solvation process.

Conference

- **8^{th} ISBOMC 2016:** Moscow, Russia, Poster Presentation, **I. Cassells**, T. Stringer, S. Prince, A. T. Hutton and G. S. Smith - *Synthesis and Biological Evaluation of PGM Complexes Based on Derivatised PTA Scaffolds.*

Abbreviations

Å	Angstrom (10^{-10}m)
δ	Chemical shift
v/v %	Percent by volume
2008	Ovarian cancer cell line
A2780	Human ovarian carcinoma
A2780cis	Human ovarian carcinoma cispatin resistant
A549	Human lung carcinoma
ATR	Attenuated total reflection
C13	Hamster kidney fibroblast cells
Caco-2	Human colorectal carcinoma
Calu	Human lung cancer cell line
CaSki	Cervical epidermoid carcinoma
CINV	Chemotherapy induced nausea vomiting
cisplatin	Diamminedichloridoplatinum(II)
COD	1,5-cyclooctadiene
COSY	^{1}H-^{1}H Correlation spectroscopy
Cp	Cyclopentadienyl
Cp*	1,2,3,4,5-Pentamethylcyclopentadienyl
d	Doublet
dec.	Decomposed
DMSO	Dimethyl sulfoxide
DMSO-d_6	Deuterated dimethyl sulfoxide
DNA	Deoxyribonucleic acid
EI-MS	Electron impact mass spectrometry
ESI-MS	Electrospray ionisation mass spectrometry
Et	Ethyl
EtOH	Ethanol

Fc	Ferrocene
Fc^+	Ferrocenium
Flt-4	FMS tyrosine kinase 4
FT-IR	Fourier transform - infrared spectroscopy
GMP	Guanosine 5′-monophosphate disodium
GSK-3	Glycogen synthase kinase 3
GST	Glutathione-S-transferase
h	Hours
HEK	Human embroyonic cancer cell line
HeLa	Human cervical cancer cell line
Hep3B	Human liver cancer cell line
HL60	Human promyelocytic leukemia cells
HR	High resolution
HSQC	Heteronuclear single quantum coherence
HT-29	Human colon adenocarcinoma cell line
IC_{50}	50% Inhibition concentration
J	Coupling constant
K562	Myelogenous leukemia cell line
KYSE	Oesophageal carcinoma cell line
L929	mouse adipose fibroblast tissue
LoVo	Male colon adrenocarcinoma
LO2	Normal liver cells
m	Multiplet
MCF-7	Human breast adrenocarcinoma

MDA-MB-	Metastatic human breast adenocarcinoma cell line
MeOH	Methanol
MTT	3-(4,5-dimethylthiazol-2-yl)-2,5-diphenyltetrazolium bromide
NMR	Nuclear magnetic resonance
PC3	Human prostate carcinoma
pcy	η^6-*para*-cymene
PGM	Platinum group metals
Pim-1	Prot-oncohene serine/treonine protein kinase
ppm	Parts per million
PTA	1,3,5-triaza-7-phosphaadamantane
r.t.	Room temperature
RAED	Ruthenium arene ethylenediammine
RAPTA	Ruthenium arene 1,3,5-triaza-7-phosphaadamantane
RAPTA-C	RAPTA- para-cymene
RI	Resistance index
RNA	Ribonucleic acid
ROS	Reactive oxygen species
$\mathbf{S_{298}}$	Solubility at 298K
S180	Sarcoma-180 tumour cells
s	Singlet
SE	Standard error
sept.	Septet
SERM	Selective estrogen receptor modulator
SI	Selectivity index
STAT	Signal transducer and transcription
T47D	Breast ductal carcinoma
t	Triplet

td	Triplet of Doublets
TMS	Tetramethylsilane
WHCO1	Oesophageal carcinoma cell line
XRD	X-ray diffraction

"Hope I made you proud, *Taichou*"

Contents

Chapter 1

Advances in the Use of Platinum Group Metals as Anticancer Agents

1.1 Introduction

1.1.1 Cancer Mortality

There are several strategies to optimise the therapeutic properties of medicinal compounds, with great emphasis on directing compounds to specific sites, lowering of healthy cellular cytotoxicity and overcoming resistance pathways.[1] The latter is essential for maintaining the longevity of the drug. Non-infectious diseases often exploit essential biological processes making them hard to target and difficult to treat. Cancers are a group of non-infectious diseases which are characterised and defined by their uncontrolled cell division.[2] This pandemic affects approximately 600 000 people a year in South Africa alone.[3,4] Of this number, approximately 7% of those diagnosed results in mortality. Since cancer is a major cause of death worldwide, it is important to understand its biology for effective drug design.

1.1.2 What is Cancer?

Benign tumours (tumours that are confined within tissue boundaries[5]) are often the easiest cancers to treat as the growth is localised. Proteases secreted from the cells often fracture the tissue boundary and pervade the adjoining cells.[5] Once this has occurred, platelets crowd the cell and often gets destroyed by immune cells, which sees a drop in the platelet count. For those cells not destroyed by the immune cells, the cancer cells can spread throughout the body by the lymphatic or bloodstream systems and settle in another locale (secondary site, Figure 1.1).[6] At this new locale the process can continue and spread to even more locations. This process is referred to as metastasis (Figure 1.1). This process can be delayed or prevented by tumour dormancy, poor vascularisation, apoptosis (programmed cell death), immune responses or induced treatments.[7,8]

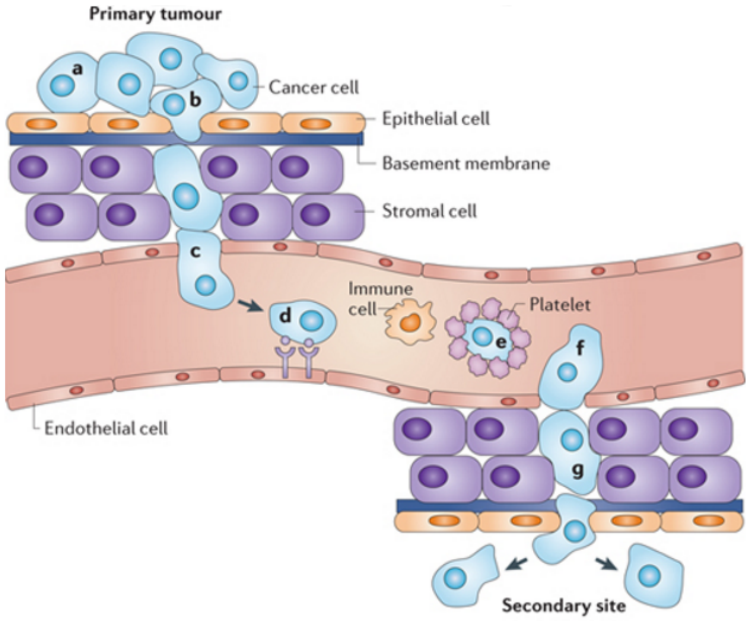

Figure 1.1: A diagram depicting the process of metastasis.[6]

1.1.3 Chemotherapy and Setbacks

Advances in the treatment of these diseases have improved dramatically over the last century.[8] Chemotherapy, the use of natural or synthetic chemicals for the treatment of diseases, is the most common treatment of cancer.[9] Often chemotherapies have negative side effects like chemotherapy-induced-nausea-vomiting (CINV),[8] caused by the non-

selective nature of many chemotherapeutic agents towards cancerous cells or oncogenes. These drugs often prevent imperative biological processes, leading to deleterious effects, such as hair loss and mild arthritis.[10]

To improve the efficacy of chemotherapeutics, researchers have identified suitable biological targets for drugs.[5] High concentrations of cancer inducing and suppressing proteins (e.g. Ras and Myc) have been found in cancerous cells,[5,11,12] making them favourable targets for selective activity. These targets have been a main focus when developing chemotherapeutics over the last few decades. Since many therapies exhibit several short-comings, the need for suitable alternatives is dire. Metal-based compounds have generated interest in recent years as a suitable alternative class of compounds. In the subsequent sections, some advances of metal-based compounds towards the treatment of cancer are discussed.

1.2 Platinum-containing Complexes

The discovery of the anticancer properties of cisplatin (**1.1**, Figure 1.2) by Rosenberg[13,14] has paved the way for the research of metal-based treatments for this disease. Based on mechanistic studies, it was concluded that cisplatin undergoes hydrolysis to form a diaqua cationic complex (**1.2**, Figure 1.2) which facilitates intermembrane transfer. The aqua complex **1.2** interacts with DNA by binding to two adjacent guanine-N7 nitrogen donor atoms (**1.3**, Figure 1.2), which leads to cell apoptosis.[15] Further mechanistic studies revealed that hydrolysis was not the only possible ligand substitution that could occur. The soft acidic nature of platinum meant it could bind to sulphur containing ligands, such as methionine and glutathione (**1.4**, Figure 1.2), which also facilitates cell membrane transfer and cell apoptosis.[16] Cisplatin is the most frequently used and effective metal-based anticancer drug against ovarian and testicular cancers, however the lack of selectivity towards cancerous cells often leads to negative side effects.[8,17]

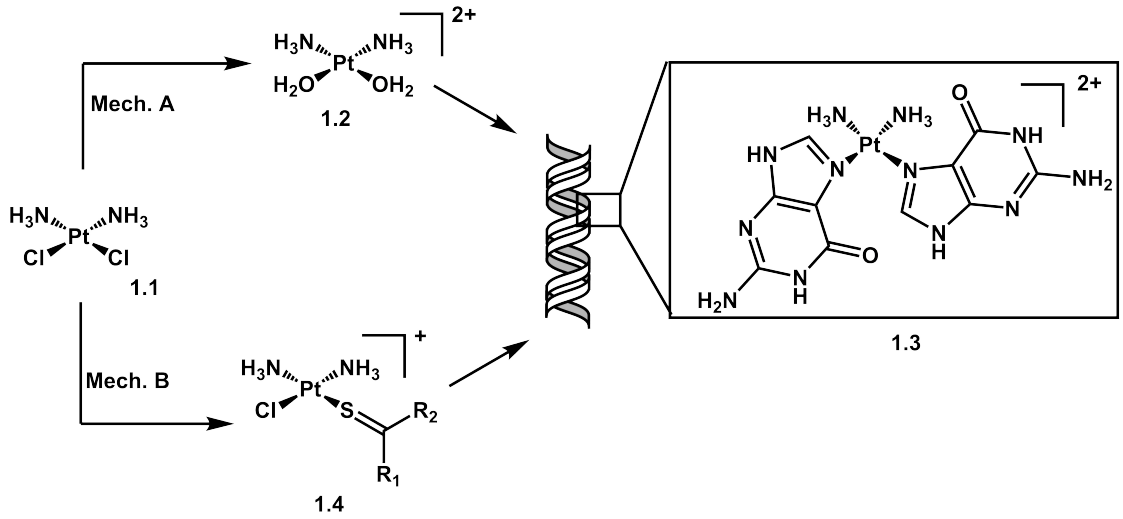

Figure 1.2: The proposed mechanism of action of cisplatin.[16]

Analogues of cisplatin have also been synthesised and biologically evaluated. The idea was to replace the chloride or/and primary amines with more labile ligands to increase the rate of aquation of the complex to increase the efficiency of DNA binding, and to increase selectivity towards cancerous cells.[16] A few analogues have been proven to be effective against various cancer types. Carboplatin (**1.5**, Figure 1.3) is a second generation derivative of cisplatin with a cyclobutane-carboxylate replacing the chlorido ligands. It has been found to have lower cytotoxicity against healthy cells relative to cisplatin; however higher dosages are required due to lower reactivity.[18] Oxaliplatin (**1.6**, Figure 1.3) is a third generation derivative of cisplatin, which has both the chlorido and ammino groups replaced by more labile groups, but maintaining the *cis* nature of the ligands. It is mostly used in the treatment of colorectal cancer,[19] the third most frequently diagnosed cancer reported in 2012 worldwide.[20] Although both of these agents are currently used in chemotherapy, they have limitations. One such limitation is that certain tumours are prone to drug resistance, which subdues the effects of the prescribed treatments.[21] Further development of drugs that possess activity against cancerous cells, as well drugs that are able to overcome resistance, is obligatory to treat cancer.[21]

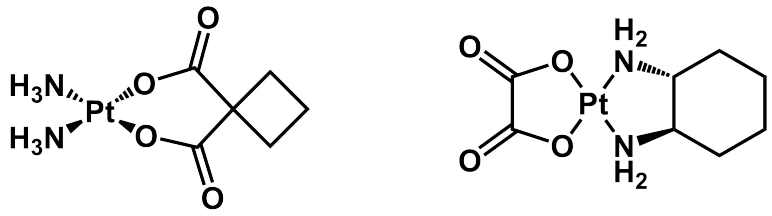

Figure 1.3: Cisplatin derivatives, carboplatin (**1.5**) and oxaliplatin (**1.6**)

Due to the efficacy of the afore-mentioned drugs, other platinum complexes have been synthesised and evaluated for their anticancer properties. In addition to this, interactions between DNA and platinum complexes were investigated. Barauah *et al.*[22] investigated the cytotoxicity and DNA binding mechanisms of acridine-thiourea platinum complexes, where acridine could be used as a DNA intercalating agent. The acridine-thiourea ligands and complexes (**1.7** and **1.8**, Figure 1.4) were found to be cytotoxic against HL-60 leukemia, 2008 (cisplatin sensitive) and C13 (cisplatin resistant) human ovarian cancer cell lines, with **1.7** being highly active in micromolar concentrations. Against the HL-60 leukaemia cancer cell line, it was found that there was approximately a 85-fold difference in activity between **1.7** and **1.8**. DNA binding studies suggested that **1.8** exclusively intercalates with DNA, while **1.7** strongly bound to DNA via two binding manifolds: intercalating and Pt-DNA binding, suggesting that cell apoptosis is strongly linked to the strength of the interactions between the complex and biomolecules.[22]

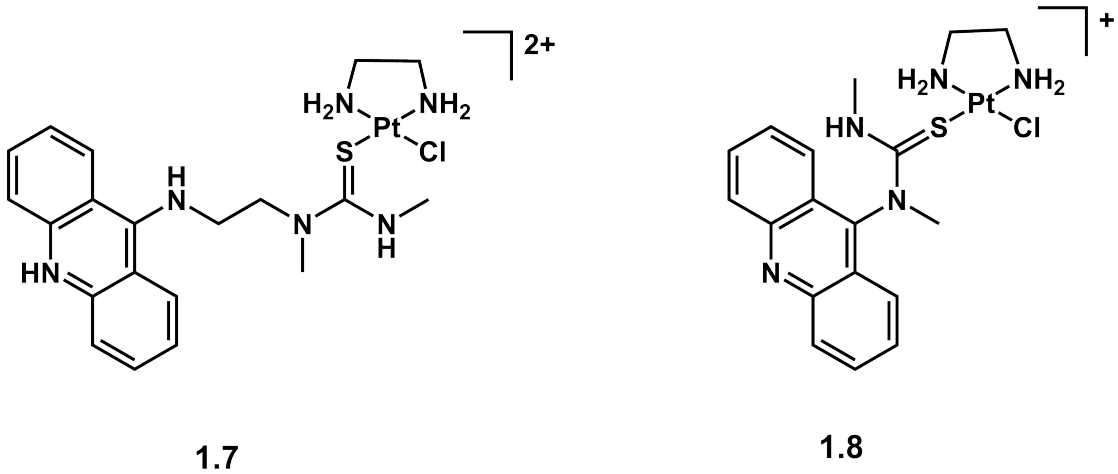

Figure 1.4: Acridinylthiourea complexes that exhibit anticancer activity.[22]

In light of the success of mononuclear platinum-based complexes, a polynuclear derivative of cisplatin with naturally occurring polyamines was investigated with partial success. BBR3464 (**1.9**, Figure 1.5) is a trinuclear platinum complex that has shown significant activity against cisplatin-sensitive and cisplatin-resistant cell lines.[23] The addition of the polyamine scaffold increased cell membrane permeability, with a different mechanism of action towards the unwinding of double stranded DNA. BBR3464 has undergone Phase II clinical trials, identifying it as a potential drug candidate, but was ultimately excluded due to the low selectivity towards cancer cells.[24]

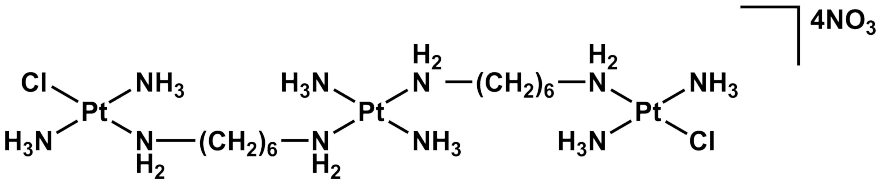

1.9

Figure 1.5: Structure of BBR3464 (**1.9**).[23]

Platinum-based treatments are still currently used today despite high levels of toxicity towards non-tumour cells. The low selectivity of platinum towards cancer cell DNA over healthy cells and the development of drug resistance has paved the way for the investigation of other platinum group metals (PGMs) in drugs for the treatment of cancer.

1.3 Palladium-containing Complexes

Palladium complexes are closely related to platinum complexes as the two metals share similar coordination chemistry.[25] Mono- and multinuclear palladium complexes have been evaluated against various cancer cell lines to determine the potency of the metal.[25] Complexes bearing structural similarities to cisplatin exhibited near identical activity against various cell lines.[25,26] In a study by Ulukaya and co-workers, palladium complexes with an *(N, N, N)*-tridendate ligand exhibited potent anti-growth, anti-invasive and apoptosis inducing activity both *in vitro* and *in vivo*.[27] In recent years cyclopalladated complexes have shown to be highly active against HeLa, HT-29, K562 and

MDA-MB-468 cancer cell lines, with the complexes showing greater activity than cisplatin.[28] Increased activity was observed in the dimeric complexes.

Smith and co-workers investigated the effect of palladium thiosemicarbozone complexes (**1.10**, Figure 1.6) against several cancer cell line families of WHCO, KYSE, CaSki and HeLA.[29] Thiosemicarbozones are robust, multidentate ligands which has shown both anticancer and antibacterial properties. The complexes showed moderate anticancer activity and were found to be less active than the free ligand. Further analysis showed, against the HeLa cell line, that these palladium complexes were apoptosis inducers. Cyclometallalated palladium complexes (**1.11**, Figure 1.6), investigated by Navarro-Ranninger *et al.* were evaluated against the triple negative MDA-MB-468 breast cancer cell line and HL-60 human cancer cells.[30] Platinum analogues of these complexes were also evaluated as a comparison of the anticancer activity between the two metals. The palladium complexes were observed to have a lower anticancer activity than the platinum analogues. It was found that palladium did not bind to DNA like platinum, which could attribute to the lower anticancer activity observed. This lack of binding suggests that palladium will not disturb DNA-dependent processes in healthy cells.

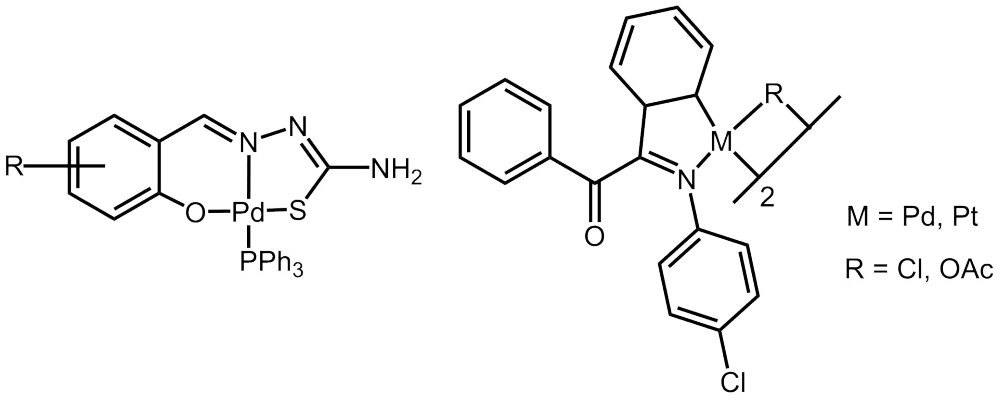

Figure 1.6: General structures of the complexes investigated by Smith *et al.* (**1.10**)[29] and Navarro-Ranninger *et al.* (**1.11**).[30]

Very few mechanistic studies has been done in order to understand the underlying reason for the activity of palladium complexes but these complexes do show great potential as anticancer agents.

1.4 Ruthenium-containing Complexes

Despite that the afore-mentioned metals and others, such as gold and copper[31] that display anticancer properties; ruthenium complexes have shown to be the most promising. The first ruthenium complex to show anticancer activity was *cis*-dichlorotetraammineruthenium chloride (**1.12**, Figure 1.7), a cisplatin derivative with a ruthenium metal centre.[31] A few years later, *cis*-[$RuCl_2(DMSO)_4$] was shown to be active against both primary and metastatic tumours, which has paved the way for ruthenium-based complexes as anticancer treatments (**1.13**, Figure 1.7).[31]

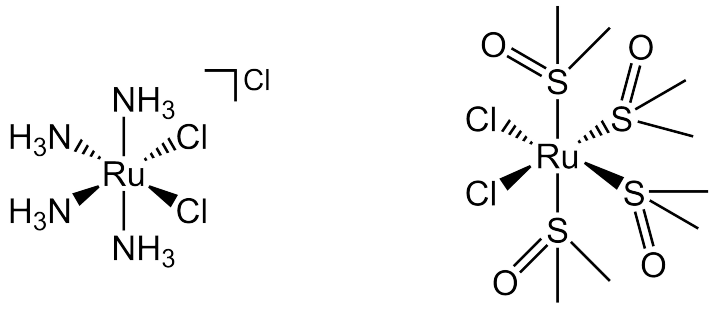

1.11 **1.12**

Figure 1.7: The first ruthenium complexes to show anticancer activity.

Some ruthenium(III) complexes are classified as prodrugs, as they are biologically inert.[31] These complexes can reduce to ruthenium(II) complexes, which is widely regarded as the active species.[32] These prodrugs are generally inactive against primary tumours, but have been found to be highly active towards preventing the development of tumours.[31,32] New Anti-tumour Metastasis Inhibitor-A (NAMI-A, **1.14**, Figure 1.8) successfully completed Phase I clinical trials. It was shown to interact with matrix metalloproteinases, which prevented tumour growth.[33] NAMI-A was found to be most effective in lung tissues, as it has the highest collagen content, to which NAMI-A binds strongly.[33] Similar ruthenium(III) complexes, such as KP1019 (**1.15**, Figure 1.8) and (N)KP1339 (**1.16**, Figure 1.8), have been shown to induce apoptosis and are currently in clinical trials.[33,34] Even though these compounds have shown activity towards metastases, their lack of activity towards primary tumours resulted in the research of ruthenium-based compounds which are active towards both metastases and primary

tumours. NAMI-A, KP1019 and (N)KP1339 all undergo a complete exchange of ligands under physiological conditions, which led researchers to believe that the more stable ruthenium(II) complexes are responsible for the anticancer properties.[33] One of the first ruthenium(II) complexes to be used as a framework was developed by Sadler *et al.*, i.e. the ruthenium arene ethylenediammine (RAED) framework (Figure 1.9).[35] Derivatives of this framework showed good *in vitro* (comparable to carboplatin) and *in vivo* activity.[35] The cytotoxicity of these complexes were largely due to the rapid aquation and DNA affinity, which is similar to cisplatin's mechanism of action. To increase the lipophilicity of the cationic RAED complexes, extended arenes were incorporated, which resulted in greater π_{purene}-π_{arene} stacking and greater DNA binding affinity.[36]

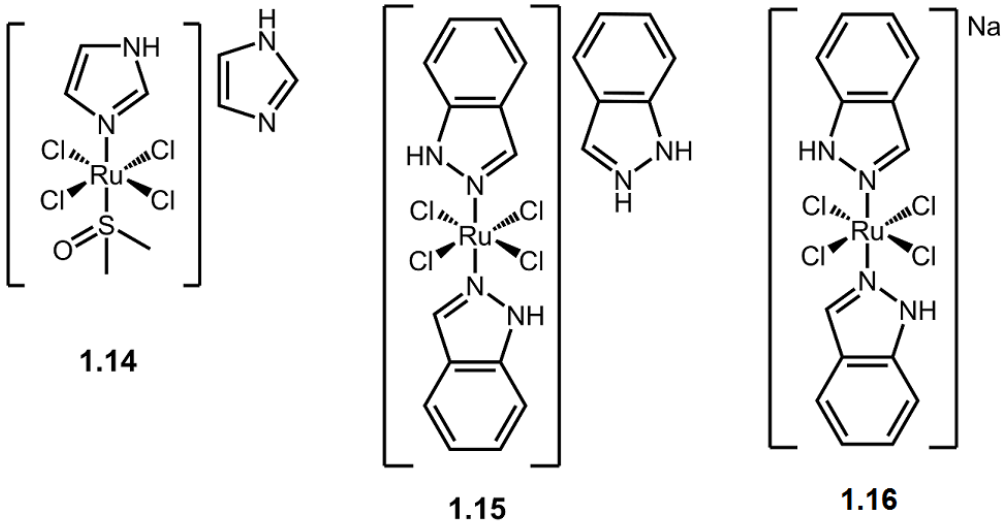

Figure 1.8: Ruthenium compounds that have shown promising biological activity.

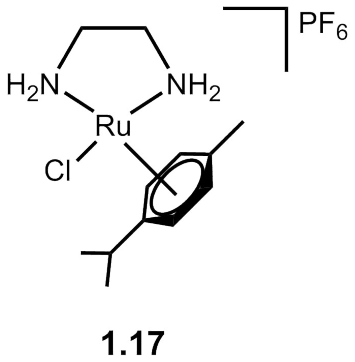

Figure 1.9: Ruthenium Arene Ethylene Diammine (RAED) complex synthesised by Sadler *et al.*[35]

Bipyridyl ligands are known to intercalate with DNA to disrupt its replication. Glazer *et al.* investigated ruthenium(II) complexes incorporating bipyiridyl ligands,[37] as these groups are light-activated, which could give insight into the anticancer properties of the ligands attached. Complexes **1.18** and **1.19** (Figure 1.10) exhibited very low anticancer activity against HL60, A549 and A549 spheroid cancer cells when tested in a dark room. Potent anticancer activity was observed when the assay was performed in conditions with light. This suggests that the activity of these complexes are largely due to an electronic transfer aided by a light source. In the light assay, complexes were found to exhibit anticancer activity superior to that of cisplatin. Agarose gel electrophoresis indicated a lack of any DNA interaction under dark conditions, but with light both DNA photocleavage and photobinding were responsible for the anticancer activity.

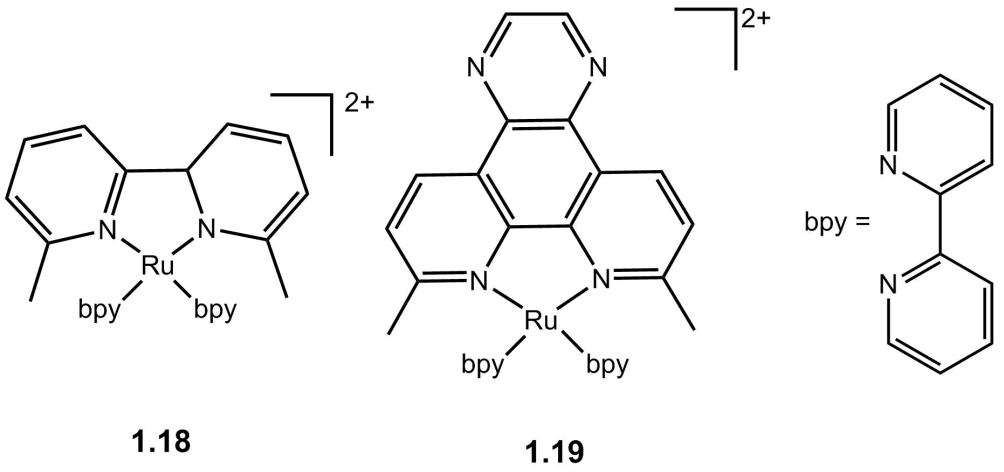

Figure 1.10: Bipyridyl complexes investigated by Glazer *et al.*[37]

Another strategy exploited to aid with toxicity and anticancer activity is to bind metals to biologically significant ligands before treating cancer cells. Incorporating amino acids as part of metal complexes has been proven to be a favourable strategy for improved selectivity. Lima and co-workers used this approach and treated sarcoma-180 tumour cells (S180) with ruthenium(II) amino acid complexes.[38] Ruthenium bipyridyl moieties were complexed with various amino acids to treat sarcoma-180 cancer and L929 normal cell lines to evaluate the biological activity and selectivity. These complexes were more cytotoxic than cisplatin against the S180 cancers but were found to be less toxic against L929. This suggests that these types of complexes are highly selective for cancer cells over normal cells. This claim was further supported with an

increase in caspases proteins (a family of cystine proteinases which are responsible for apoptosis) and an increase in mitochondrial dysfunction levels upon treatment with the complex. Due to the success of this strategy, many other non-cancer systems are being treated using the same strategy.[39]

The success of ruthenium complexes *in vitro* and *in vivo*, strategies used to overcome detrimental pathways and the rise in resistance strains probed the use of other metals using the same approaches.

1.5 Osmium-containing Complexes

Analogous to ruthenium, osmium piano-stool complexes have been investigated with some success. Osmium complexes have shown promise as protein-DNA binding inhibitors which are strongly associated with the progression of human cancers. An osmium(II) complex with a chlorophenazine bipyridyl ligand showed promise in the inhibition of DNA and tyrosine kinase product (signal transducer and transcription proteins, STAT) binding.[40] These STAT families are essential for the development of cancers and inflammation. A strong binding of the complex to STAT5B (has a role in apoptosis) was observed while a weak bond was observed for the cancer causing STAT5A.

Osmium derivatives of NAMI-A and the Keppler series (Figure 1.8) were synthesised and evaluated for their anticancer properties. The osmium complexes were significantly more active than the ruthenium analogues when tested against the HT-29 and SK-BR-3 cancer cell lines.[41] The inert nature of these complexes showed that hydrolysis is not essential for the activity, as observed with the ruthenium analogues. These complexes can be used as models to study biodistribution of unhydrolysed NAMI-A type complexes. The Keppler series analogues possessing osmium(II) and osmium(IV) oxidation states were tested *in vivo* using a Hep3B SCID mouse model and were well tolerated with good activities observed. In contrast, the ruthenium analogues of the azolium salts showed weaker cytotoxicity than the osmium counterparts. The authors

reasoned this to the cellular uptake of the complexes.[41–43] Osmium(IV) complexes have been investigated as potential anticancer agents against various cancer cell lines. Exceptional cytotoxicity of osmium(IV) bipyridyl complexes were reported by Lippard *et al.*[44] These complexes were observed to have two separate pathways that inhibit cell growth, namely the p53 dependant and p53 independent pathways. Similar to the ruthenium analogues of the complexes investigated, the ligand system determines the apoptosis pathway.

Even though osmium complexes do show a great deal of promise, the high levels of normal cell toxicity is not favourable for use of some of these compounds as biological agents.

1.6 Rhodium-containing Complexes

The success of ruthenium(II) complexes as potential anticancer agents has led researchers to take interest in the isoelectronic metal centre, rhodium(III).[45] The first rhodium complex shown to exhibit anticancer properties was a dirhodium complex, $[Rh_2(RC\,OO)_2(S)_2]$ (where S = coordinating solvent e.g. H_2O). The use of carboxylatorhodium complexes as anticancer agents extends to more recent rhodium(II) citrate complexes for the treatment of breast cancer.[46] The kinetically inert rhodium(III) centre can be made labile by using cyclopentadienyl (Cp) and pentamethylcyclopentadienyl (Cp*) ligands.[45] Due to its unique chemistry, rhodium(III) Cp* complexes often show similar activity to that of their ruthenium arene counterparts.[45] This relation has sparked interest in using rhodium(III) complexes as potential anticancer agents.

Based on the success of imidazole-based ruthenium(III) complexes (**1.14**, Figure 1.8), other metals have been investigated as anticancer agents. Mestroni *et al.* investigated rhodium(III) imidazole-based complexes which are similar to the ruthenium(III) complexes in Figure 1.8.[47] The complexes were tested against A2780, A2780/cp8, LoVo and Calu cells with cisplatin as the positive control. Complexes **1.20** and **1.21** (Figure 1.11) exhibited greater anticancer activity than cisplatin against the tested cell

lines. Strong DNA interactions were observed for these complexes resulting in early stage DNA termination during DNA synthesis. Unlike cisplatin or the ruthenium analogues, no preferential binding of the rhodium complexes to guanine was observed. The success of these complexes *in vitro* sparked research using nitrogen donor ligands with rhodium centres.

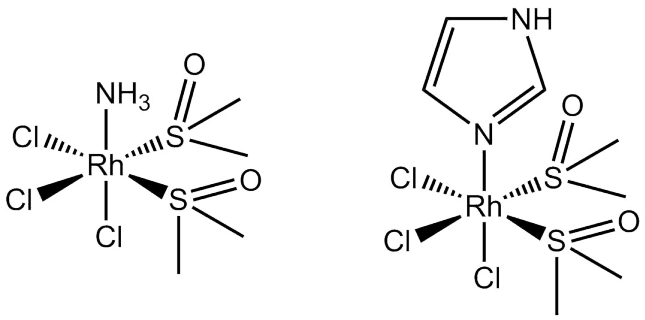

1.20 **1.21**

Figure 1.11: Most active rhodium(III) imidazole-based complexes investigated by Mestroni *et al.*[47]

A study has been conducted using rhodium Cp* picolinamide (*N,N*-chelating derivative of the natural occurring nicotinamide) complexes as potential anticancer agents (**1.22**, Figure 1.12).[48] Screening of the complex against the A2780 human ovarian cell line revealed an IC_{50} value of 28.8 μM, significantly less active than the cisplatin standard.[48] DNA interaction studies suggests binding of the complex in a similar manner to cisplatin.[48,49] A study using *N,N*-chelating ligands (**1.23**, Figure 1.12) showed improved results to the picolinamide complex.[50] The dipyridophenazine ligand was found to intercalate between the base pairs of the DNA double helix, similar to the complexes investigated by Baruah *et al.*[22,50] Compound **1.23** and its derivatives exhibited up to 70 fold greater activity than cisplatin against the MCF7 and HT-29 cell lines. Fluorescence studies showed $\sim$ 88 % cell apoptosis, which was due to the generation of reactive oxygen species (ROS) within the cell.[50] A significant decrease in the activity was observed when only the ligands were tested.

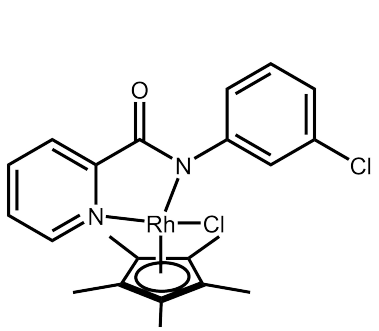

1.22

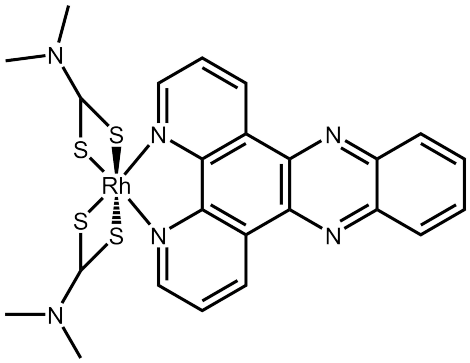

1.23

Figure 1.12: General structures investigated by Almondares *et al.*[48] (**1.22**) and Hackenberg *et al.*[50] (**1.23**).

Ott *et al.*[51] investigated the effects of different *N*-heterocyclic carbene complexes using rhodium(I) with 1,5-cyclooctadiene (COD) and carbon monoxide ligands, against the MCF7 breast cancer cell line, HT-29 colon carcinoma and TrxR, a thioredoxin reductase. These complexes exhibited great activity against the tested cell lines and reductase with strong inhibition of the TrxR.[51] Inhibition of the TrxR was independent of the ligand but the rhodium centre was required to showcase the inhibition effect. A stronger binding affinity to albumin and DNA was observed compared to cisplatin. Reduced rhodium uptake was observed when albumin was present, showing that rhodium can bind to various biological entities. Rhodium clusters have shown to unpair DNA base pairs to inhibit DNA synthesis. Carneiro *et al.*[52] investigated the effects of citrate ligands on the anticancer properties of rhodium(II) citrate clusters against MCF7 breast cancer cells. The anticancer activity was found to be low ($IC_{50} > 200\mu M$). At higher concentrations, blebbing of cells were observed. Blebbing is a process of the cytoskeleton breaking up due to stress, an indication of apoptosis. Due to the strong interactions with DNA, these complexes were toxic to healthy cells as well.

1.7 Iridium-containing Complexes

A large number of organometallic complexes have been researched for their anticancer properties; however there are very few iridium complexes that have been researched.

Iridium(III) is commonly kinetically inert,[31] and by coordinating strong field ligands to the metal centre, it can be liberated to its more reactive d^6 low spin state.[31] Like rhodium, Cp and Cp* ligands are responsible for the increased lability of the inert metal centre.[31] Compounds **1.24** and **1.25** were observed to have comparable cytoactivity to that of cisplatin against the A2780 cell line, and $\simeq$ 10-fold greater activity against A2780cisR and MCF-7 cell lines.[53] These iridium compounds were also observed to accumulate more efficiently in the cancer cells in comparison to cisplatin; a desirable property for anticancer agents. Changing the bipyridyl ligand to an azopyridyl group increased activity by $\sim$ 1.5-2 fold (likely due to the lipophilic arene and the charge aiding in hydrophilicity).[54]

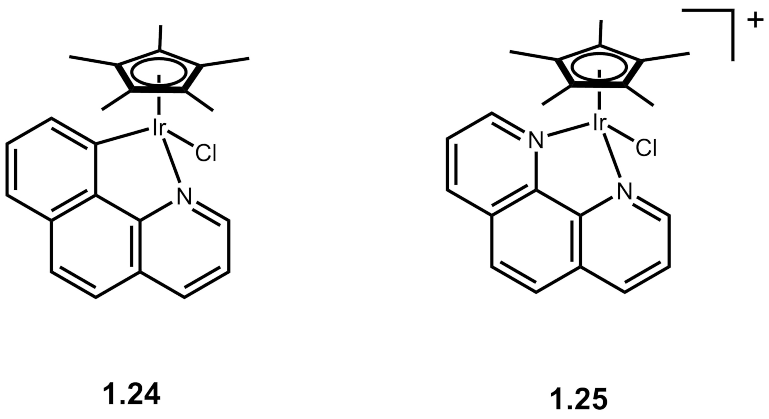

1.24 **1.25**

Figure 1.13: Iridium Cp* complexes, **1.24** and **1.25** investigated for cell accumulation.[53]

In a separate study by Kasparkova and workers, another *N,N*-chelating iridium complex with a functionalised Cp* ring (**1.26**, Figure 1.14) was investigated for its apoptosis inducing properties. It was found that the complex was cytoactive against various cisplatin sensitive and resistant cell lines.[55] It was found that **1.26** is amongst the DNA damaging class of therapeutic compounds, and binds more effectively to DNA than the other iridium complexes tested.[55] Apoptosis was induced more by **1.26** than cisplatin, with a concentration-dependant florescence - a definitive indication of ROS formation.

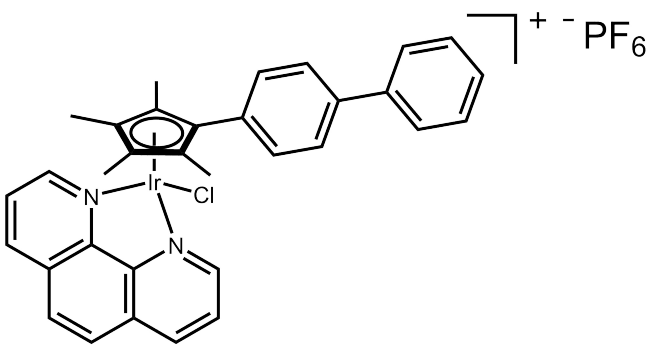

1.26

Figure 1.14: Iridium complex investigated for induced cell apoptosis.[55]

A study using multiple *(N,N)*- and *(N,C)*- pyridyl moieties to enhance activity was investigated by Lu *et al.*[56] These iridium complexes were found to be substitutionally inert. The complexes showed strong inhibition against various cancer cell lines and were found to be more active than the cisplatin standard.[56] This strong inhibition is most likely due to intercalation with DNA since the metal centre was found to be inert. These complexes also showed potent inhibition activity against *S. aureus*, a common bacterium responsible for skin disease in mammals. Meggers and co-workers investigated the antiangiogenic properties of (*N,N*)-pyridocarbozole iridium COD complexes against Flt-4.[57] Complex **1.27** (Figure 1.15) showed high *in vitro* selectivity for the Flt-4 kinase, nanomolar inhibition of the kinase and very low cytotoxicity *in vivo*. This complex served as a scaffold for iridium(III) octahedral complexes as potential anticancer agents. More recently, Mao and co-workers have used this concept by incorporating C-H activated ligands.[58] The C-H activated complexes were tested against HeLa, A549(S/R), MDA-MB-231, PC3 and LO2 cancer cell lines and were found to be more active than the commercially used cisplatin - particularly in the A549-R assay where complexes were up to 180 times more active. This effect was also observed for Payne and co-workers using C-H activated propylbenzylimine complexes.[59] Mito-Tracker Deep Red (MTDR) tests on **1.27** revealed that the complexes penetrate the cell membrane via an energy-dependent mechanism, as opposed to an endocytic pathway.

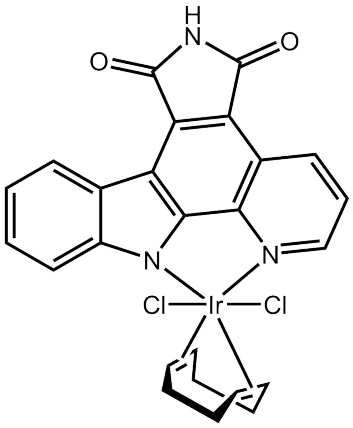

1.27

Figure 1.15: Most active iridium complex discussed in Meggers *et al.*[57]

1.8 RAPTA complexes

As shown in the previous sections, the ligand system plays a vital role in the cytotoxicity of the complex. One of the more promising ligand systems, PTA (1,3,5-triaza-7-phosphaadamantane), has been studied extensively.

Piano-stool complexes (**1.28** and **1.29**, Figure 1.16) such as ruthenium arene 1,3,5-triaza-7-phosphaadamantane (RAPTA) complexes have shown potential as anticancer agents. In the case of the RAPTA complexes, both lipophilic and hydrophilic entities are present which is favourable for bio-availability.[60] These complexes showed promise *in vivo*.[33] The low cytotoxicity against non-tumorous cells and selectively targeting tumour cells via protein binding, provided the rationale for additional studies with other metals.[45] The most active primary RAPTA series is RAPTA-C (**1.28** with R = *p*-cymene, $R_1 = R_2 =$ Cl, Figure 1.16), due to the strong binding strength to sulfur donor atoms in proteins.[45] The mechanism of action was proposed to be similar to that of cisplatin (see Figure 1.2), with the exception that ruthenium(II) complexes stabilise DNA at pH > 7, which prevents replication.[61] However, at pH < 7, RAPTA compounds caused DNA damage.[61] Ruthenium(II) has also been observed to mimic endogenous iron by binding to proteins.[62] Piano-stool complexes (**1.29**, Figure 1.16) prefer binding to proteins over DNA, which is an advantage as this reduces the cytotoxicity towards normal cells.[63]

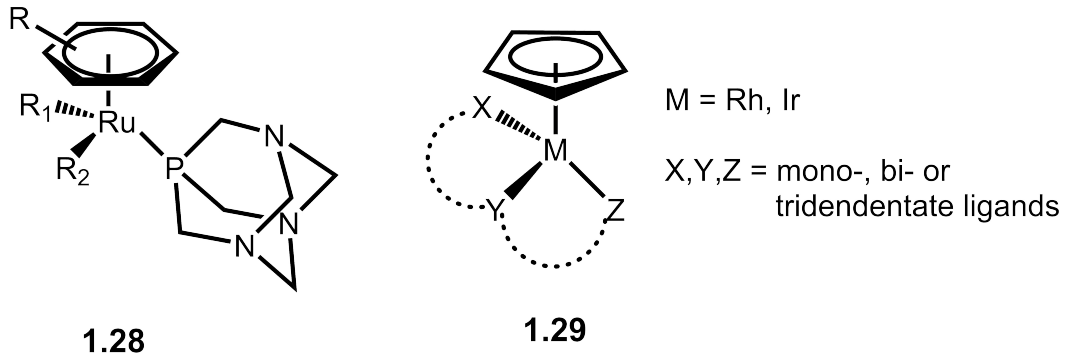

1.28 **1.29**

Figure 1.16: General structures of piano-stool complexes of RAPTA (**1.28**), and rhodium and iridium (**1.29**).

Variations based on the RAPTA-C complex have been synthesised to improve the cytotoxicity and the bio-availability in cells. One such modification is to use biologically active, naturally occurring compounds and modify these using the RAPTA metalloframework. Novel ruthenium complexes bearing curcumin-like structures have been synthesised and tested for biological activity (**1.30**, Figure 1.17).[64] These complexes were found to be highly toxic towards both A2780 and A2780cisR cell lines (0.36 μM $< IC_{50} <$ 1.18 μM), as well as having a low affinity toward healthy cells at these concentrations. The derivatised curcumin complexes, under high chloride concentration, reverted to RAPTA-C, as well as an aqua species (Scheme 1.1).[64]

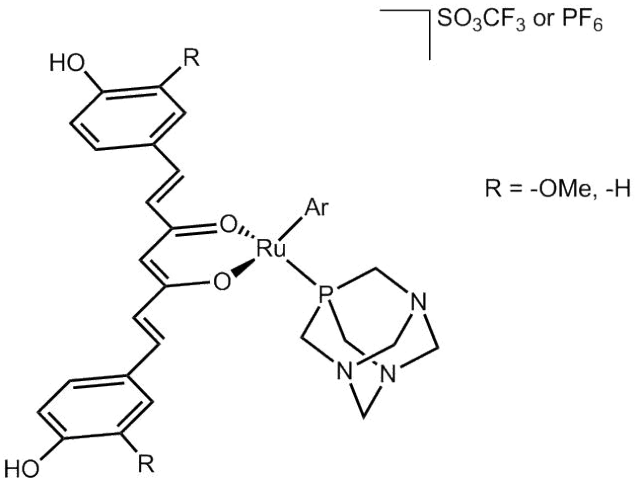

1.30

Figure 1.17: General structure of ruthenium curcumin based complexes investigated by Dyson and co-workers.[64]

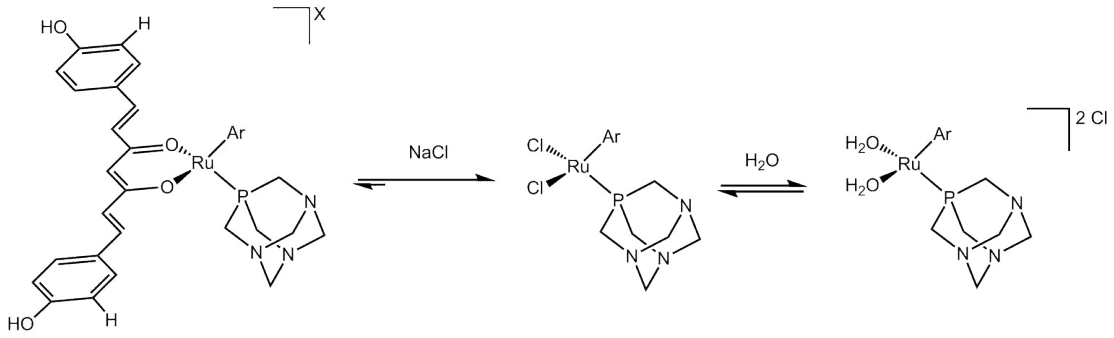

Scheme 1.1: Aquation of ruthenium bisdemethoxycurcumin complexes investigated in 100 mM NaCl(aq)/DMSO at 37 °C for 7 days.[64]

Another study investigated the impact of enantiomerically pure chiral ligands coordinated to the RAPTA framework.[65] Different optical isomers have been found to exhibit different biological activities; tragically discovered with the administration of thalidomide for the treatment of pregnancy pains.[66] Dyson and co-workers derivatised the arene group of the RAPTA framework using *R*- and *S*- amido moieties (**1.31** and **1.32**, Figure 1.18).[65] Upon addition of water, a similar trend in the hydrolysis of RAPTA compounds was observed (see Scheme 1.1), and the labile chlorido ligands were displaced. In comparison to oxaloRAPTA-C (**1.32**, Figure 1.18) and the *R*-configuration, the *S*-configuration was found to be highly active against A2780 and A2780cisR cell lines. However, at the most active concentration, low selectivity between the A2780 cell lines and the HEK (human embryonic kidney) cell line was observed.[65]

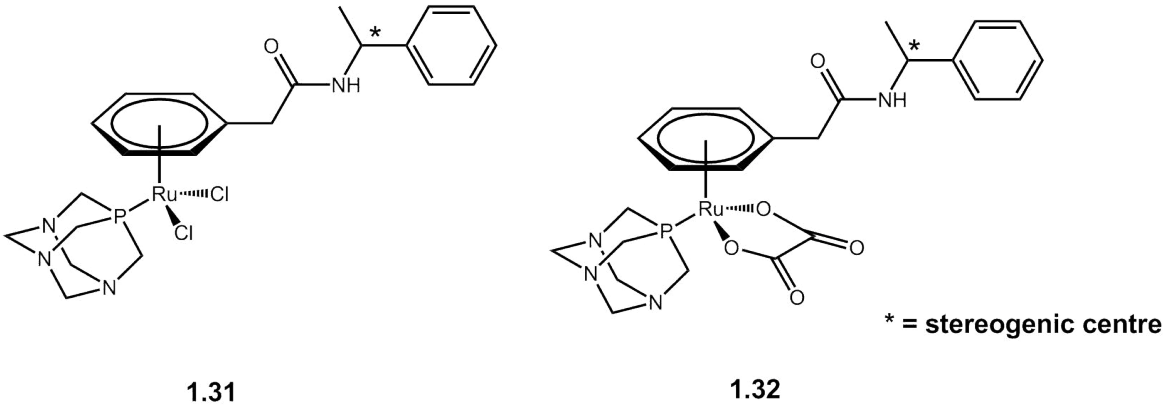

1.31 **1.32**

Figure 1.18: Structures of enantiomeric ruthenium complexes investigated by Dyson and co-workers.[65]

Dyson's RAPTA complexes have been the most successful piano-stool ruthenium-based

drug candidates to date.[33] Another study investigated the effects of different metals with PTA as the ligand based on the RAPTA structure.[67] Rhodium (**1.33**, Figure 1.19) and Osmium derivatives (**1.34**, Figure 1.19) of RAPTA were evaluated against the HT29, A549 and T47D cell lines. Complexes **1.33** showed comparative, and some better, antiproliferative activity than the ruthenium analogues *in vitro*.[67] These complexes were observed to hydrolyse almost completely, making both DNA and proteins possible targets.[67]

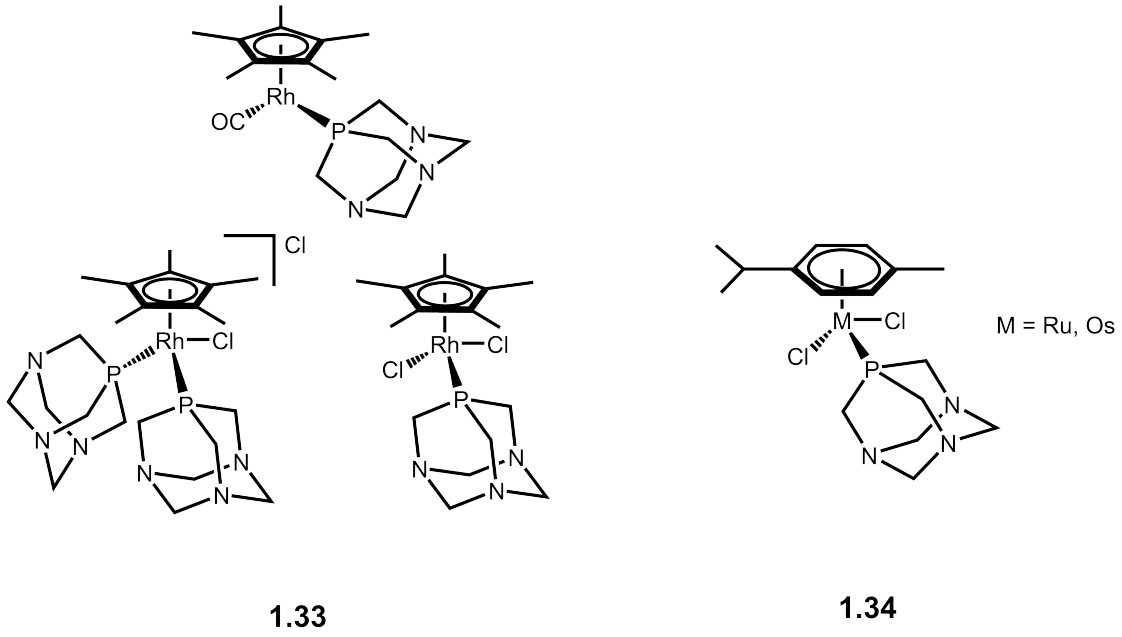

1.33 **1.34**

Figure 1.19: Generic structures of Rhodium (**1.33**) and Osmium (**1.34**) derivatives of RAPTA complexes investigated by Dyson and co-workers.[67]

1.9 Rationale for the Current Study

Based on the favourable properties of metal-based drugs, there is a need for further development to enhance the effects observed. Incorporating two or more successful strategies into a single metal-based drug can potentially enhance or compliment the effects of the individual strategies.

Two strategies extensively investigated by Smith *et al.* is the use of functionalised *(N,O)*-salicylaldimine complexes and the use of a PTA derivative to increase the water solubility of these complexes.[59,68–73] The first series of these complexes to show com-

parable activity to cisplatin was prepared by Govender and co-workers[70], where the investigation of propyl-terminated salicylaldimines with ruthenium *p*-cymene as the metal component was examined. The use of rhodium and iridium Cp* with various *(N,O)*-salicylaldimine ligands were also investigated with largely similar success as the ruthenium compounds.[59,71,72,74] Substitution of the chlorido ligand with a phosphorus donor ligand, such as PTA, resulted in an increase in biological activity in both A2780 and A2780cis ovarian cancer cell lines.[68,71] This shows the importance of the PTA moiety for biological activity, as observed for Dyson's original RAPTA complexes.[33] Figure 1.20 is a representative structure of the complexes investigated by Govender and co-workers.[59,68,70,71]

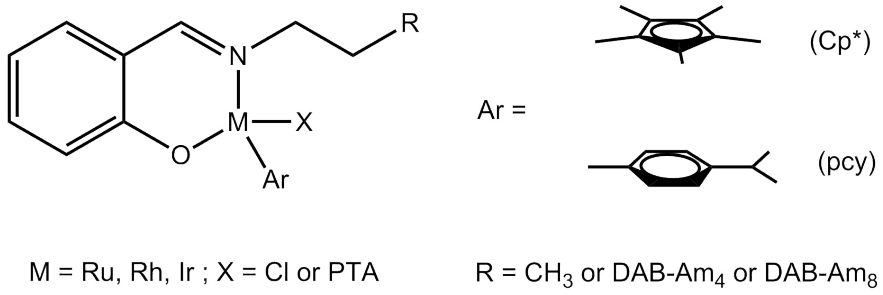

Figure 1.20: General structure of the complexes investigated by Govender and co-workers.[59,68,70,71]

A balance between hydrophilicity and lipophilicity is a key component for the cytotoxicity of compounds. Water soluble drugs have gathered interest recently since water is the main component in biological processes.[33,35] RAPTA complexes have shown how effective PTA is to both water solubility and anticancer properties.[21,33,35,67] A method to change the degree of solubility is to quaternise the PTA moiety using organohalides. Cerrada *et al.* investigated gold(I) complexes which incorporated various groups attached to PTA.[75] Free PTA ligands exhibited no cytoactivity, however the complexes of these ligands were more active than cisplatin against two Caco-2 colon cancer cell lines. In addition to the high levels of cytotoxicity against cancerous cells, no activity was observed against enterocytes when tested at the IC_{50} concentrations. Burgoyne *et al.* investigated the effects of similar quaternary derivatives of PTA using benzyl halides and platinum group metals.[73] These PTA complexes were found to have a degree of water solubility similar to free PTA, which is favourable for the distribution of

drugs in a biological system. The complexes were tested and exhibited activity against the WHCO1 cell line, but were found to be considerably less effective than cisplatin.

Incorporation of both alkylated PTA and salicylaldimine PGM complexes and their effect on activity is yet to be investigated. The lipophilicity of the salicylaldimine complexes and the water solubility of the PTA moiety can potentially enhance the biological activity of the overall complex. In this study, we aimed to investigate a series of neutral salicylaldimine PGM complexes and their cationic PTA derivatives against the MCF-7 breast carcinoma cell line.

1.10 Aims and Specific Objectives

1.10.1 Aims

As discussed in this chapter, it may be interesting to investigate the benefits of both salicylaldimine PGM complexes[68,70,74,76] and an alkylated PTA scaffold as part of the same complex.[73,77] This study therefore is aimed to synthesise a range of PGM salicylaldimine complexes and evaluate their biological activity against the MCF7 breast adenocarcinoma cell line. These complexes were reacted with an alkylated PTA scaffold[77] and the biological significance was evaluated and compared to the non-PTA analogues.

1.10.2 Specific Objectives

1. To synthesise a series of salicylaldimine ligands (Figure 1.21) containing various groups on the imine nitrogen.

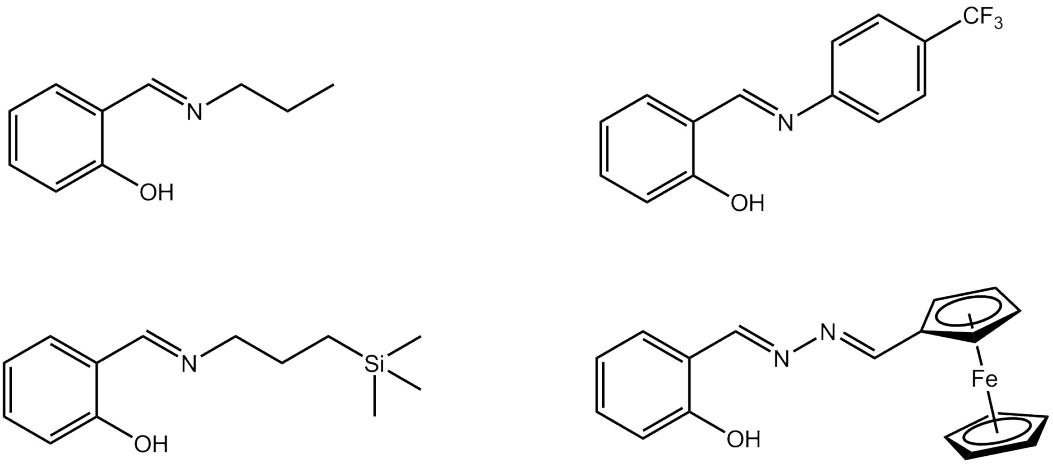

Figure 1.21: Salicylaldimine ligands synthesised in this study.

2. To prepare a series of Ru(II), Rh(III) and Ir(III) salicylaldimine complexes (Figure 1.22). Six of these complexes were previously reported to show activity against the A2780 human ovarian cell line.[68–70,70]

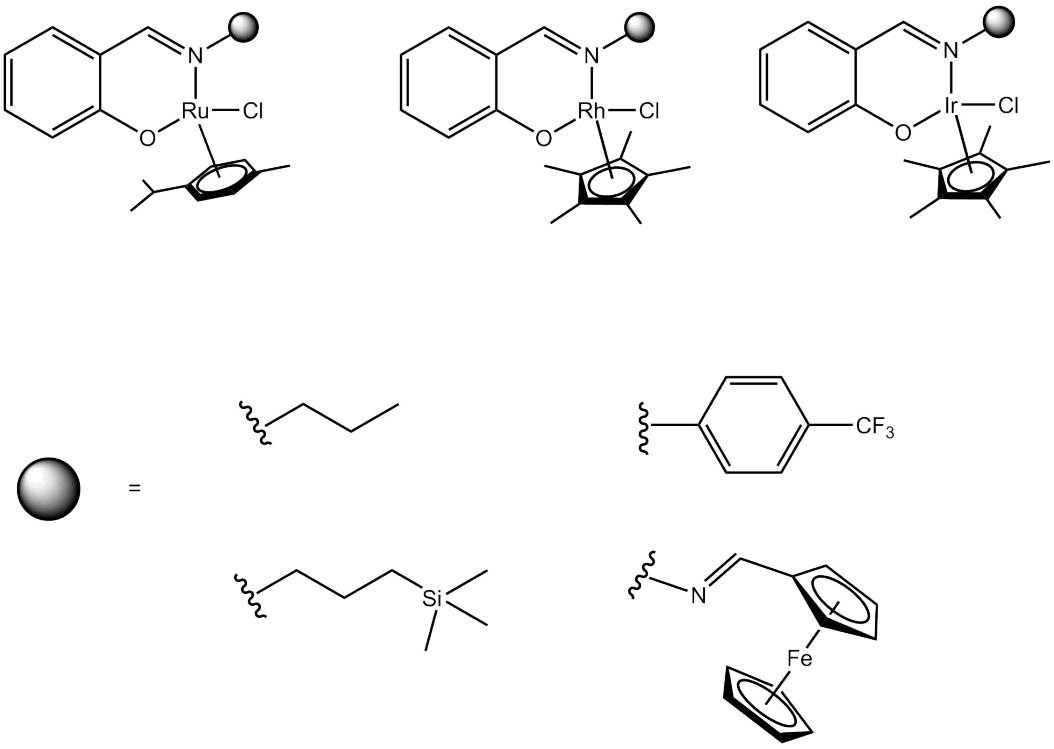

Figure 1.22: General structures of *(N,O)*-salicylaldimine complexes synthesised in this study.

3. Using the complexes outlined in Figure 1.22, a PTA scaffold to be incorporated as part of the complexes to afford PTA derivatives (Figure 1.23). PTA complexes

have shown great *in vitro* activity,[35] as well as favourable biological significant features such as enhanced water solubility.

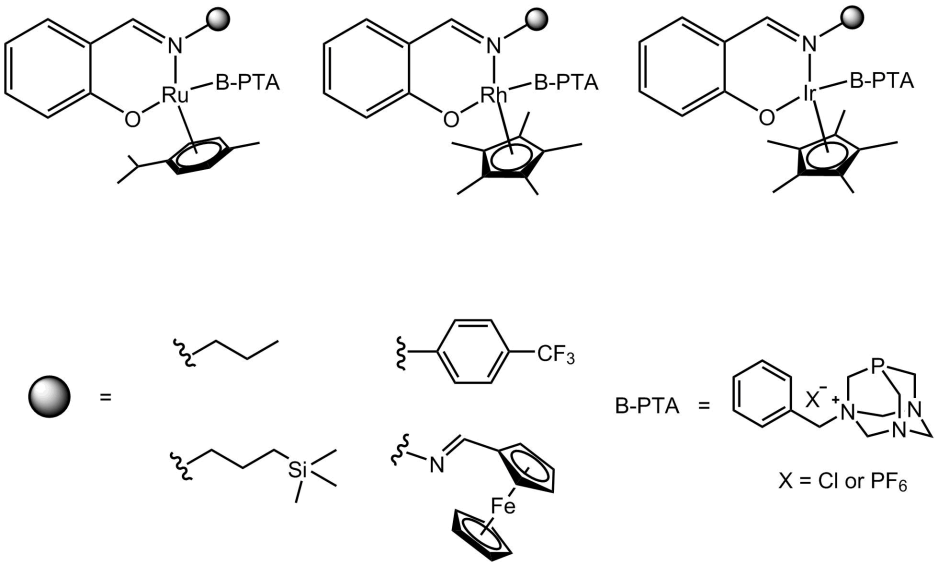

Figure 1.23: General structures of *(N,O)*-salicylaldimine PTA complexes synthesised in this study.

4. To characterise all of the compounds synthesised using Nuclear Magnetic Resonance spectroscopy (NMR), Fourier Transform - Infrared spectroscopy (FT-IR), Elemental Analysis (EA) and Electrospray Ionisation (positive mode) or Electron Impact Mass Spectroscopy (ESI-MS or EI-MS). Single crystal X-ray diffraction (XRD) analysis was used on single crystals to provide further insight into the structure of some of the isolated complexes.

5. Lastly, to investigate the *in vitro* activity of these complexes against the MCF7 breast cancer cell line. To conduct NMR studies to determine a potential biological pathway for the most active complex.

1.11 References

1. L. Ronconi and P. J. Sadler, *Coord. Chem. Rev.*, 2007, **251**, 1633–1648.

2. NIH, *NIH: National Cancer Institute*, http://www.cancer.gov/about-cancer/what-is-cancer, (accessed Jan. 2016).

3. WHO, *WHO: Cancer*, http://www.who.int/entity/cancer/country-profiles/zaf_en.pdf, (accessed Dec. 2015).

4. *CANSA: Statistics*, http://www.cansa.org.za/south-african-cancer-statistics/, (accessed Jan. 2016).

5. Nature, *Cell Division and Cancer*, http://www.nature.com/scitable/topicpage/cell-division-and-cancer-14046590, (accessed Jan. 2016).

6. A. Schroeder, D. A. Heller, M. M. Winslow, J. E. Dahlman, G. W. Pratt, R. Langer, T. Jacks and D. G. Anderson, *Nat. Rev. Cancer*, 2012, **12**, 39–50.

7. J. A. Aguirre-Ghiso, *Nature*, 2007, **7**, 834–846.

8. P. R. Bhandari, *J. Adv. Pharm. Technol. Res.*, 2012, **3**, 202–209.

9. N. Farrell, *Coord. Chem. Rev.*, 2002, **232**, 1–4.

10. A. H. Amiri and A. Rafiei, *Indian J. Med. Sci*, 2010, **64**, 197–203.

11. M. Malumbres and M. Barbacid, *Nature Rev. Cancer*, 2003, **3**, 459–465.

12. J. L. Bos, *Cancer Res.*, 1989, **49**, 4682–4689.

13. M. Perone, *Ann. Chemie. Pham.*, 1884, **51**, 1–29.

14. B. Rosenberg, L. VanCamp, J. E. Trosko and V. H. Mansour, *Nature*, 1969, **222**, 385–386.

15. M. J. Hannon, *Pure Appl. Chem.*, 2007, **79**, 2243–2261.

16. J. Reedijk, *Platinum Met. Rev.*, 2008, **52**, 2–11.

17. N. Farrell, *Coord. Chem. Rev.*, 2002, **232**, 1–4.

18. L. Kelland, *Nat. Rev. Cancer*, 2007, **7**, 573–584.

19. D. Simpson, C. Dunn, M. Curran and K. L. Goa, *Drugs*, 2003, **63**, 2127–2156.

20. *Globocan*, http://globocan.iarc.fr/Pages/factsheetspopulation.aspx, (accessed Jan. 2015).

21. S. Chatterjee, S. Kundu, A. Bhattacharyya, C. G. Hartinger and P. J. Dyson, *J. Biol. Inorg. Chem.*, 2008, **13**, 1149–1155.

22. H. Baruah, C. L. Rector, S. M. Monnier and U. Bierbach, *Biochem. Pharmacol.*, 2002, **64**, 191–200.

23. C. Manzotti, G. Pratesi, E. Menta, R. D. Domenico, E. Cavalletti, H. H. Fiebig, L. R. Kelland, N. Farrel, D. Polizzi, R. Supino, G. Pezzoni and F. Zunino, *Clin. Cancer Res.*, 2000, **6**, 2626–2634.

24. D. I. Jodrell, T. R. J. Evans, W. Steward, D. Cameron, J. Prendiville, C. Aschele, C. Noberasco, M. Lind, J. Carmichael, N. Dobbs, G. Camboni, B. Gatti and F. D. Braud, *Eur. J. Cancer*, 2004, **40**, 1872–1877.

25. A. R. Kapdi and I. J. S. Fairlamb, *Chem. Soc. Rev.*, 2014, **43**, 4751–4777.

26. G. Zhao, H. Lin, Y. Ping, H. Sun, S. Zhu, S. Xuncheng and Y. Chen, *J. Inorg. Biochem.*, 1999, **73**, 145–149.

27. E. Ulukaya, F. Ari, K. Dimas, E. I. Ikitimur, E. Guney and V. T. Yilmaz, *Eur. J. Med. Chem.*, 2011, **46**, 4957–4963.

28. K. Karami, M. H. Kharat, H. Sadeghi-Aliabadi, J. Lipkowski and M. Mirian, *Polyhedron*, 2012, **50**, 187–192.

29. P. Chellan, N. Shunmoogam-Gounden, D. T. Hendricks, J. Gut, P. J. Rosenthal, C. Lategan, P. J. Smith, K. Chibale and G. S. Smith, *Eur. J. Inorg. Chem.*, 2010, 3520–3528.

30. C. Navarro-Ranninger, I. López-Solera, V. M. González, J. M. Pérez, A. Alvarez-Valdés, A. Martín, P. R. Raithby, J. R. Masaguer and C. Alonso, *Inorg. Chem.*, 1996, **35**, 5181–5187.

31. S. Medici, M. Peana, V. Marina, J. I. Lachowicz, G. Crisponi and M. Antonietta, *Coord. Chem. Rev.*, 2015, **284**, 329–350.

32. A. Bergamo and G. Sava, *Dalton Trans.*, 2011, **40**, 7817–7823.

33. P. J. Dyson and G. Sava, *Dalton Trans.*, 2006, 1929–1933.

34. K. D. Mjos and C. Orvig, *Chem. Rev.*, 2014, **114**, 4540–4563.

35. C. S. Allardyce and P. J. Dyson, *Dalton Trans.*, 2016, **45**, 3201–3209.

36. G. Süss-Fink, *Dalton Trans.*, 2010, **39**, 1673–1688.

37. B. S. Howerton, D. K. Heidary and E. C. Glazer, *J. Am. Chem. Soc.*, 2012, **134**, 8324–8327.

38. A. P. Lima, F. C. Pereira, M. A. P. Almeida, F. M. S. Mello, W. C. Pires, T. M. Pinto, F. K. Delella, S. L. Felisbino, V. Moreno, A. A. Batista and E. de Paula Silveira-Lacerda, *PLOS ONE*, 2014, **9**, 1–11.

39. G. W. Karpin, J. S. Merola and J. O. Falkinham, *Antimicrob. Agents Chemother.*, 2013, **57**, 3434–3436.

40. L.-J. Liu, W. Wang, T.-S. Kang, J.-X. Liang, C. Liu, D. W. J. Kwong, V. K. W. Wong, D.-L. Ma and C.-H. Leung, *Sci. Rep.*, 2016, **6**, 36044–36052.

41. B. Cebrián-Losantos, A. A. Krokhin, I. N. Stepanenko, R. Eichinger, M. A. Jakupec, V. B. Arion and B. K. Keppler, *Inorg. Chem.*, 2007, **46**, 5023–5033.

42. G. E. Büchel, I. N. Stepanenko, M. Hejl, M. A. Jakupec, B. K. Keppler, P. Heffeter, W. Berger and V. B. Arion, *J. Inorg. Biochem.*, 2012, **113**, 47–54.

43. C. Hartinger, M. Jakupec, S. Zorbas-Seifried, M. Groessl, A. Egger, W. Berger, H. Zorbas, P. Dyson and B. Keppler, *Chem. Biodivers.*, 2008, **5**, 2140–2155.

44. K. Suntharalingam, T. C. Johnstone, P. M. Bruno, W. Lin, M. T. Hemann and S. J. Lippard, *J. Am. Chem. Soc.*, 2013, **135**, 14060–14063.

45. A. Casini, F. Edafe, M. Erlandsson, L. Gonsalvi, A. Ciancetta, A. I. N. Re, L. Messori, M. Peruzzini and P. J. Dyson, *Dalton Trans.*, 2010, **39**, 5556–5563.

46. M. L. B. Carneiro, R. C. A. Peixoto, G. A. Joanitti, R. G. S. Oliveira, L. A. M. Telles, A. L. Miranda-Vilela, A. L. Bocca, L. M. S. Vianna, I. C. R. da Silva, A. R. de Souza, Z. G. M. Lacava and S. N. Báo, *J. Nanobiotechnology*, 2013, **11**, 4–16.

47. G. Mestroni, E. Alessio, A. S. o Santi, S. Geremia, A. Bergamo, G. Sava, A. Boccarelli, A. Schettino and M. Coluccia, *Inorgan. Chim. Acta*, 1998, **273**, 62–71.

48. Z. Almodares, S. J. Lucas, B. D. Crossley, A. M. Basri, C. M. Pask, A. J. Hebden, R. M. Phillips and P. C. McGowan, *Inorg. Chem.*, 2014, **53**, 727–736.

49. D. L. Ma, D. S. Chan and C. H. Leung, *Acc. Chem. Res.*, 2014, **47**, 3614–3631.

50. F. Hackenberg, L. Oehninger, H. Alborzinia, S. Can, I. Kitanovic, Y. Geldmacher,

M. Kokoschka, S. Wölfl, I. Ott and W. S. Sheldrick, *J. Inorg. Biochem.*, 2011, **105**, 991–999.

51. L. Oehninger, L. N. Küster, C. Schmidt, A. Muñoz-Castro, A. Prokop and I. Ott, *Chem. Eur. J.*, 2013, **19**, 17871–17880.

52. M. L. Carneiro, E. S. Nunes, R. C. Peixoto, R. G. Oliveira, L. H. Lourenço, I. C. da Silva, A. R. Simioni, A. C. Tedesco, A. R. de Souza, Z. G. Lacava and S. N. Báo, *J. Nanobiotechno.*, 2011, **9**, 11–27.

53. V. Novohradsky, Z. Liu, M. Vojtiskova, P. J. Sadler, V. Brabec and J. Kasparkova, *Metallomics*, 2014, **6**, 682–690.

54. J. M. Hearn, I. Romero-Canelón, B. Qamar, Z. Liu, I. Hands-Portman and P. J. Sadler, *ACS Chem. Biol.*, 2013, **8**, 1335–1343.

55. V. Novohradsky, L. Zerzankova, J. Stepankova, A. Kisova, H. Kostrhunova, Z. Liu, P. J. Sadler, J. Kasparkova and V. Brabec, *Metallomics*, 2014, **6**, 1491–1501.

56. L. Lu, L.-J. Liu, W.-c. Chao, H.-J. Zhong, M. Wang, X.-P. Chen, J.-J. Lu, R.-n. Li, D.-L. Ma and C.-H. Leung, *Sci. Rep.*, 2015, **5**, 14544–14552.

57. A. Wilbuer, D. Vlecken, D. Schmitz, K. Kräling, K. Harms, C. Bagowski and E. Meggers, *Angew. Chem. Int. Ed.*, 2010, **49**, 3839–3842.

58. J.-J. Cao, C.-P. Tan, M.-H. Chen, N. Wu, D.-Y. Yao, X.-G. Liu, L.-N. Ji and Z.-W. Mao, *Chem. Sci.*, 2017, **8**, 631–640.

59. R. Payne, P. Govender, B. Therrien, C. M. Clavel, P. J. Dyson and G. S. Smith, *J. Organomet. Chem.*, 2013, **729**, 20–27.

60. C. A. Lipinski, F. Lombardo, B. W. Dominy and P. J. Feeney, *Adv. Drug Deliv.*, 1997, **23**, 3–25.

61. C. Scolaro, A. Bergamo, L. Brescacin, R. Delfino and M. Cocchietto, *J. Med. Chem.*, 2005, **48**, 4161–4171.

62. E. Menéndez-Pedregal, J. Díez, A. Manteca, J. Sánchez, A. C. Bento, R. García-Navas, F. Mollinedo, M. P. Gamasa and E. Lastra, *Dalton Trans.*, 2013, **42**, 13955–13967.

63. M. Pongratz, P. Schluga, M. A. Jakupec, V. B. Arion, C. G. Hartinger, G. Allmaier and B. K. Keppler, *J. Anal. At. Spectrom.*, 2004, **19**, 46–51.

64. R. Pettinari, F. Marchetti, F. Condello, C. Pettinari, G. Lupidi, R. Scopelliti, S. Mukhopadhyay, T. Riedel and P. J. Dyson, *Organometallics*, 2014, **33**, 3709–3715.

65. K. J. Kilpin, S. M. Cammack, C. M. Clavel and P. J. Dyson, *Dalton Trans.*, 2013, **42**, 2008–2014.

66. M. E. Franks, G. R. Macpherson and W. D. Figg, *Lancet*, 2004, **363**, 2008–2014.

67. A. Dorcier, W. H. Ang, S. Bolan, L. Gonsalvi, L. Juillerat-Jeannerat, M. Peruzzini, A. D. Phillips, F. Zanobini and P. J. Dyson, *Organometallics*, 2006, **25**, 4090–4096.

68. P. Govender, L. C. Sudding, C. M. Clavel, P. J. Dyson, B. Therrien and G. S. Smith, *Dalton Trans.*, 2013, **42**, 1267–1277.

69. W. Nkoana, D. Nyoni, P. Chellan, T. Stringer, D. Taylor, P. J. Smith, A. T. Hutton and G. S. Smith, *J. Organomet. Chem.*, 2014, **752**, 67–75.

70. P. Govender, A. K. Renfrew, C. M. Clavel, P. J. Dyson, B. Therrien and G. S. Smith, *Dalton Trans.*, 2011, **40**, 1158–1167.

71. P. Govender, H. Lemmerhirt, A. T. Hutton, B. Therrien, P. J. Bednarski and G. S. Smith, *Organometallics*, 2014, **33**, 5535–5545.

72. P. Govender, T. Riedel, P. J. Dyson and G. S. Smith, *Dalton Trans.*, 2016, **45**, 9529–9539.

73. A. R. Burgoyne, C. H. Kaschula, M. I. Parker and G. S. Smith, *Eur. J. Inorg. Chem.*, 2016, 1267–1273.

74. P. Govender, B. Therrien and G. S. Smith, *Eur. J. Inorg. Chem.*, 2012, 2853–2862.

75. E. Atrián-Blasco, S. Gascón, M. J. Rodríguez-Yoldi, M. Laguna and E. Cerrada, *Eur. J. Inorg. Chem.*, 2016, 2791–2803.

76. L. C. Sudding, R. Payne, P. Govender, F. Edafe, C. M. Clavel, P. J. Dyson, B. Therrien and G. S. Smith, *J. Organomet. Chem.*, 2014, **774**, 79–85.

77. P. Servin, R. Laurent, L. Gonsalvi, M. Tristany, M. Peruzzini, J.-P. Majoral and A.-M. Caminade, *Dalton Trans.*, 2009, 4432–4434.

Chapter 2

Synthesis and characterisation of neutral Ru(II), Rh(III) and Ir(III) salicylaldimine complexes

2.1 Introduction

In light of the high levels of toxicity and unfavourable side effects of cisplatin, a range of biologically active organometallic complexes have been researched in order to treat various cancers with minimal side effects.[1] Platinum group metals have shown exceptional promise, with a few complexes performing well in clinical trials.[2,3] Many of these organometallic compounds have a piano-stool structure, with a η^6-*para*-cymene (pcy) or η^5-pentamethylcyclopentadienyl (Cp*) seat with three legs (Figure 2.1). The dimeric precursors ($[MCl_2(pcy \text{ or } Cp^*)]_2$) of these complexes have been shown to exhibit little biological activity,[4,5] strongly suggesting that the activity of these complexes is determined by the nature of the ligands attached to the metal. Recently, McGowan and co-workers[4,5] have observed an increase in activity of these organometallic complexes when the dimer was coordinated to *N,N*-, *N,O*- or *O,O*- bis-chelating ligands, where the *N,O* complexes were found to exhibit the greatest activity amongst the three types. This result suggests that *N,O*- bis-chelating ligands coordinated to these metals can produce highly cytotoxic complexes, making them favourable for anticancer research.

Figure 2.1: Structure of piano stool complexes, with a piano-stool in the centre for comparison.

Salicylaldimines are versatile and easily functionalised building blocks for larger macromolecules and can be used in a wide range of biological applications.[6–12] Many salicylaldimines enhance the distribution of the metal into organelles and interrupt DNA processes, increasing the activity of the complex.[13] In addition to this, the *N,O*-chelating ligand can be attached to a pharmacophore to infiltrate biological targets.[9,14,15] Various salicylaldimine PGM complexes exhibit moderate or low activity against the human ovarian cancer cell lines, A2780 and A2780cis (I, Figure 2.2),[9,16]. However, in other cell lines, namely MCF7 (human breast carcinoma) and A549 (lung cancer), similar complexes showed comparable activity to cisplatin (II, Figure 2.2).[17,18]

Three biologically active groups of interest for this project are the ferrocenyl, trifluoromethyl and trimethylsilane groups, which have shown biological activity in previous studies.[19–21] Ferrocene is chemically robust and highly versatile. The most promising feature of ferrocene for biological applications is its ability to promote single electron redox transfers.[22] Ferrocenyl analogues of biologically active tamoxifen and raloxifene (ferrocifens and ferrocenyl raloxifenes) have been shown to have high cytotoxicity in various invasive cancer cell lines *in vitro*, as well as following the same selective estrogen receptor modulator (SERM) mechanism of action.[23] Fluorine groups have shown promise in the inhibition of various important biological processes for tumour growth.[19,24] The small size of the fluorine group, its high electronegativity and resistance to chemical degradation, makes fluorine-containing compounds favourable for enzyme inhibition.[24] Various fluorine-containing compounds have shown potent anticancer properties, for example TAS-102. TAS-102 is a potent combination anti-

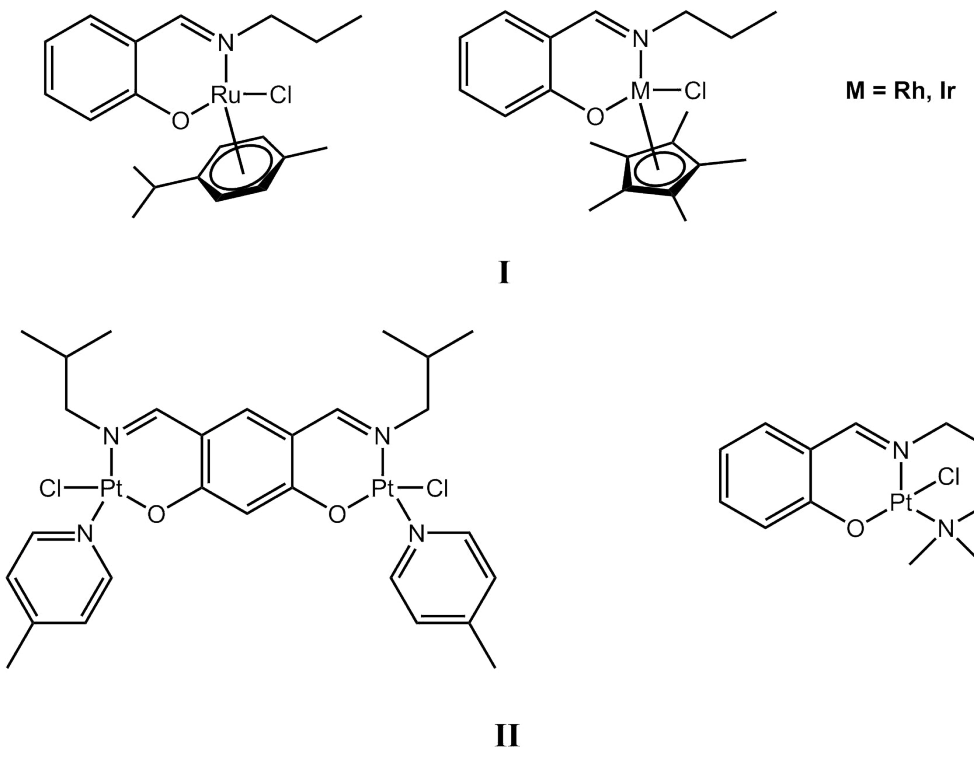

Figure 2.2: Selected salicylaldimine complexes investigated by Smith *et al.*[9,16] (I) and Zhang *et al.*[10,11,17,18] (II).

cancer treatment for third- and fourth- line colorectal cancers. The treatment combines both antiangiogenic and thymidylate synthase inhibition properties, with Trifluricine, a (trifluoromethyl)pyrimidine-2,4-dione deoxyribose compound, responsible for the inhibition of tumour growth.[25] Very few silane-based compounds are reported in the literature as potential anticancer agents. A few reports have shown these groups to be more active than analogous carbon derivatives.[20,21] Silanes are highly lipophilic in nature, which can be advantageous for cross-membrane transfer between lipo- and hydrophilic boundaries.

Since very little research has been done to investigate the biological activity of trifluoromethane and organosilane salicylaldimine complexes, this study investigates the synthesis and characterisation of trifluoromethane- and organosilane- derivatised salicylaldimine complexes, as well as ferrocenyl- and propylsalicylaldimine complexes previously reported by Smith and co-workers.[9,15,16,26]

2.2 Synthesis of *(N,O)*-salicylaldimine ligands

2.2.1 Synthesis

Four salicylaldimine ligands were synthesised using modified literature methods.[16,27] Salicylaldehyde was reacted with either *n*-propylamine, 4-trifluoroaniline or 3-aminopropyl trimethylsilane via a Schiff-base condensation reaction to afford ligands **2.1**-**2.3** (Scheme 2.1).[16,27] The electrophilic formyl carbon of salicylaldehyde undergoes nucleophilic attack from the electron-rich nitrogen of the amine (Scheme 2.2). The oxygen atom accepts the electrons from the carbonyl bond and by means of a proton transfer reduces to a hydroxyl group. A sequence of bond forming (C-N to C=N) and bond breaking (C–OH) due to rearrangement results in the formation of the imine product and water. The Schiff-base products were isolated as either viscous yellow oils (compounds **2.1** and **2.3**) or an amorphous yellow powder (**2.2**) in high yields (91-93%).

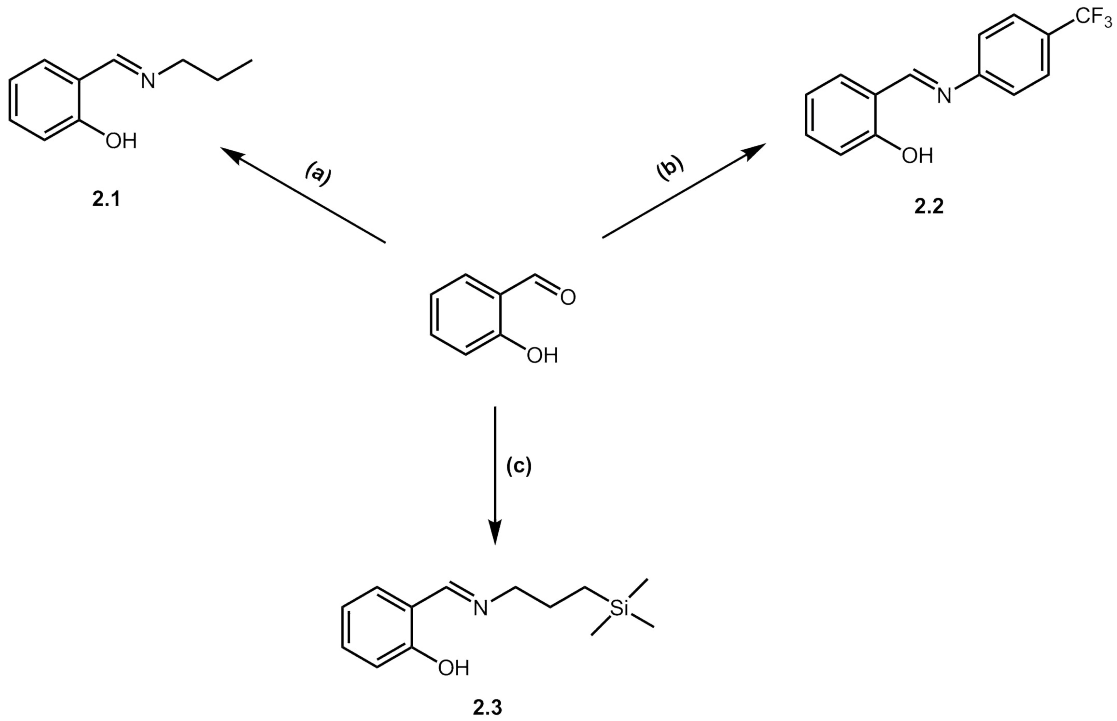

Scheme 2.1: Synthesis of *(N,O)*-chelating Ligands, **2.1**-**2.3**. Reagents and conditions: (a) *n*-propylamine / Et_2O / 18 h / r.t.; (b) 4-trifluoromethylaniline / Et_2O / 16 h / r.t.; (c) 3-aminopropyltrimethylsilane / Et_2O /16 h / r.t.

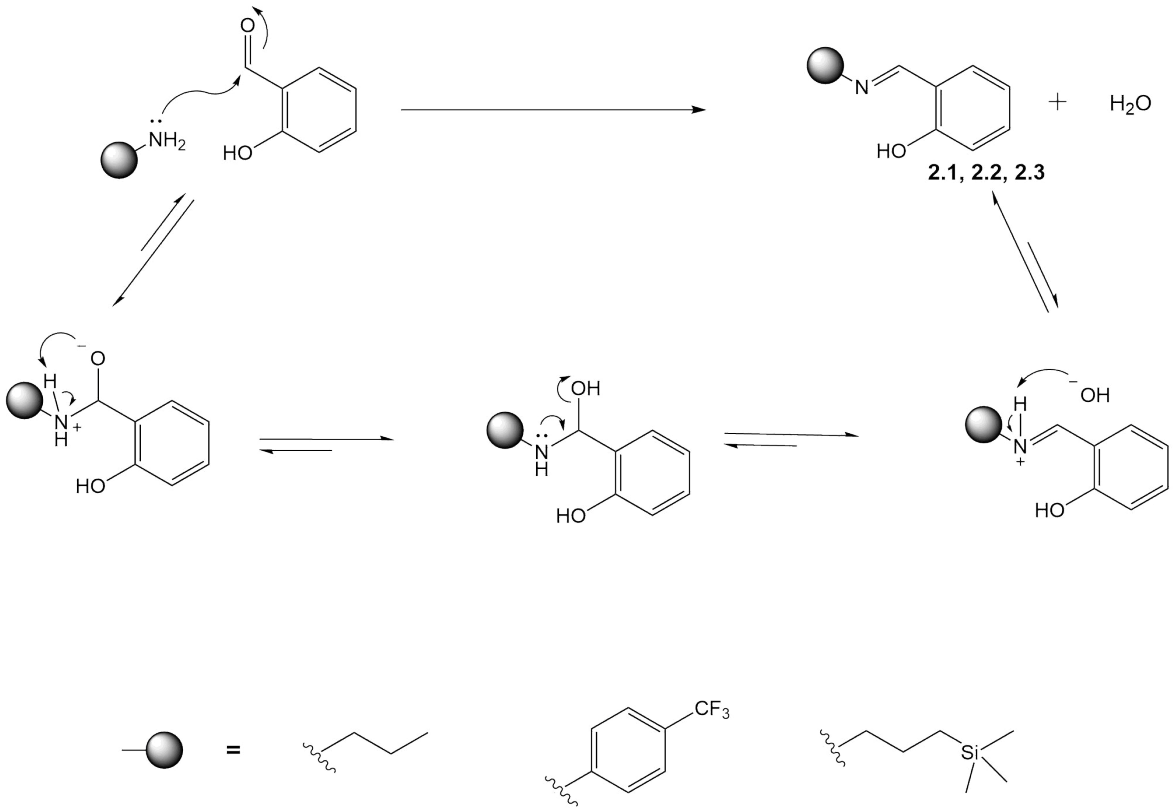

Scheme 2.2: Reaction mechanism of the Schiff-base condensation reaction to afford **2.1**-**2.3**.

Compound **2.4** was synthesised in a two-step process from salicylaldehyde hydrazone, **L1**, which was prepared by reacting salicylaldehyde and hydrazine hydrate (Scheme 2.3), using a modified literature method,[15] and was isolated as a beige crystalline solid in low yield (34%). Compound **2.4** was synthesised via the same mechanism as outlined before (Scheme 2.2) using **L1** and ferrocenecarboxaldehyde (Scheme 2.4). Compound **2.4** was isolated as a deep red amorphous solid in high yield (75%).

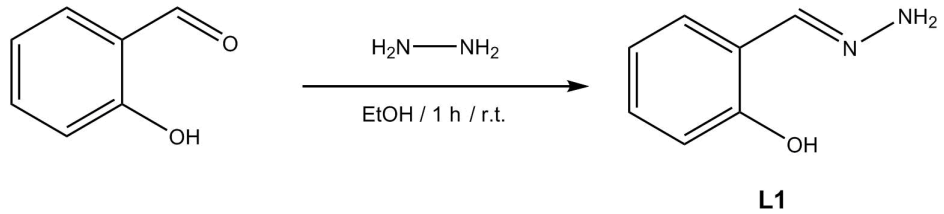

Scheme 2.3: Synthesis of **L1**.

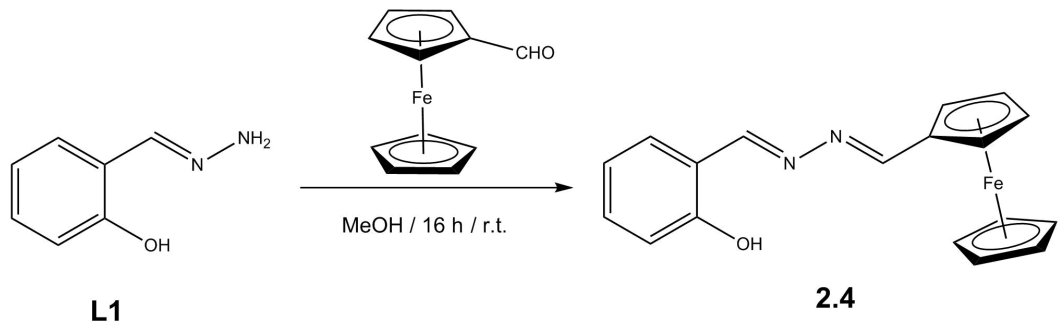

L1 **2.4**

Scheme 2.4: Synthesis of **2.4**.

2.2.2 Characterisation

Ligands **2.1**-**2.4** and **L1** were characterised by various spectroscopic and analytical techniques, namely ^{1}H, ^{13}C{^{1}H}, ^{19}F{^{1}H} (compound **2.2**), ^{1}H-^{1}H correlation spectroscopy (COSY) and heteronuclear single quantum coherence (HSQC) nuclear magnetic resonance (NMR) spectroscopy, infrared (IR) spectroscopy, and electron impact (EI-MS).

NMR Spectroscopy

Analysis of the ^{1}H NMR spectra of compounds **2.1**-**2.4** and **L1** confirmed that the proposed compounds were obtained. All spectra were recorded in $CDCl_3$ and the absence of the C**H**O resonance at δ_H 9.87 ppm, observed in the spectrum of the aldehyde, confirmed successful Schiff-base condensation. The presence of a singlet in the ^{1}H NMR spectra of **2.1**-**2.4**, in the region of δ_H 8.3-8.7 ppm, confirmed the presence of the imine group (Table 2.1). Phenyl proton resonances for the salicylaldimine spin system were observed in the region of δ_H 6.7-7.6 ppm, integrating for four protons. The hydroxyl proton is deshielded because of the attached phenyl group and was found to be in the region above δ_H 11 ppm in spectra of **2.1**-**2.4** (Table 2.1). The integration of the proton resonances were consistent with the proposed structures.

The spectrum of **2.1** displayed signals pertaining to the propyl chain which was observed at δ_H 1.00 (t), 1.74 (m) and 3.56 (td) ppm for the $CH_2C\mathbf{H}_3$, $C\mathbf{H}_2CH_3$ and $NC\mathbf{H}_2CH_2$ protons, respectively. Due to the effect of the trimethylsilane group in **2.3**, the signals of the propyl chain differ to those of **2.1**. In comparison to the spectrum of

2.1, the C**H**$_2$Si(CH$_3$)$_3$ proton resonance was observed at δ_H 0.58 ppm. Signals for the C**H**$_2$CH$_2$Si and NC**H**$_2$CH$_2$ protons were observed at δ_H 1.72 (m) and 3.60 (t) ppm, which are comparable to resonances observed for the same protons in **2.1**. In the ^{1}H NMR spectrum of **2.2**, additional aromatic signals were observed at δ_H 7.36 (2H) and 7.77 (2H) ppm as doublets due to the 1,4-substituted ring.

The synthesis of **L1** was supported by the appearance of a singlet at δ_H 7.87 ppm (CHN), integrating for 1H. Confirmation of the monofunctionalised product was the appearance of a broad singlet at δ_H 5.43 ppm, integrating for 2H, which was assigned to the NH$_2$ of the hydrazone. The O**H** resonance was observed at δ_H 11.05 ppm, and integrated for a single proton. In the ^{1}H NMR spectrum of **2.4** a shift of the imine resonance in **L1** from δ_H 7.87 ppm to 8.56 ppm suggests a change in the environment of the CHN moiety. An additional imine proton resonance was observed at δ_H 8.67 ppm for the imine group adjacent to the ferrocenyl moiety. In the COSY spectrum of **2.4** the imine signal at δ_H 8.70 ppm was observed to be correlated with one of the aromatic signals of the salicylaldimine (Figure 2.3), confirming the correct assignment. Signals for both the substituted (δ_H 4.51 (2H) and 4.74 (2H) ppm) and unsubstituted (δ_H 4.25 (5H) ppm) cyclopentadienyl groups are observed, confirming successful synthesis.

Table 2.1: Selected resonances observed in the ^{1}H NMR spectra of ligands **2.1**-**2.4**, recorded in CDCl$_3$

Compound	C**H**N (δ_H, ppm)	RC$_6$H$_4$O**H** (δ_H, ppm)
2.1	8.33	13.66
2.2	8.68	12.80
2.3	8.35	13.71
2.4	8.70	11.84

^{13}C{^{1}H} NMR spectroscopy was used to further characterise compounds **2.1-2.4**. Signals pertaining to the imine carbon atoms (**C**=N) were assigned at approximately δ_C 164 ppm for compounds **2.1**-**2.4**. Signals for the **C**OH carbon were observed at δ_C 161 ppm. In the spectrum of **2.2**, C-F coupling was observed for the carbons closest to the fluorine atoms. Coupling constants for $^1J_{C-F}$, $^2J_{C-F}$ and $^3J_{C-F}$ were observed and

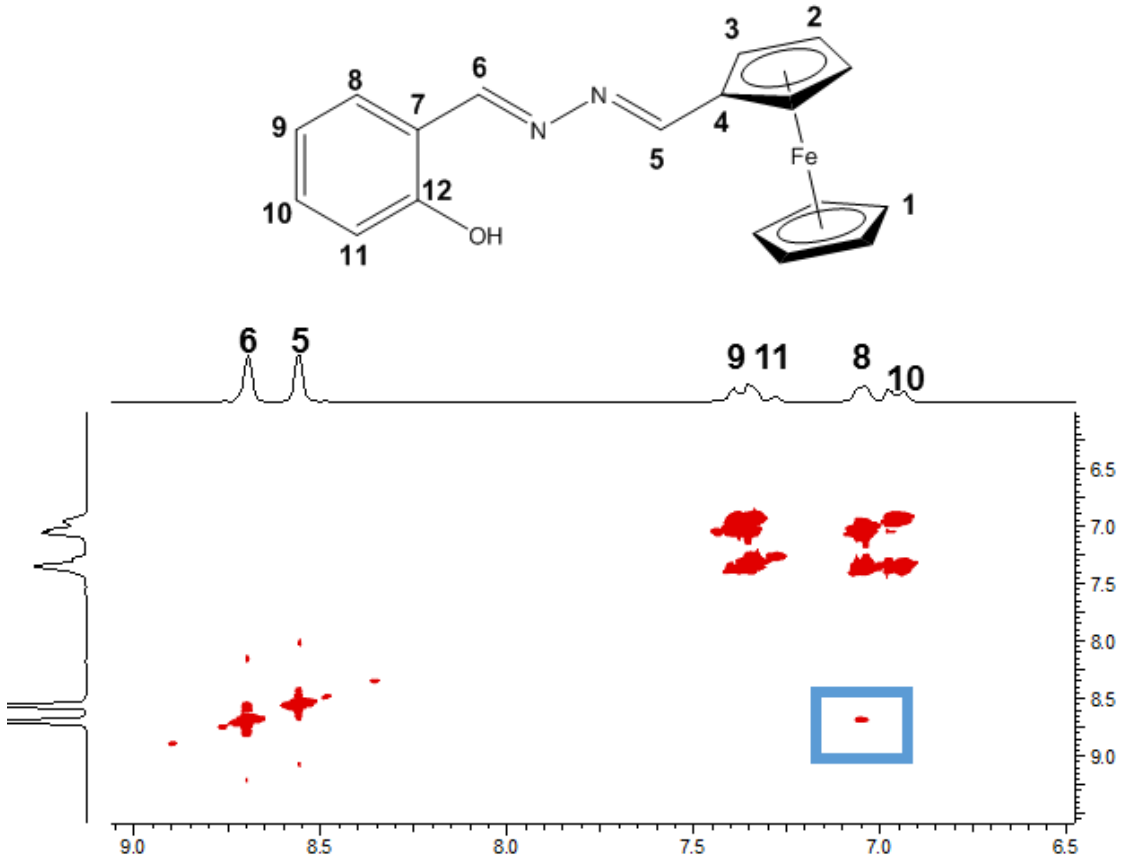

Figure 2.3: COSY spectrum of **2.4**, in $CDCl_3$, with a box enclosing the cross-peak of protons 6 and 8.

found to be 272.0 Hz, 32.5 Hz and 3.7 Hz, respectively, and the signals were observed as quartets (Figure 2.4). This phenomenon is consistent with the reported literature of similar compounds.[28] In the spectrum of **2.3**, the signal associated with $Si(\mathbf{C}H_3)_3$ was observed at δ_C -1.79 ppm due to the high shielding nature of the silicon atom. Compound **2.2** was analysed using $^{19}F\{^1H\}$ NMR spectroscopy. A single resonance was observed at δ_F -62 ppm, evidence of a single fluorine species.

Infrared Spectroscopy and EI Mass Spectrometry

Infrared (IR) spectroscopy is a technique used to identify various functional groups within a given molecule. The IR spectra of **2.1**-**2.4** were recorded in the solid state using the attenuated total reflection (ATR) sampling technique. The spectra of compounds **2.1**-**2.4** displayed absorption bands for the imine C=N between 1585 and 1618 cm^{-1}.

EI-MS analysis further confirmed the proposed structures. Molecular ion peaks were

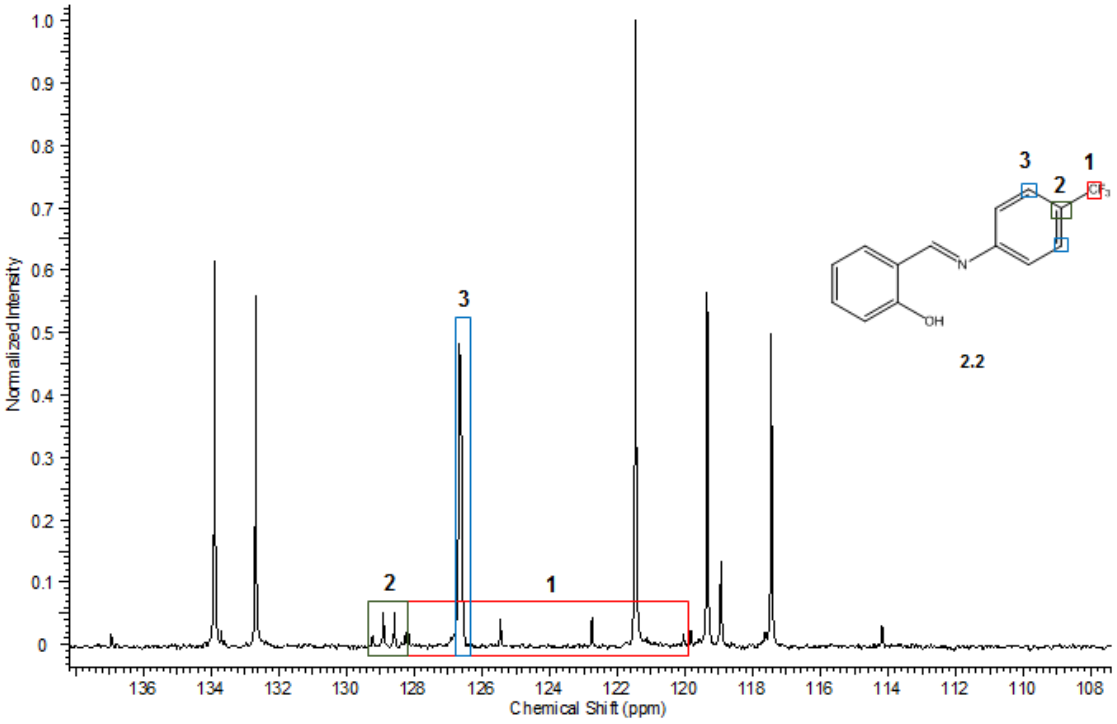

Figure 2.4: $^{13}C\{^{1}H\}$ NMR spectrum of **2.2** in $CDCl_3$, highlighting key carbon regions and assignments.

observed at *m/z* 163.00, 265.01, 235.13 and 332.05 in the spectra of **2.1**, **2.2**, **2.3** and **2.4**, respectively, further supporting the proposed structure.

Based on the characterisation data obtained, it was concluded that a series of *(N,O)*-salicylaldimine ligands were successfully synthesised. All spectroscopic and analytical evidence confirmed the integrity of the compounds synthesised.

2.3 Synthesis of *(N,O)*-salicylaldimine Ru(II), Rh(III) and Ir(III) complexes

2.3.1 Synthesis

A series of *(N,O)*-salicylaldimine Ru(II), Rh(III) and Ir(III) complexes, **2.5-2.16**, was synthesised using the afore-mentioned synthesised ligands via a bridge splitting reaction of $[RuCl(\mu\text{-}Cl)(p\text{-cymene})]_2$, $[RhCl(\mu\text{-}Cl)(Cp^*)]_2$ or $[IrCl(\mu\text{-}Cl)(Cp^*)]_2$ (Scheme 2.5).

Complexes **2.5**-**2.7**, **2.8**-**2.10**, **2.11**-**2.13** and **2.14**-**2.16** were synthesised by reacting **2.1**, **2.2**, **2.3** and **2.4**, respectively, in the presence of triethylamine to deprotonate the hydroxyl group, with the corresponding metal dimer to form the *(N,O)*-complexes. Complexes **2.5**-**2.10** were synthesised in dichloromethane, whereas **2.11**-**2.13** and **2.14**-**2.16** were synthesised in diethyl ether and ethanol, respectively.

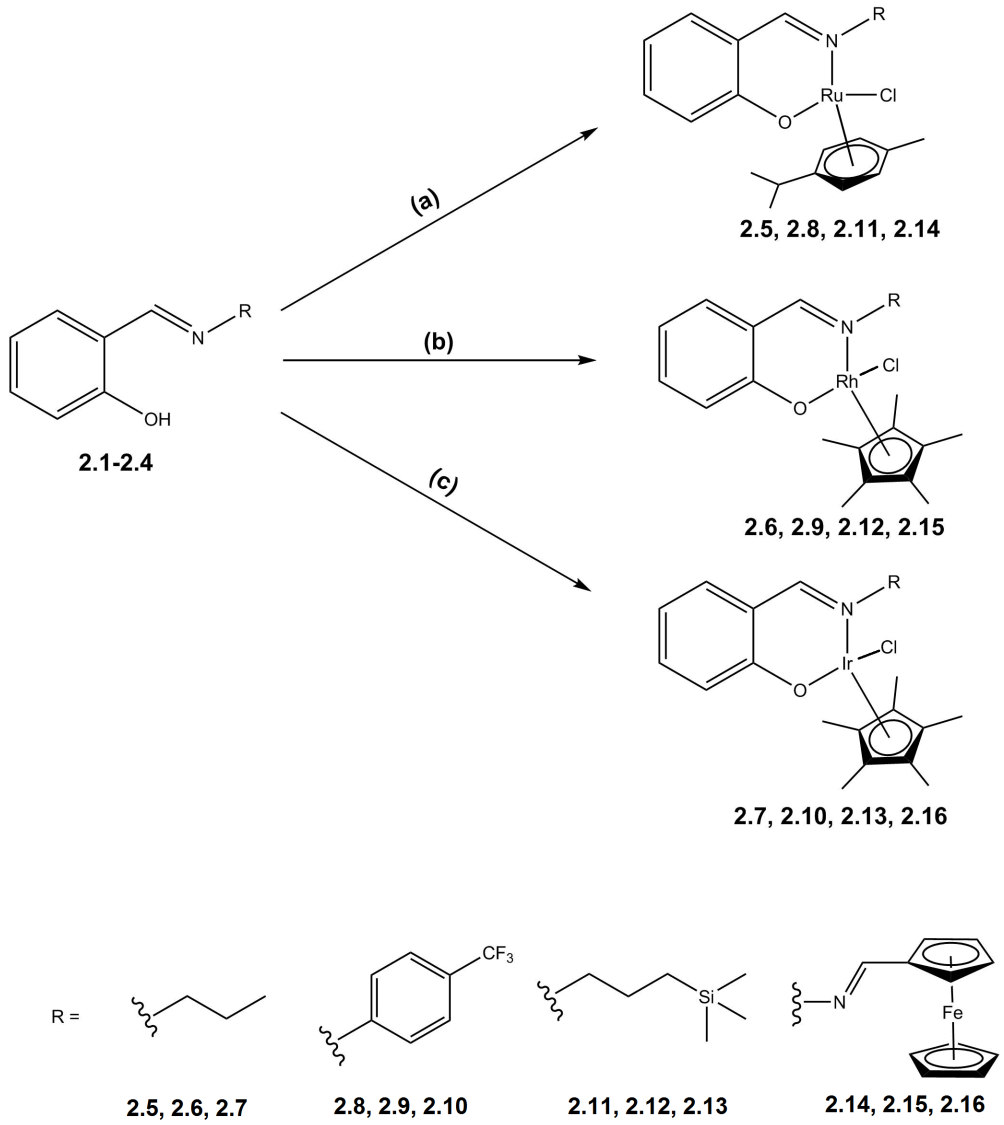

Scheme 2.5: Synthesis of *(N,O)*-complexes, **2.5**-**2.16**. Reagents and conditions: (a) Et_3N, $[RuCl(\mu\text{-}Cl)(p\text{-cymene})]_2$ / r.t.; (b) Et_3N, $[RhCl(\mu\text{-}Cl)(Cp^*)]_2$/ r.t.; (c) Et_3N, $[IrCl(\mu\text{-}Cl)(Cp^*)]_2$/ r.t.

2.3.2 Characterisation

NMR Spectroscopy

The ^{1}H and ^{13}C{^{1}H} NMR spectra of **2.5**-**2.16** were recorded in $CDCl_3$ and are consisted with the proposed structures.

Coordination was confirmed by an upfield shift in the imine proton (C**H**N) resonance. A shift from δ_H 8.33 ppm in **2.1** to δ_H 7.67-7.80 ppm in the complexes confirmed coordination to the imine nitrogen. The absence of the phenolic proton signal of the salicylaldimine moiety further supports the proposed bidentate chelation of the ligand to the metal centre. A consequence of this is metal chirality, as the metal becomes a stereogenic centre. Since there are no factors influencing the coordination site of the imine, two enantiomers are formed in equal probability (racemic mixture). Evidence of this is the diastereotopic behaviour of signals **2** and **3** (Figure 2.5), where the CH_2 protons are seen as non-equivalent in complex **2.5**, but are equivalent in the spectrum of ligand **2.1**. The same diastereotopic behaviour is observed in **2.6** and **2.7**. In the ^{13}C{^{1}H} NMR spectra of **2.5**-**2.7**, an upfield shift of the imine carbon resonance from the free ligand (δ_C 164.5 ppm) to the complex (δ_C 159-163 ppm) is also observed, thus confirming coordination to the imine nitrogen. A downfield shift of the carbon resonance adjacent to the oxygen atom (δ_C 161 ppm to 165-166 ppm) strongly suggests a metal-oxygen bond thus supporting the notion of the ligand behaving as an (N,O)-chelating ligand.

In the ^{1}H NMR spectra of **2.8**-**2.10**, an upfield shift in the imine proton signal was observed (δ_H 7.7-8.0 ppm) when compared to the free ligand (δ_H 8.68 ppm). Minute shifts in the (trifluoromethyl)phenyl group suggest little to no interaction with the *p*-cymene or Cp* ligands on the metal. A small shift in the carbon resonance for the imine group was observed. In the ^{13}C{^{1}H} NMR spectra of **2.8**-**2.10**, a distinct downfield shift of the carbon adjacent to the nitrogen from δ_C 151 ppm to 160-161 ppm (Figure 2.6) confirmed bonding of the nitrogen atom to the metal centre. The imine carbon resonance exhibited minor shifts from δ_C 164 ppm to 161-164 ppm. Coupling constants and carbon resonances for the trifluoromethylaniline group observed in the ^{13}C{^{1}H} NMR spectrum of **2.2** are unaffected in the complexes **2.8**-**2.10**, further suggesting

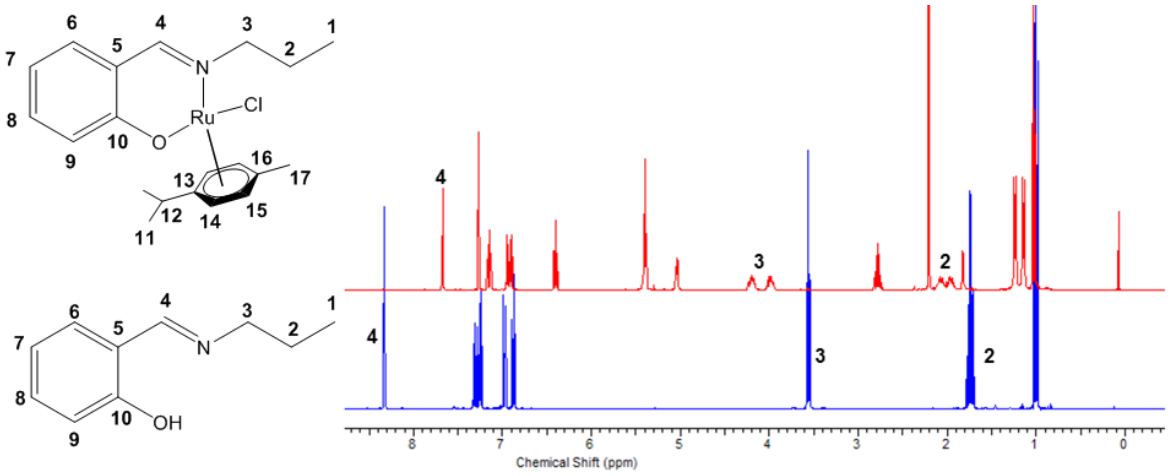

Figure 2.5: ^{1}H NMR spectra comparison of **2.1** and **2.5** in $CDCl_3$.

that there is no interaction of the *p*-cymene or Cp* ligands with the trifluormethane group. This was further confirmed using $^{19}F\{^{1}H\}$ NMR spectroscopy. As observed in **2.2**, a single resonance was observed at δ_F -62 ppm for **2.8**-**2.10** which supports the notion of a single fluorine species.

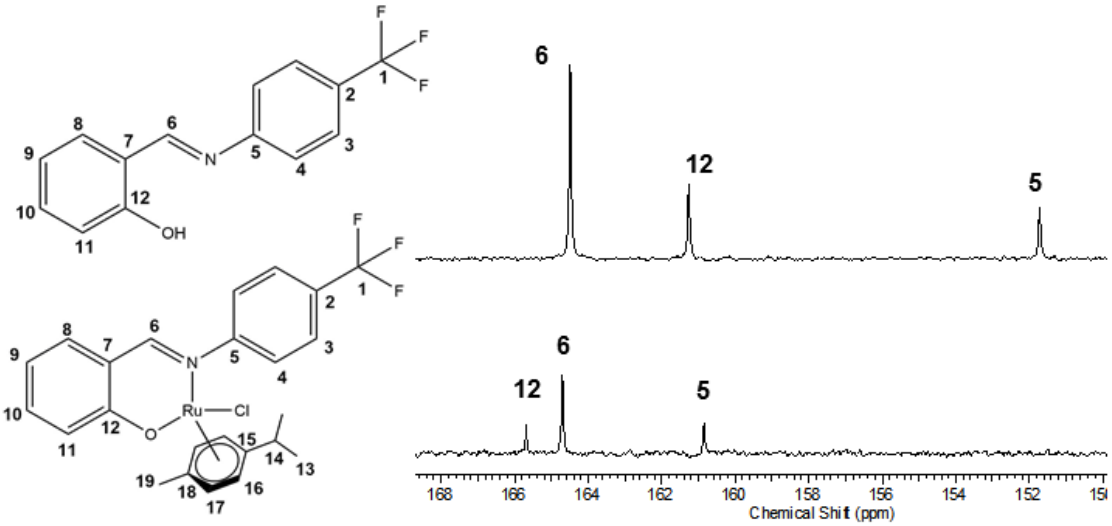

Figure 2.6: $^{13}C\{^{1}H\}$ NMR spectra comparison in the region between δ_C 150 and 170 ppm of **2.2** and **2.8** in $CDCl_3$.

The ^{1}H NMR spectra of complexes **2.11**-**2.13** display similar phenomena to those observed in complexes **2.5**-**2.7**. Evidence of chirality is observed in the signals associated with the propyl chain. Each CH_2 proton of the propyl chain was observed at its own chemical shift and integrates for a solitary proton. An upfield shift of the imine signal from δ_H 8.35 ppm to 7.6-7.6 ppm (Figure 2.7) is indicative of a change in the chemical

environment of the imine substructure. No hydroxyl signal (Figure 2.7) was observed in the ^{1}H NMR spectra, strongly suggesting that the ligand was deprotonated in the synthesis process. As found for complexes **2.5**-**2.7**, resonances for the imine and **C**O-M carbon atoms in the ^{13}C{^{1}H} NMR spectra were observed to have an upfield or downfield shift, respectively.

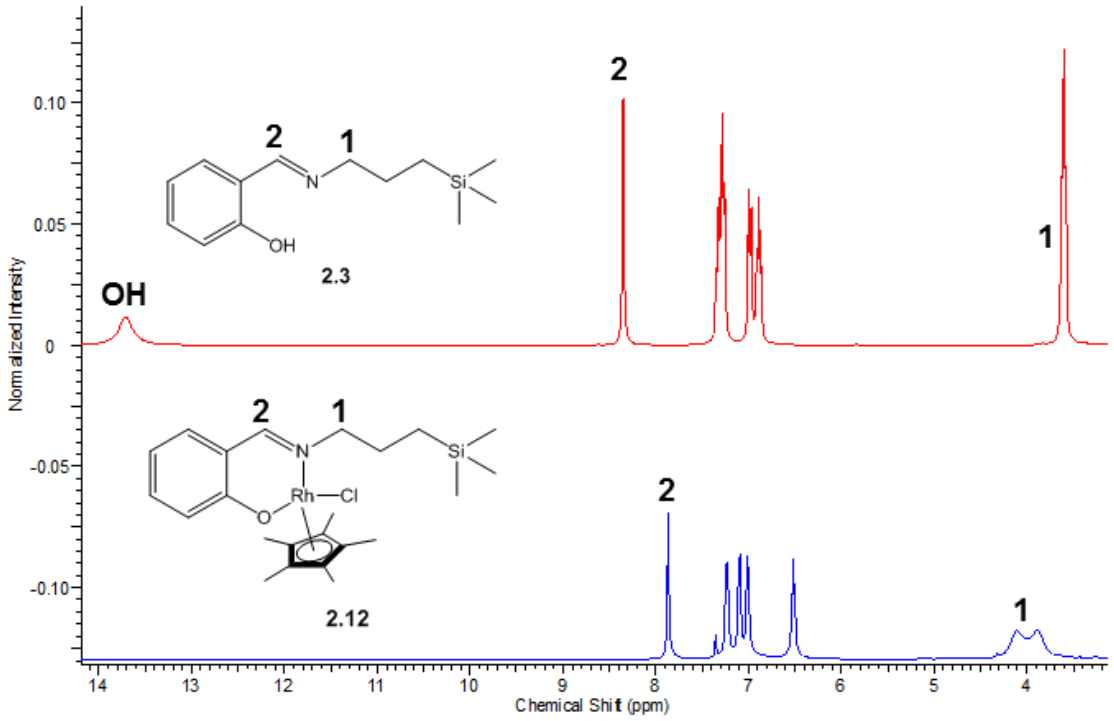

Figure 2.7: ^{1}H NMR spectra comparison in the region between δ_H 6.0 and 8.5 ppm of **2.3** and **2.12** in $CDCl_3$.

A shift of the imine proton signal in the ^{1}H NMR was observed upon complexation from **2.4** (δ_H 8.70 ppm) to **2.14**-**2.16** (δ_H 7.80-8.31 ppm). A minor shift in the imine proton resonance adjacent to the ferrocenyl group, confirms that the nitrogen adjacent to the salicylaldimine moiety coordinates to the metal centre. The protons for the substituted Cp ring are observed in the region of δ_H 4.2-4.9 ppm and are inequivalent.

Infrared Spectroscopy and Mass (EI and ESI) Spectrometry

For complexes **2.5**-**2.16**, a shift to lower wavenumbers of the C=N stretching vibration from the free ligands ($\approx$ 1630 cm^{-1}) to the complexes ($\approx$ 1615 cm^{-1}) supports complexation (Figure 2.8). The lower wavenumber suggests a weakening of the C=N bond. The metal-nitrogen bond is strengthened by back-bonding of the metal into

the nitrogen π^* orbital, which in turn reduces the bond order between the carbon and nitrogen. This synergistic effect is commonly observed in metal-imine systems.[16,29]

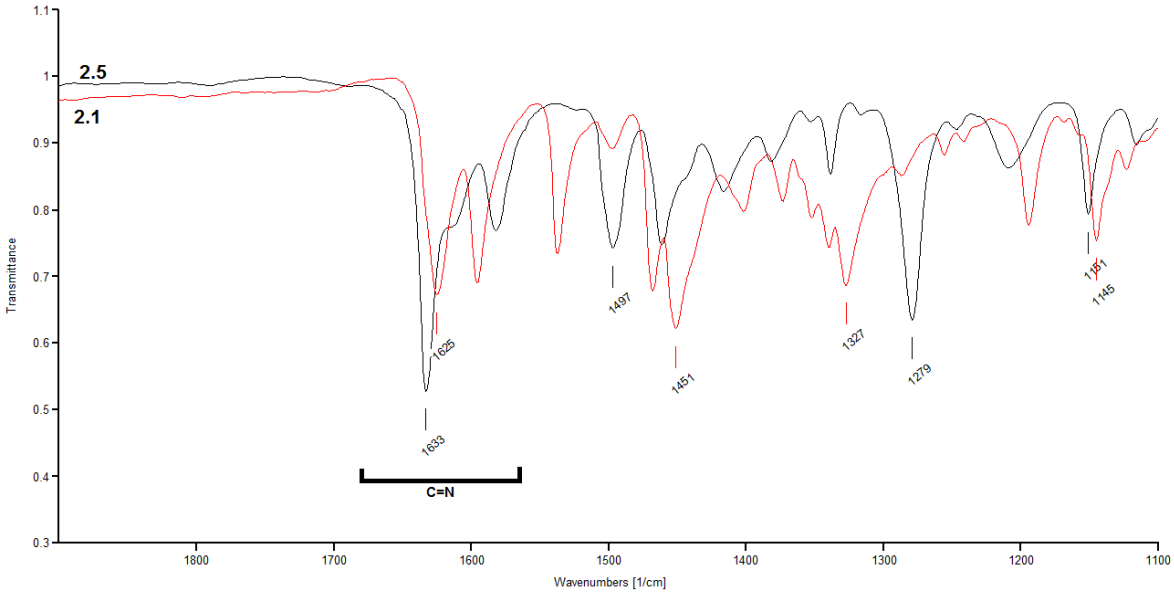

Figure 2.8: Representative IR spectra comparison between the ligand (**2.1**) and complex (**2.5**) highlighting the region of the imine absorbance.

The EI-MS spectra of complexes **2.5**-**2.7** and **2.14**-**2.16** and ESI-MS spectra of complexes **2.8**-**2.13** supports the synthesis of the proposed structures. Complexes were either ionised as M^+ or $[M+H]^+$ and corresponded well to the calculated values, with the exception of **2.13**. Compound **2.13** was observed to lose both the Cl and three methyl groups of the silane ($[M\text{-}Cl\text{-}(CH_3)_3]^{2+}$), with an overall charge of 2+.

Single Crystal X-Ray Diffraction (XRD)

Single crystal XRD is a useful technique to confirm the molecular structures of proposed compounds. Single crystals of **2.8**-**2.10** were obtained by slow diffusion of diethyl ether into methanol and the structures of these complexes elucidated (Figure 2.9). These complexes crystallised in the $P2_1/c$ space group with 4 molecules present in a given unit cell. The geometry about the metal is consistent with the proposed piano-stool geometry, with the angles between the N,O and Cl donor atoms ranging between 85 and 89°, indicative of a pseudo-tetrahedral arrangement (Table 2.2). This

is consistent with the data obtained by Smith *et al.* for complex **2.5**.[16] The two phenyl groups are observed to be $\sim 90^{\circ}$ in relation to each other. A six-membered ring is formed between the *(N,O)*-chelating ligand and the metal centre, further supporting the proposed bidentate structure. Bond distances between the metal and chlorido ligand are 20% larger in comparison to the *N,O*-chelate and the arene/Cp* group (2.0 Å for *N,O* compared to 2.4 Å for chlorido, see Table 2.2). Torsion angles about the imine bond are observed to be 179°, confirming a *trans*-configuration of the imine. The crystal data are provided in Table 2.3.

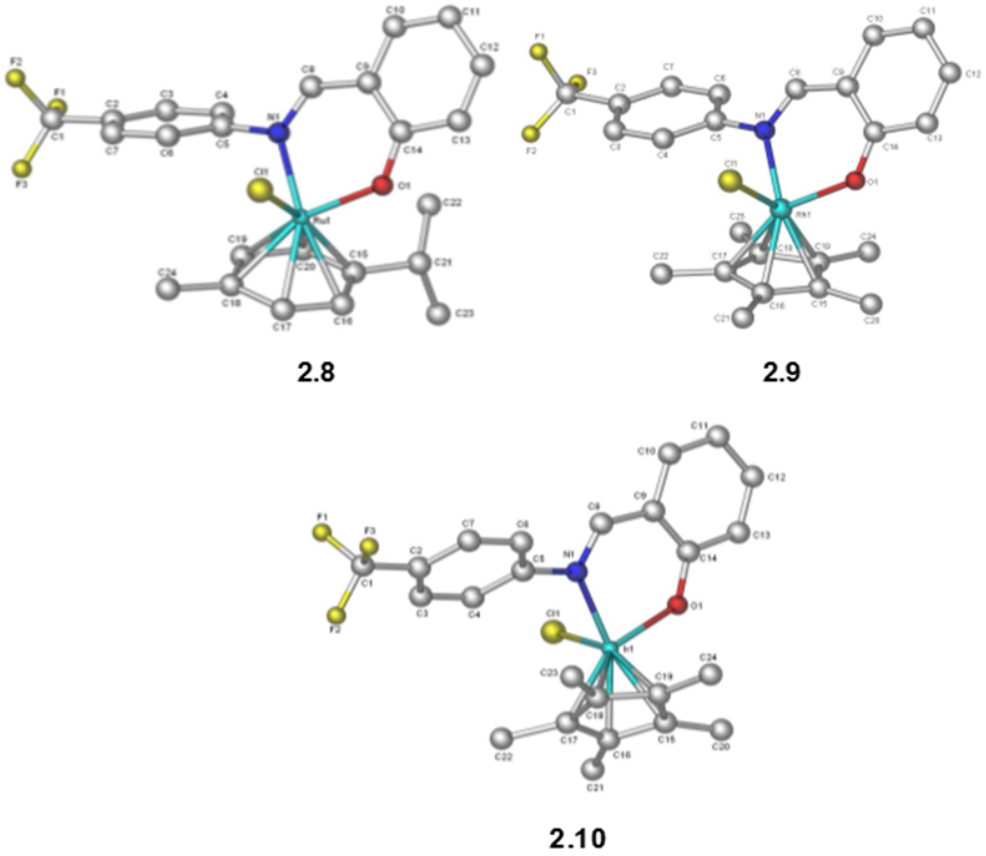

Figure 2.9: Ball and stick representation of the molecular structures of **2.8**-**2.10** determined by single crystal XRD. Hydrogen atoms are omitted for clarity.

Table 2.2: Selected bond distances and angles of complexes **2.8**-**2.10**

	Bond distance (Å) / angle (°)		
Entity	**2.8**	**2.9**	**2.10**
M-N	2.088(2)	2.109(2)	2.095(3)
M-Cl	2.4288(8)	2.4258(9)	2.4210(9)
M-O	2.0594(18)	2.068(2)	2.084(2)
N-M-O	88.01(7)	88.42(8)	88.02(10)
N-M-Cl	89.89(9)	85.18(7)	85.59(7)
O-M-Cl	85.38(6)	88.89(7)	85.58(7)
C=N-C-C	179.9(3)	179.9(3)	178.7(3)

Table 2.3: Crystal data and structure refinement for complexes **2.8**-**2.10**

	2.8	**2.9**	**2.10**
Empirical Formula	$C_{24}H_{23}ClF_3NORu$	$C_{24}H_{24}ClF_3NORh$	$C_{24}H_{24}ClF_3IrNO$
Formula Weight (g.mol^{-1})	534.95	537.80	627.11
Temperature (K)	110	173	173
Radiation (Å)	0.71073	0.71073	0.71073
Crystal System	Monoclinic	Monoclinic	Monoclinic
Space Group	$P2_1$/c	$P2_1$/c	$P2_1$/c
Unit Cell dimensions			
a (Å)	9.6891(5)	11.8815(14)	7.7409(6)
b (Å)	13.8341(7)	24.057(3)	22.0339(15)
c (Å)	16.7075(7)	7.8436(10)	12.9297(9)
α (°)	90	90	90
β (°)	96.279(1)	103.124(3)	95.103(2)
γ (°)	90	90	90
V (Å^3)	2226.04(19)	2183.4(5)	2196.6(3)
Z	4	4	4
Density (calc.) (g·cm^{-1})	1.596	1.636	1.896
$F(000)$	1080	1088	1216
Crystal size (mm)	0.07 x 0.08 x 0.08	0.13 x 0.14 x 0.15	0.09 x 0.13 x 0.16
$\theta_{min,max}$ (°)	1.9, 27.9	1.7, 28.0	1.8, 28.0
Data set	-12 : 12 ; -18 : 18;	-15 : 15 ; -31 : 31;	-10 : 10 ; -29 : 29;
	-21 : 21	-10 : 9	-17 : 17
Total reflections	43241	26557	44304
Unique reflections	5332	5269	5291
R indices (R_1, wR_2)	0.0320, 0.0666	0.0359, 0.0837	0.0224, 0.0516
Res. Dens. (e Å^{-3})$_{min,max}$	-0.52, 0.46	-0.55, 0.60	-0.59, 0.96

Based on the correlation between the proposed structures and the spectroscopic data, it can be concluded that the desired metal complexes were synthesised.

2.4 Summary

A series of salicylaldimine complexes was prepared, characterised and the data obtained from compounds **2.5**-**2.8** and **2.14**-**2.16** corresponded well to the literature.[9,15,16,26] Two new series of trifluoromethane (**2.8**-**2.10**) or organosilane (**2.11**-**2.13**) complexes bearing Ru(II), Rh(III) or Ir(III) metal centres, derived from two salicylaldimine ligands (**2.2**[27] and **2.3**) were synthesised and characterised. Single crystals of **2.8**-**2.10** were analysed by X-ray diffraction and further confirmed the molecular structure of the complexes in the solid state. All of the compounds were characterised using NMR (^{1}H, ^{13}C{^{1}H}, HSQC, COSY) and IR spectroscopies, elemental analysis, and EI (**2.5**-**2.7** and **2.14**-**2.16**) or ESI (**2.8**-**2.13**) mass spectrometry and correlate well with the proposed structures.

2.5 References

1. A. Alama, B. Tasso, F. Novelli and F. Sparatore, *Drug Discov. Today*, 2009, **14**, 500–508.
2. A. Bergamo, A. Masi, A. Peacock, A. Habtemariam, P. Sadler and G. Sava, *J. Inorg. Biochem.*, 2010, **104**, 79–86.
3. G. Sava, A. Bergamo and P. J. Dyson, *Dalton Trans.*, 2011, **40**, 9069–9075.
4. S. J. Lucas, R. M. Lord, R. L. Wilson, R. M. Phillips, V. Sridharan and P. C. McGowan, *Dalton Trans.*, 2012, **41**, 13800–13802.
5. S. J. Lucas, R. M. Lord, A. M. Basri, S. J. Allison, R. M. Phillips, A. J. Blacker and P. C. McGowan, *Dalton Trans.*, 2016, **45**, 6812–6815.
6. J. Yang, R. Shi, P. Zhou, Q. Qiu and H. Li, *J. Mol. Structure*, 2016, **1106**, 242–258.
7. T. Stringer, D. T. Hendricks, H. Guzgay and G. S. Smith, *Polyhedron*, 2012, **31**, 486–493.
8. I. Correia, S. Roy, C. P. Matos, S. Borovic, N. Butenko, I. Cavaco, F. Marques, J. Lorenzo, A. Rodríguez, V. Moreno and J. C. Pessoa, *J. Inorg. Biochem.*, 2015, **147**, 134–146.

9. P. Govender, L. C. Sudding, C. M. Clavel, P. J. Dyson, B. Therrien and G. S. Smith, *Dalton Trans.*, 2013, **42**, 1267–1277.

10. F.-U. Rahman, A. Ali, I. Khan, R. Guo, L. Chen, H. Wang, Z.-T. Li, Y. Lin and D.-W. Zhang, *Polyhedron*, 2015, **100**, 264–270.

11. F.-U. Rahman, A. Ali, R. Guo, W.-K. Wang, H. Wang, Z.-T. Li, Y. Lin and D.-W. Zhang, *Dalton Trans.*, 2015, **44**, 9872–9880.

12. A. M. Abu-Dief and I. M. Mohamed, *Beni-Seuf Univ. J. Appl. Sci.*, 2015, **4**, 119–133.

13. V. Sharma, A. Beatty, S. P. Wey, J. Dahlheimer, C. M. Pica, C. L. Crankshaw, L. Bass, M. A. Green, M. J. Welch and D. Piwnica-Worms, *Chem. Biol.*, 2000, **7**, 335–343.

14. T. Stringer, D. Taylor, H. Guzgay, A. Shokar, A. Au, P. J. Smith, D. T. Hendricks, K. M. Land, T. J. Egan and G. S. Smith, *Dalton Trans.*, 2015, **44**, 14906–14917.

15. W. Nkoana, D. Nyoni, P. Chellan, T. Stringer, D. Taylor, P. J. Smith, A. T. Hutton and G. S. Smith, *J. Organomet. Chem.*, 2014, **752**, 67–75.

16. P. Govender, A. K. Renfrew, C. M. Clavel, P. J. Dyson, B. Therrien and G. S. Smith, *Dalton Trans.*, 2011, **40**, 1158–1167.

17. F.-U. Rahman, A. Ali, R. Guo, Y.-C. Zhang, H. Wang, Z.-T. Li and D.-W. Zhang, *Dalton Trans.*, 2015, **44**, 2166–2175.

18. F.-U. Rahman, A. Ali, R. Guo, W.-K. Wang, H. Wang, Z.-T. Li, Y. Lin and D.-W. Zhang, *Dalton Trans.*, 2015, **44**, 9872–9880.

19. C. Isanbor and D. O'Hagan, *J. Fluorine Chem.*, 2006, **127**, 303–319.

20. M. Adams, L. Barnard, C. de Kock, P. J. Smith, L. Wiesner, K. Chibale and G. S. Smith, *Dalton Trans.*, 2016, **45**, 5514–5520.

21. M. Adams, C. de Kock, P. J. Smith, K. M. Land, N. Liu, M. Hopper, A. Hsiao, A. R. Burgoyne, T. Stringer, M. Meyer, L. Wiesner, K. Chibale and G. S. Smith, *Dalton Trans.*, 2015, **44**, 2456–2468.

22. J. Kühnert, P. Ecorchard and H. Lang, *Eur. J. Inorg. Chem.*, 2008, 5125–5137.

23. C. Ornelas, *New J. Chem.*, 2011, **35**, 1973–1985.

24. K. L. Kirk, *J. Fluorine Chem.*, 2006, **127**, 1013–1029.

25. O. H. Temmink, T. Emura, M. De Bruin, M. Fukushima and G. J. Peters, *Cancer Sci.*, 2007, **98**, 779–789.

26. R. Payne, P. Govender, B. Therrien, C. M. Clavel, P. J. Dyson and G. S. Smith, *J. Organomet. Chem.*, 2013, **729**, 20–27.

27. L. Maqeda, B. C. Makhubela and G. S. Smith, *Polyhedron*, 2015, **91**, 128–135.

28. M. Carril, P. Altmann, M. Drees, W. Bonrath, T. Netscher, J. Schütz and F. E. Kühn, *J. Cat.*, 2011, **283**, 55–67.

29. L. C. Sudding, R. Payne, P. Govender, F. Edafe, C. M. Clavel, P. J. Dyson, B. Therrien and G. S. Smith, *J. Organomet. Chem.*, 2014, **774**, 79–85.

Chapter 3

Synthesis and characterisation of cationic Ru(II), Rh(III) and Ir(III) alkylated PTA complexes

3.1 Introduction

Despite extensive investigation of the potential anticancer activity of various metal-based compounds, only a few have entered clinical trials.[1,2] Three platinum-containing complexes are currently used clinically.[3] Issues such as *in vivo* toxicity, drug resistance and low aqueous solubility all contribute to the low success rate of metal complexes as anticancer agents.[4] The severe side-effects of widely-used cisplatin and problems such as tumour resistance, have led to the investigation of more effective and less toxic alternatives.

Ruthenium complexes such as NAMI-A and KP1019 have shown promise and have been evaluated in clinical trials.[5–9] Recently, ruthenium(II) arene complexes have become a popular alternative to these ruthenium(III) coordination complexes. Specifically, compounds of the RAPTA variety ([Ru(η^6-arene)(PTA)L_2], **1a**, Figure 3.1) have shown great promise and could be used as anticancer agents in the future.[10,11] Generally, RAPTA complexes contain a ruthenium core, an arene group and the PTA (1,3,5-

triaza-7-phosphaadamantane) ligand, which promotes aqueous solubility, as well as two labile chlorido ligands. These complexes have shown potent antitumour activity against both primary and metastatic tumours *in vivo*.[12–15] Increasing the cellular uptake and changing the metal can increase the bio-activity of these complexes. Dyson and co-workers[16] investigated the effect of lipophilicity by changing the arene, changing a Cl ligand to PPh_3, and altering the counter ion to increase cellular uptake. A 10-fold increase in cytotoxicity was observed by changing the counterion to a BF_4 species (**1a, 2a** to **1b, 2b**, respectively, Figure 3.1), whilst the *p*-cymene arene complex showed the greatest activity. A slight increase in the uptake of **1b** in comparison to **1a** (Figure 3.1) in cells (0.13 vs 0.12 μg per 10^6 cells) suggests that a small change in the uptake can assist with the activity of the complex in question.

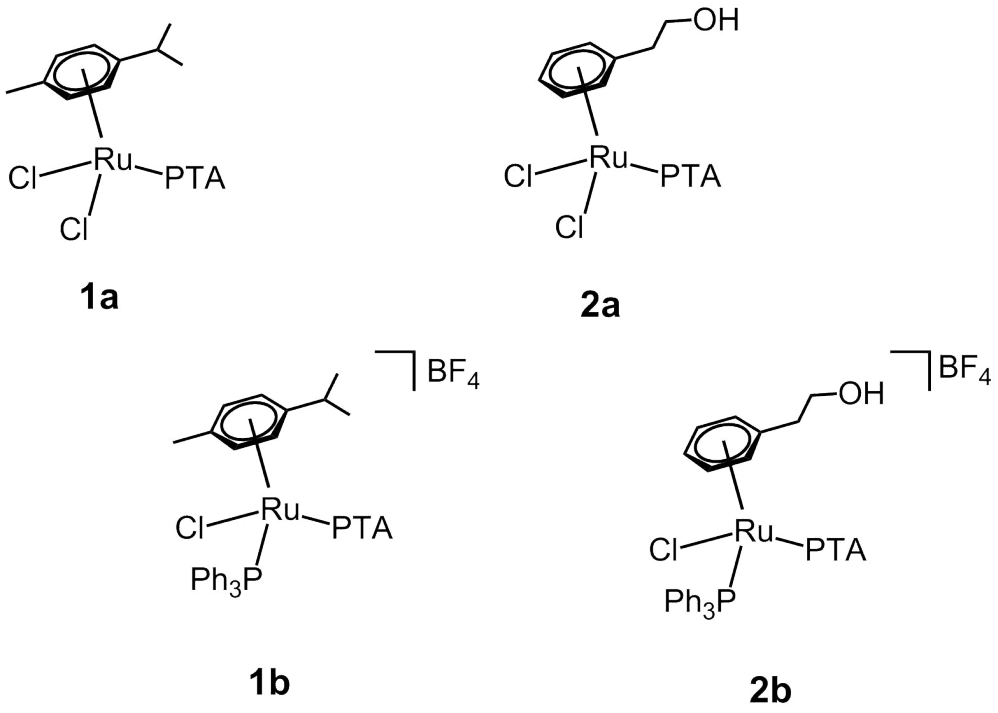

Figure 3.1: PTA complexes investigated by Dyson and co-workers.[16]

Another way to tailor RAPTA complexes to biological assays is to increase the solubility of the complexes in the medium. To increase the water solubility, Burgoyne and co-workers[17] used benzyl chloride and 1,3,5-tris(chloromethyl)benzene to create a charge on the PTA ligand using an alkylation reaction. These complexes, shown in Figure 3.2, exhibit significant water solubility, as well as biological activity. These complexes were evaluated against an oesophageal cancer cell line (WHCO1), and was observed to have

a biological profile 5-33 times less effective than cisplatin against the WHCO1 cell line. The other way to tailor these complexes is to replace the chlorido ligands with more biologically significant entities. Changing the ligands can significantly change the interaction with biomolecules and may display more effective modes of action.[18] Pettinari *et. al.*[12] displaced these chlorido ligands with (*O,O*)-curcumin derivatives, which have shown promise in a previous study.[19] In comparison to cisplatin, these complexes were more active against the ovarian carcinoma sensitive and resistant A2780 and A2780cis cancer cell lines, and display comparable activity against the non-tumorous human embryonic kidney cells (HEK293), with the most active complex being 71% less toxic to HEK293. These complexes also exhibited no preference between the resistant and sensitive cancer cell lines (Resistance Index (RI) $\simeq$ 1, A2780cis/A2780 (cisplatin, RI = 17)), as well as high selectivity for A2780 over HEK293, with the selectivity indices (SI) of these complexes ranging between 12 and 65 in comparison to cisplatin (SI = 5).[19]

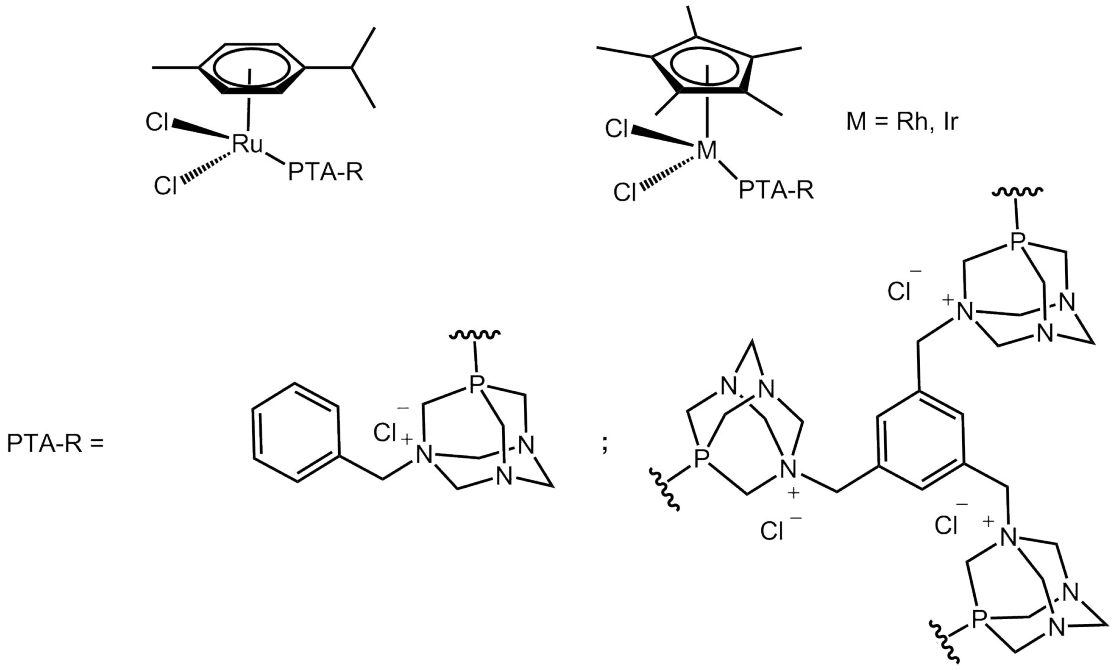

Figure 3.2: Alkylated PTA complexes investigated by Burgoyne and co-workers.[17]

These changes to the RAPTA series have yielded significant improvements in the uptake, solubility and selectivity of these compounds.[12,16,17,19] In this chapter, a series of alkylated PTA Ru(II), Rh(III) and Ir(III) complexes, an extension of the work conducted by Burgoyne and co-workers[17] were prepared in order to investigate the effect

of incorporating an alkylated PTA scaffold and its influence on biological activity in comparison to the complexes discussed in Chapter 2. The biological activity of PTA complexes containing metals other than ruthenium has been infrequently explored.[20] The synthesis and characterisation of the complexes are reported herein.

3.2 Synthesis of the alkylated PTA scaffold and monocationic complexes (3.1-3.4)

3.2.1 Synthesis

A benzyl alkylated PTA scaffold (**3.1**) was synthesised by reacting one molar equivalent each of benzyl chloride and 1,3,5-triaza-7-phosphaadamantane via a quaternisation reaction to afford the benzyl PTA scaffold (**3.1**, Scheme 3.1). The reaction proceeds via a nucleophilic substitution reaction of the chloride with a tertiary PTA amine (Scheme 3.1). No bis-functionalised product was obtained, even when reacting 2.5 molar equivalents of benzyl chloride, likely due to the close proximity of the positive charges. The atom economic product was isolated as a white solid, in high yield (99 %) and was found to be soluble in water, dimethyl sulfoxide, alcohols and sparingly soluble in chloroform.

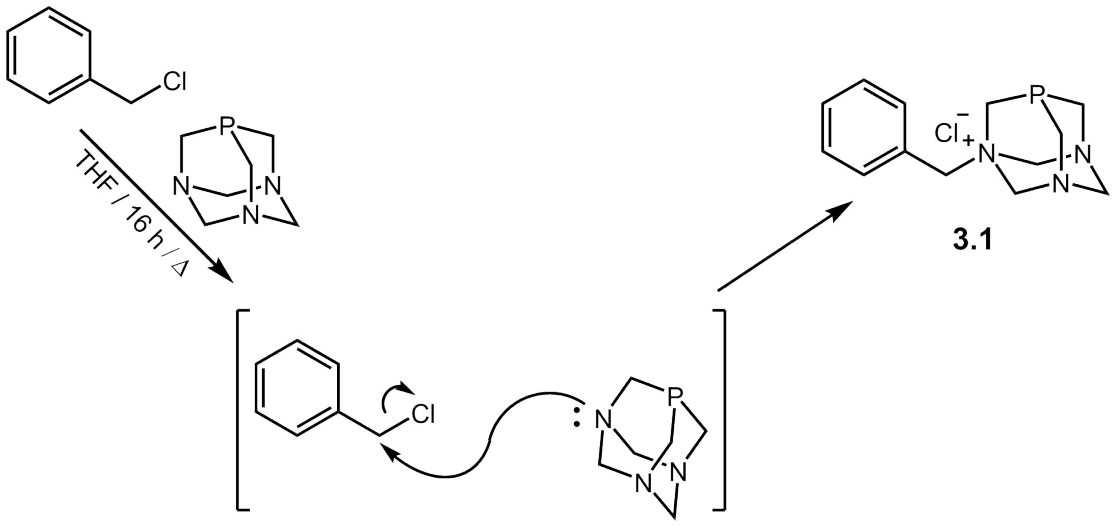

Scheme 3.1: Synthesis of the benzyl PTA scaffold, **3.1**, with the reaction mechanism.

RAPTA-type complexes were synthesised by reacting [RuCl(μ-Cl)(p-cymene)]$_2$, [RhCl(μ-Cl)(Cp*)]$_2$ or [IrCl(μ-Cl)(Cp*)]$_2$ with the benzyl PTA scaffold (**3.1**) via a bridge-splitting reaction (**3.2-3.4**, Scheme 3.2). The complexes were isolated as red crystalline (**3.2** and **3.3**) or orange amorphous (**3.4**) powders in moderate yields (50-70 %), and were found to be highly water-soluble, in contrast to the metal dimers.

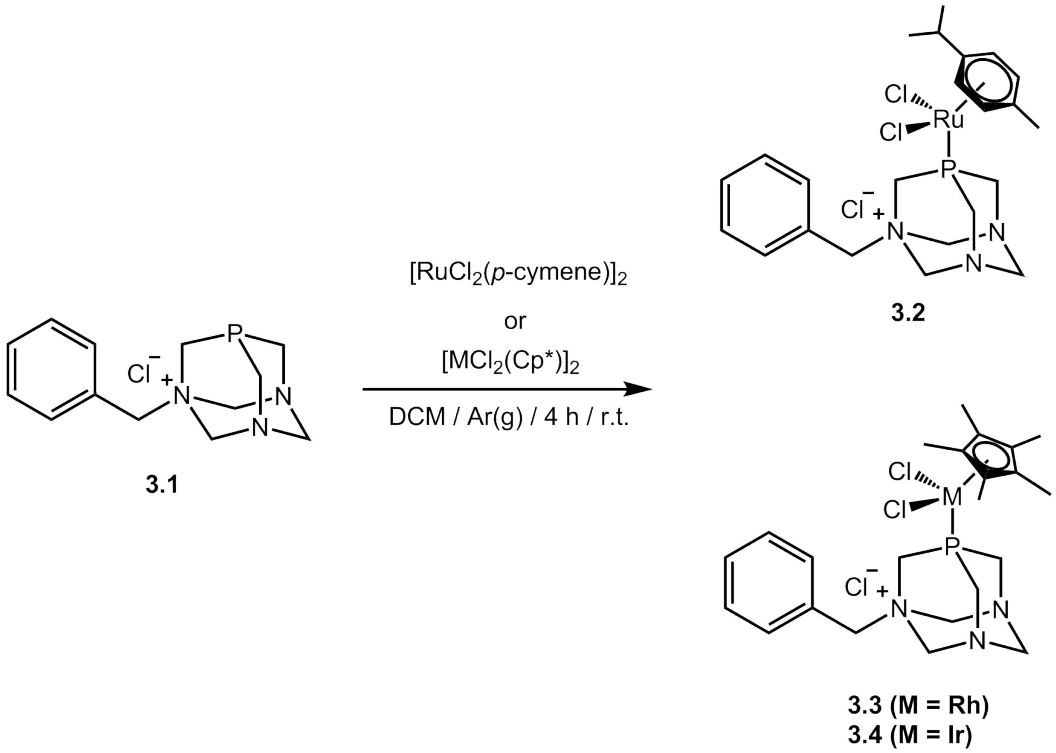

Scheme 3.2: Synthesis of the metal PTA complexes **3.2-3.4**.

3.2.2 Characterisation

NMR Spectroscopy

Analysis of the ^{1}H NMR spectrum of **3.1** shows that the mono-quaternised PTA scaffold was obtained. Two AB-spin quartets, integrating for 4H and 2H, were observed in the spectrum, supporting a loss of the C_{3v} symmetry. These signals were assigned to the lower cage protons of the PTA moiety (signals 6 and 7, Figure 3.3). The protons of the upper cage (carbon atoms adjacent to the phosphorus atom) were also observed as two sets of signals, with an undefined splitting pattern, further supporting the loss of symmetry of the free PTA precursor and coupling to the NMR active ^{31}P nucleus. A

singlet for the benzyl CH_2 protons was observed at δ_H 4.2 ppm and integrated for 2H. A broad multiplet was observed at δ_H 7.5-7.6 ppm assigned to the aromatic protons, integrating for 5H. Upon complexation with the metal dimers, the AB-spin system was not observed, supporting a change in the PTA environment. Upon complexation of **3.1**, proton resonances for the aromatic signals (signals 1-3, Figure 3.3) appear more distinct.

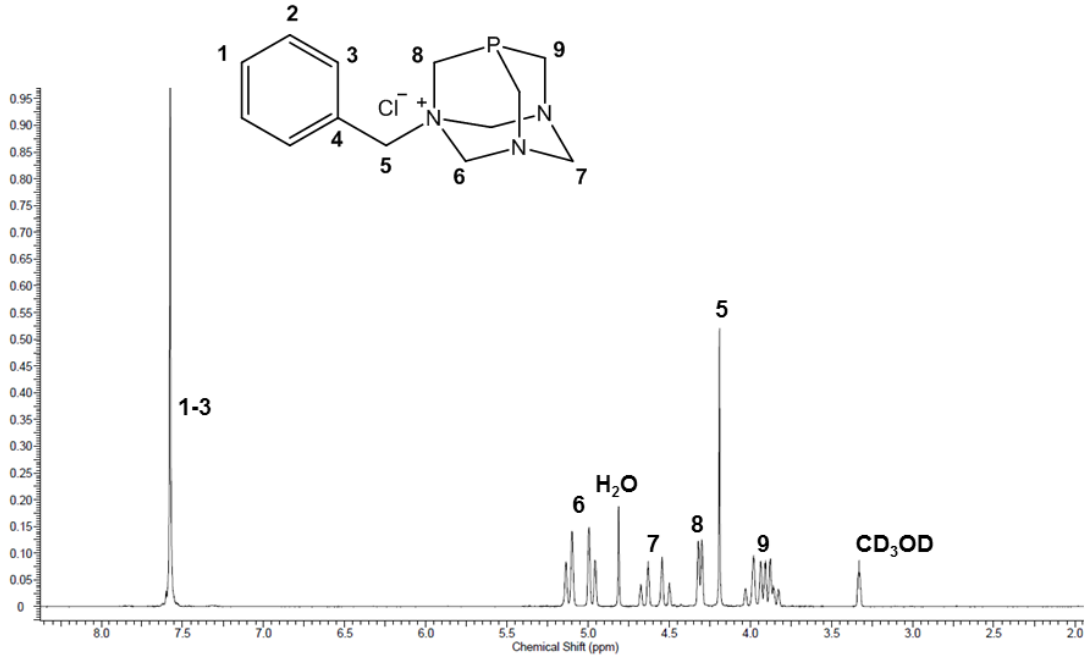

Figure 3.3: ^{1}H NMR spectrum of **3.1** in CD_3OD-d_4.

Two signals for the methyl carbon atoms of the Cp* moiety of **3.3** in the $^{13}C\{^1H\}$ NMR spectrum are observed in CD_3OD-d_4 (Figure 3.4). This phenomenon was not observed in $CDCl_3$ (Figure 3.4), for complexes **3.2** and **3.4** and the dimeric precursor. Further investigations are required to understand this phenomenon. The $^{31}P\{^1H\}$ NMR spectra of compounds **3.1**-**3.4** provided further support that the proposed compounds were synthesised. A singlet at δ_P -81 ppm (**3.1**, Figure 3.5) for the phosphorus atom of the PTA ligand **3.1** was observed (a significant shift from the free PTA precursor, which was observed at δ_P -98 ppm). Upon complexation, a downfield shift of the phosphorus resonance from δ_P -81 ppm to $\sim$ -21 ppm for **3.2** and **3.3** and δ_P -55 ppm for **3.4** (Figure 3.5) confirms a change in the environment of the phosphorus atom, evidence of the formation of a metal-phosphorus bond. Coupling of the rhodium centre and the phosphorus atom is evident in the $^{31}P\{^1H\}$ NMR spectrum of **3.3**, with the phosphorus

signal observed as a doublet with a coupling constant of $J_{Rh-P} = 150$ Hz.

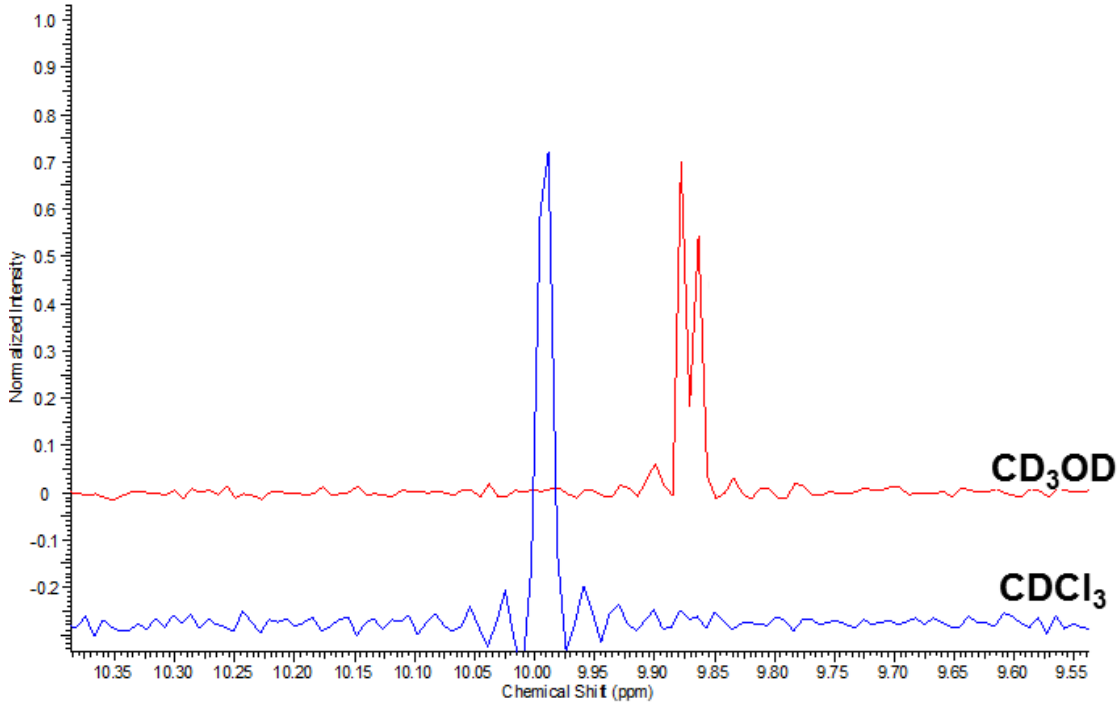

Figure 3.4: $^{13}C\{^1H\}$ NMR spectra of **3.3** in CD_3OD-d_4 and $CDCl_3$, showing the Cp* methyl carbon signals.

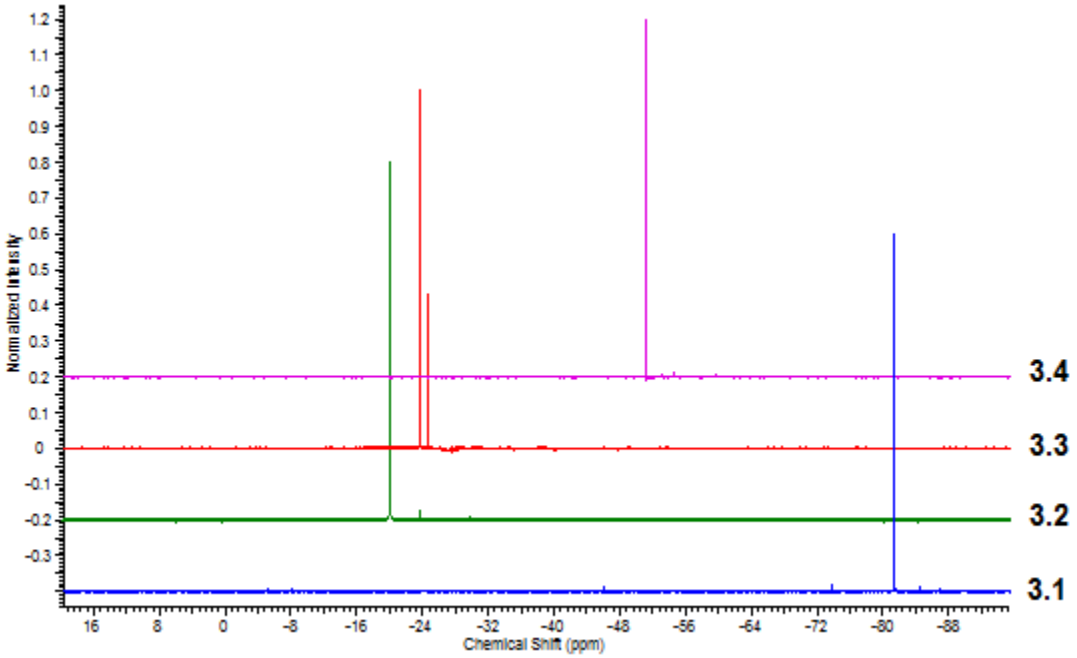

Figure 3.5: $^{31}P\{^1H\}$ NMR spectra comparison of **3.1**-**3.4**, in CD_3OD-d_4 (**3.1**) and $CDCl_3$ (**3.2**-**3.4**).

ESI Mass Spectrometry

The ESI mass spectra, recorded in the positive-ion mode, of **3.1**-**3.4** confirmed the successful synthesis of the proposed compounds. The spectra of compounds **3.1**-**3.3** display a base peak of $[M\text{-}Cl]^+$ (248.1318, 554.0833, 556.0906 respectively), while a peak for $[M\text{-}2Cl]^{2+}$ (305.5901) is observed for **3.4**. These results are consistent with the proposed structures.

3.3 Synthesis of dicationic (*N,O*)-salicylaldimine PTA complexes (3.5-3.15)

3.3.1 Synthesis

Complexes **2.5**-**2.11** and **2.13**-**2.16** (discussed in Chapter 2) were reacted with **3.1** to afford complexes **3.5**-**3.15** (Scheme 3.3). Complexes **2.5**-**2.7**, **2.11**, **2.13** and **2.14** were reacted under an inert atmosphere with **3.1** in dry ethanol for 16 hours to afford complexes **3.5**-**3.7** and **3.11**-**3.13** as highly water-soluble powders. Complexes **3.8**-**3.10**, **3.14** and **3.15** (unstable as chloride salts) were prepared by abstracting the chlorido ligand of **2.8**-**2.10** and **2.15**-**2.16** using silver hexafluorophosphate in acetone, under argon, and subsequently reacted with **3.1** to afford the desired complexes as sparingly water-soluble powders. Complex **2.12** was reacted with **3.1**; however the product formed was not stable as chloride or hexafluorophosphate salts and therefore could not be isolated for analysis. Ruthenium complexes (**3.5**, **3.10** and **3.13**), though hygroscopic, formed insoluble products in water which could be solubilised using DMSO.

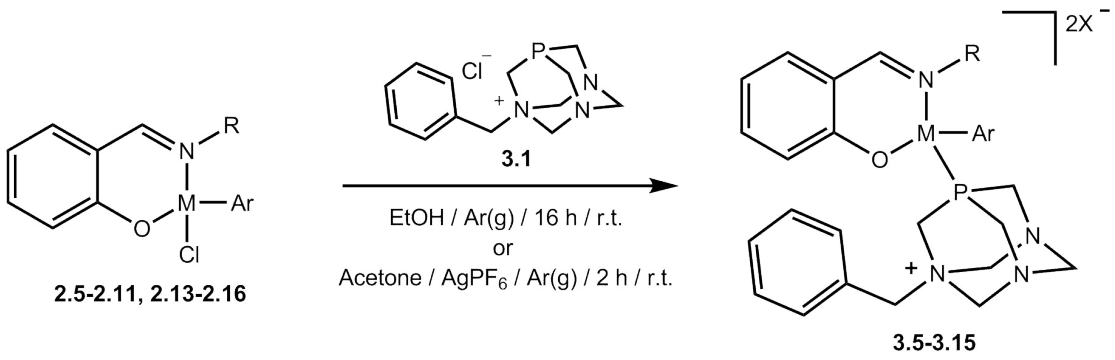

For R = Pr, X = Cl

3.5 - M: Ru; Ar: *p*-cymene
3.6 - M: Rh; Ar: Cp*
3.7 - M; Ir ; Ar: Cp*

For R = Pr-Si(Me)$_3$, X = Cl

3.11 - M: Ru; Ar: *p*-cymene
3.12 - M; Ir ; Ar: Cp*

For R = Ph-CF$_3$, X = PF$_6$

3.8 - M: Ru; Ar: *p*-cymene
3.9 - M: Rh; Ar: Cp*
3.10 - M; Ir ; Ar: Cp*

For R = NCHFc, X = Cl (**3.13**)
PF$_6$ (**3.14**-**3.15**)

3.13 - M: Ru; Ar: *p*-cymene
3.14 - M: Rh; Ar: Cp*
3.15 - M; Ir ; Ar: Cp*

Scheme 3.3: Synthesis of the dicationic PTA complexes **3.5**-**3.15**.

3.3.2 Characterisation

NMR Spectroscopy

Analysis of the ^{1}H NMR spectra of complexes **3.5**-**3.15** provides strong evidence for the synthesis of the proposed complexes.

For complexes **3.5**-**3.7**, the most shielded methylene protons of the propyl chain were observed as a multiplet (δ_H 1.7-2.2 ppm, Figure 3.6), as opposed to the two multiplets observed in **2.5**-**2.7**. A similar phenomenon was observed in the spectra of **3.11** and **3.13**. Overlap of the upper cage PTA proton resonances and the methylene protons adjacent to the imine group was observed. A loss of the AB-spin system was observed for the lower cage proton resonances (signals 6 and 7, Figure 3.3), suggesting coordination of the PTA moiety to the metal (A, Figure 3.7). The aromatic signals of the PTA scaffold (**3.1**) split into an array of signals in the complexes (B, Figure 3.7), further supporting the proposed structures. In the ^{13}C{^{1}H} NMR spectra, a downfield shift

of the imine proton resonance was observed from ≈ δ_C 165 ppm to ≈ 169 ppm. In contrast to **3.1**, three carbon resonances were observed in the spectra of complexes **3.5**-**3.7**, **3.11** and **3.13** for the upper cage of the PTA moiety as opposed to two observed in **3.1**. Signals for the aromatic carbons of **3.1** are observed, with minor changes upon complexation.

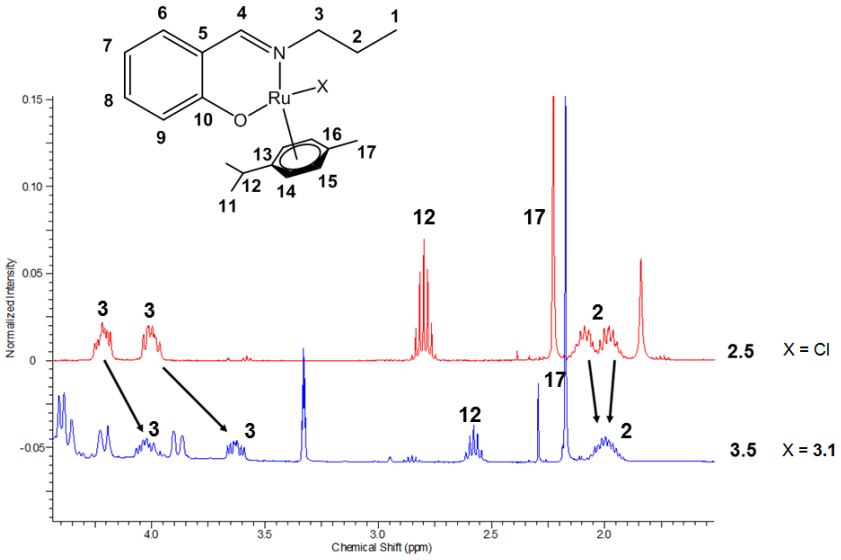

Figure 3.6: ^{1}H NMR spectra of **2.5** and **3.5** emphasising change in the splitting patterns from **2.5** ($CDCl_3$) to **3.5** (CD_3OD-d_4)

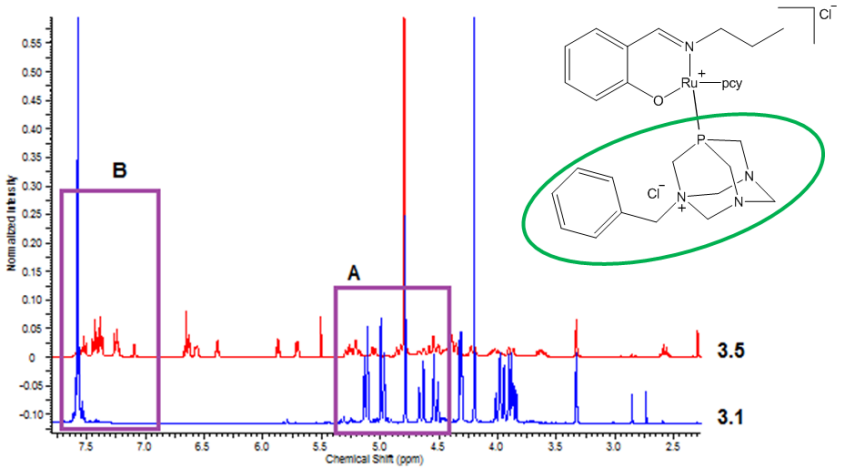

Figure 3.7: ^{1}H NMR spectra comparison of **3.1** (circled in green) and ruthenium propyl PTA complex (**3.5**) in CD_3OD-d_4.

Analysis of the ^{1}H NMR spectra of **3.8**-**3.10** and **3.13**-**3.15** confirmed that the proposed structures were afforded. An upfield shift of the imine resonance was observed

for **3.8-3.10** and **3.13-3.15**. The Cp* proton resonance of complexes **3.9**, **3.10**, **3.14** and **3.15** was observed to be a multiplet, likely due to coupling to the phosphorus, which is observed in literature.[21] Significant overlap of the PTA and ferrocenyl protons are observed in the region of 4.2-4.9 ppm for complexes **3.13-3.15**, and signals were assigned with the aid of 2D NMR techniques. The aromatic protons were observed as 5 multiplets, integrating for 13 protons, which is consistent with the proposed structure. Due to the low solubility of **3.8-3.10** and **3.14-3.15** in common NMR solvents, $^{13}C\{^1H\}$ spectra were not obtained for these compounds.

As observed for compounds **3.2-3.4**, upon reacting with the complexes obtained in Chapter 2 (**2.5-2.11** and **2.13-2.16**), an upfield shift of the phosphorus NMR resonance was observed. Signals for the phosphorus atoms of the ruthenium and iridium complexes were observed as singlets in the region of δ_P -20 to -24 ppm (Figure 3.8) and δ_P -40 to -55 ppm, respectively. The same signals for the rhodium complexes are observed as doublets, as the rhodium centre is spin-active, giving rise to a large coupling constant of 150 Hz. This strongly suggests coordination of the phosphorus atom to the metal centre. A septet integrating for 2P, resonating at δ_P -144 ppm with $^1J_{P-F}$ = 708.8 Hz, is observed in the spectra of **3.8** (Figure 3.8), **3.9**, **3.10**, **3.14** and **3.15** and was assigned to the two PF_6 counterions.

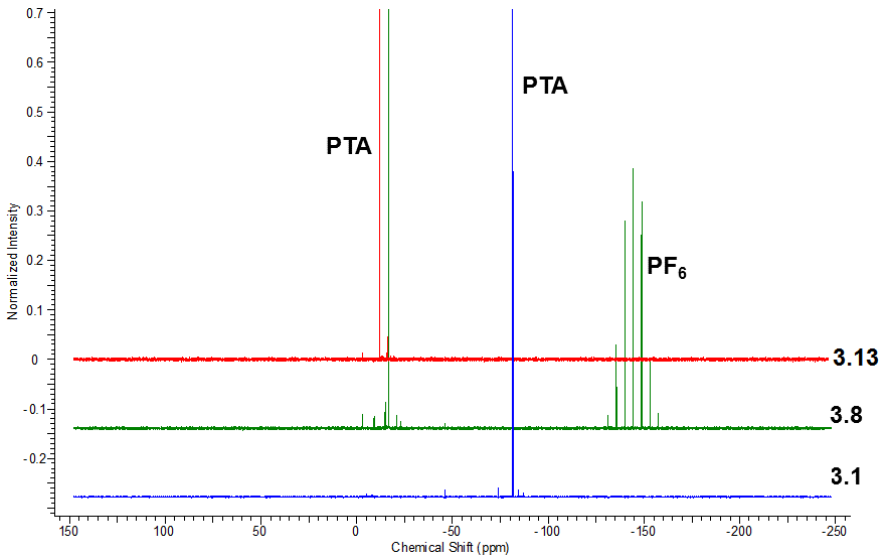

Figure 3.8: $^{31}P\{^1H\}$ NMR spectra comparison of complexes with Cl (**3.13**), PF_6 (**3.8**) counterions and **3.1** in CD_3OD-d_4.

IR Spectroscopy and ESI Mass Spectrometry

Infrared spectroscopy was used to determine the effect of the PTA scaffold on the imine bond character. A shift of ν(C=N) to lower wavenumbers strongly suggests a strengthening of the metal-nitrogen bond, lowering the bond order of the C=N bond. A general trend in a shift towards lower wavenumbers of the imine bands (Figure 3.9) was observed upon substitution of the chlorido ligand with **3.1** (Table 3.1). Charged complexes such as **3.5-3.15** have less electron density on the metal, decreasing the π*-donor capacity of the metal. This increases the δ-donation of the N→M interaction, decreasing the bond order of the C=N bond, thus weakening the bond and resulting in a lower absorption frequency.

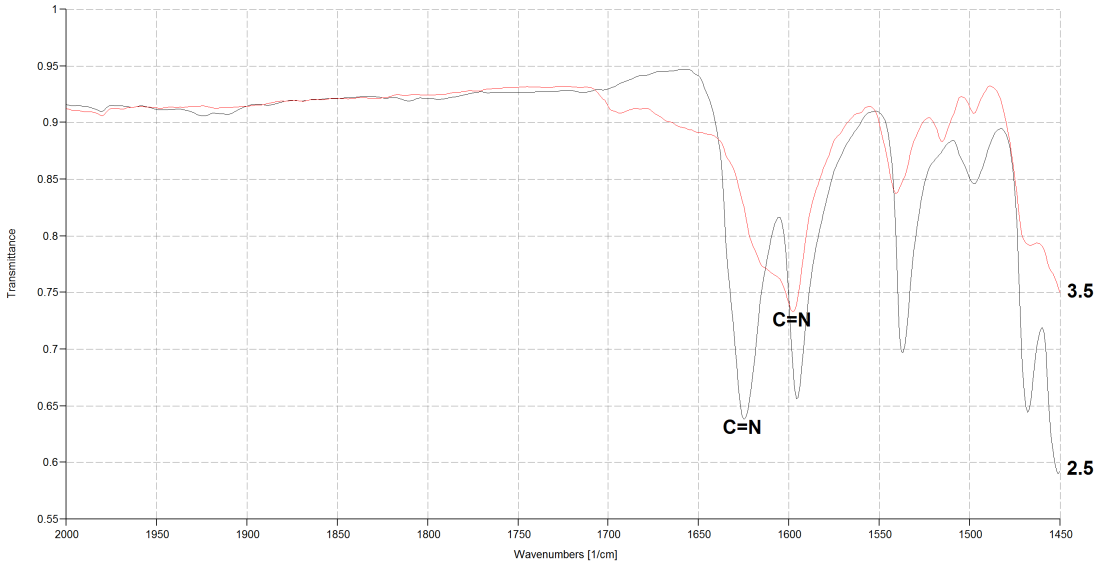

Figure 3.9: IR spectrum comparison of **2.5** and **3.5**, indicating the imine ν(C=N) absorption bands.

The ESI-MS spectra further confirmed that the desired complexes were afforded. Complexes **3.5**, **3.6** and **3.7** were ionised to $[M\text{-}Cl]^+$, with peaks corresponding at m/z 681.2059, 683.2157 and 773.2709, respectively. In the spectrum of **3.11**, a peak of 75% relative intensity at m/z 735.2667 was observed. This corresponds to the loss of both chlorido counterions from the proposed structure, but with addition of a hydroxyl counterion ($[M\text{-}2Cl\text{+}OH]^+$). The chloride salt complexes (**3.5-3.7** and **3.11-3.13**) are hygroscopic and this fragment is likely a product that forms upon contact with at-

Table 3.1: Comparison of ν(C=N) absorption bands for complexes **2.5**-**2.11**, **2.13**-**2.16** and **3.5**-**3.15**.

M-Cl	ν/cm^{-1}	M-PTA	ν/cm^{-1}
2.5	1624	**3.5**	1598
2.6	1627	**3.6**	1619
2.7	1625	**3.7**	1625
2.8	1615	**3.8**	1600
2.9	1603	**3.9**	1599
2.10	1615	**3.10**	1602
2.11	1618	**3.11**	1601
2.13	1619	**3.12**	1607
2.14	1600	**3.13**	1599
2.15	1611	**3.14**	1600
2.16	1618	**3.15**	1601

mospheric moisture. No dihydroxy species were observed in the high resolution mass spectra of these complexes. The ferrocenyl complexes, **3.13**-**3.15**, display peaks corresponding to the loss of both counterions. In the negative mode for complexes **3.8**, **3.9**, **3.10**, **3.14** and **3.15**, a peak at m/z 144.9647 was observed and assigned to the PF_6 counterion. For these complexes, no peak in the region of m/z 35 (Cl^-) was observed, evidence of the successful counterion exchange.

Single crystal X-ray Diffraction

Single crystals of **3.8** were obtained in deuterated methanol in an NMR tube, and the molecular structure of this complex determined (Figure 3.10). Complex **3.8**, like the precursor **2.8**, crystallised in the $P2_1/c$ space group with four molecules observed in each unit cell. A disordered arrangement, with a site occupancy factor less than 1.0, about the *p*-cymene moiety was observed. The geometry around the metal is pseudo-tetrahedral, similarly observed in **2.8**. Minor changes in bond lengths were observed

for the Ru-N and Ru-O bonds (Table 3.2), suggesting that substitution of the chlorido group does not affect the electronics in the bis-chelate to any significant extent. The phosphorus atom of the PTA group of **3.8** is observed to be in a closer proximity to the ruthenium centre than the chlorido atom of **2.8** (2.31Å vs 2.43Å, Table 3.2). Two PF_6 ions are observed to stabilise the overall +2 charge with no chloride ions present; this further confirms a complete ion exchange in the synthesis of **3.8**. A slight lengthening of the Ru-N and C=N bonds are observed from **2.8** to **3.8** (Table 3.2), supporting the conclusion obtained from IR spectroscopic analysis. A small change in the chelation angle (N-Ru-O, Table 3.2) is observed from **2.8** to **3.8**, which suggests the chelate is unaffected by the change in ligand. No interesting crystal structure characteristics were observed. The crystallographic data and structure refinement parameters for complex **3.8** is shown in Table 3.3.

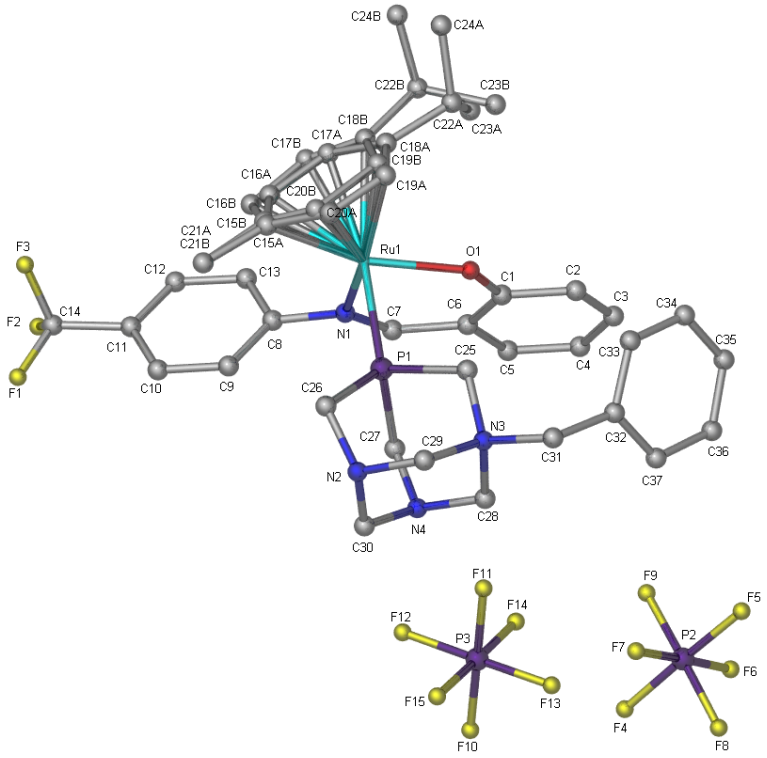

Figure 3.10: Ball and stick representation of the molecular structure of **3.8** determined by single crystal XRD. Hydrogen atoms were omitted for clarity.

Table 3.2: Selected bond distances (Å) and angle (°) comparisons for **2.8** and **3.8**.

	Bond distance (Å)	
Entity	**2.8**	**3.8**
Ru-N	2.088(2)	2.098(3)
Ru-O	2.0594(18)	2.060(3)
Ru-Cl	2.4288(8)	-
Ru-P	-	2.3108(9)
N-C	1.440(3)	1.447(4)
N=C	1.292(3)	1.296(5)
	Bond angle (°)	
N-Ru-O	88.01(7)	88.33(10)
N-Ru-Cl	85.38(6)	-
N-Ru-P	-	88.82(8)
O-Ru-Cl	84.61(5)	-
O-Ru-P	-	81.61(7)

Table 3.3: Crystallographic data and structure refinement parameters for complex **3.8**

Empirical Formula	$C_{37}H_{42}F_3N_4OPRu \cdot 2\,PF_6$
Formula Weight (g·mol^{-1})	1037.73
Temperature (K)	173
Radiation (Å)	0.71073
Crystal System	Monoclinic
Space Group	$P2_1/c$
Unit Cell dimensions	
a (Å)	19.6879(12)
b (Å)	13.8716(8)
c (Å)	17.1161(10)
α (°)	90
β (°)	113.905(1)
γ (°)	90
V (Å^3)	4273.5(4)
Z	4
Density (calc.) (g·cm^{-1})	1.613
$F(000)$	2096
Crystal size (mm)	0.11 x 0.11 x 0.18
$\theta_{min,max}$ (°)	2.0, 26.4
Data set	-24: 24 ; -17: 17 ; -21: 21
Total reflections	61100
Unique reflections	8762
R indices (R_1, wR_2)	0.0416, 0.1053
Res. Dens. (e Å^{-3})$_{min,max}$	-1.10, 1.38

3.4 Cyclic Voltammetry Study

To gain understanding into the electronic effects of the PTA scaffold (**3.1**) on the metal, the electrochemical behaviour of the ferrocenyl PTA complexes (**3.13-3.15**) was examined by cyclic voltammetry. The complexes were analysed in acetonitrile solutions (2-5 mM) using 0.1 M *n*-tetrabutylammonium perchlorate as the background electrolyte. A scan rate of 100 $mV{\cdot}s^{-1}$ was employed with ferrocene used as the external standard. A comparison of the relevant electrochemical data of **2.14-2.16**[22] and **3.13-3.15** is given in Table 3.4. The ferrocene standard exhibited a reversible wave with a half-wave potential of +0.10 V relative to the Ag/Ag^+ reference electrode. The ratio of the anodic and cathodic currents (i_{pa}/i_{pc}) was found to be 0.96, which is close to unity. This reveals that the Fc/Fc^+ couple was a reversible single-electron redox process. This was further confirmed by the value of $\Delta E_p = 0.10$ V, an acceptable value for the peak separation indicating a single electron redox process.

Previously, complexes **2.14-2.16** were analysed by Nkoana *et al.*[22] These complexes demonstrated a reversible single-electron redox wave for the Fc/Fc^+ redox couple. In addition to the Fc/Fc^+ couples, irreversible anodic peak potentials for $Ru^{II} \rightarrow Ru^{III}$, $Rh^{III} \rightarrow Rh^{IV}$ and $Ir^{III} \rightarrow Ir^{IV}$ were observed in the region of 0.6 to 0.8 V. A loss of the Fc/Fc^+ couples was observed in the voltammograms after substitution of the Cl ligand for the alkylated benzyl PTA scaffold **3.1** (complexes **3.13-3.15**). Two oxidation peak potentials were observed in the voltammogram of **3.13**, at 0.73 V and 0.93 V, with no corresponding ferrocenium reduction on the return scan. Similarly for complex **3.15**, two irreversible oxidation peaks were observed at -0.13 V and 0.36 V when scanning from -1.2 V and 1.5 V (**A**, Figure 3.11). However, changing the scan range to -1.2 V to 0.7 V, a reversible Fc/Fc^+ wave with half-potential of 0.32 V was observed (**B**, Figure 3.11). As observed for the ferrocene standard, an i_{pa}/i_{pc} value close to unity confirmed a reversible redox wave. The change in scan range suggests that once the complex undergoes oxidative stress above a potential of 0.7 V, an additional oxidation product is formed which cannot be reduced (i.e. product is unstable). No additional studies have been done to characterise the unstable species further.

Complex **3.14** was observed to be unstable in the acetonitrile solution and was monitored using peak potentials over a period of 60 minutes at 20 minute intervals. Two oxidative peaks (**a** and **b**, Figure 3.12) were observed in a similar potential range to **3.13** and **3.15**. After 20 minutes in the acetonitrile solution these two peaks shifted closer to each other (**B**, Figure 3.12). Overlap of the two peak potentials after 40 minutes in the acetonitrile solution (**ab**, **C**, Figure 3.12) was observed. These temporal changes in the results suggest decomposition of the complex in the acetonitrile solution.

Based on this result, it can be concluded that substituting the chloride ligand with the alkylated benzyl PTA scaffold (**3.1**) interferes with the reversible single-electron redox processes of the Fc/Fc^+ couple.

Table 3.4: Redox potentials (V vs. Ag/Ag^+) of compounds **2.14-2.16** from Nkoana *et al.*,[22] compounds **3.13-3.15** analysed in this study and ferrocene (Fc)[a] as the standard.

	Fe(II)/Fe(III)					**Other**
Comp.	E_{pa}	E_{pc}	$E^b_{1/2}$	$\Delta E^c_{1/2}$	i_{pc}/i_{pa}	E_{pa}
2.14	0.36	0.28	0.32	0.19	1.43	0.65
2.15	0.35	0.25	0.30	0.17	1.43	0.77
2.16	0.35	0.27	0.31	0.18	1.17	0.72
3.13	0.73	-	-	-	-	0.93
3.14[d]	-0.04	-	-	-	-	0.64
3.15	0.36	0.28	0.32	0.22	0.96	-0.13
Fc	0.15	0.05	0.10	0.00	0.96	-

[a] Measured in acetonitrile at a scan rate of 100 mV/s and referenced to Ag/Ag^+.

[b] $E_{1/2} = \frac{E_{pa} + E_{pc}}{2}$. [c] $\Delta E_{1/2} = E_{1/2}(Comp.) - E_{1/2}(Fc)$.[d] Initial scan results.

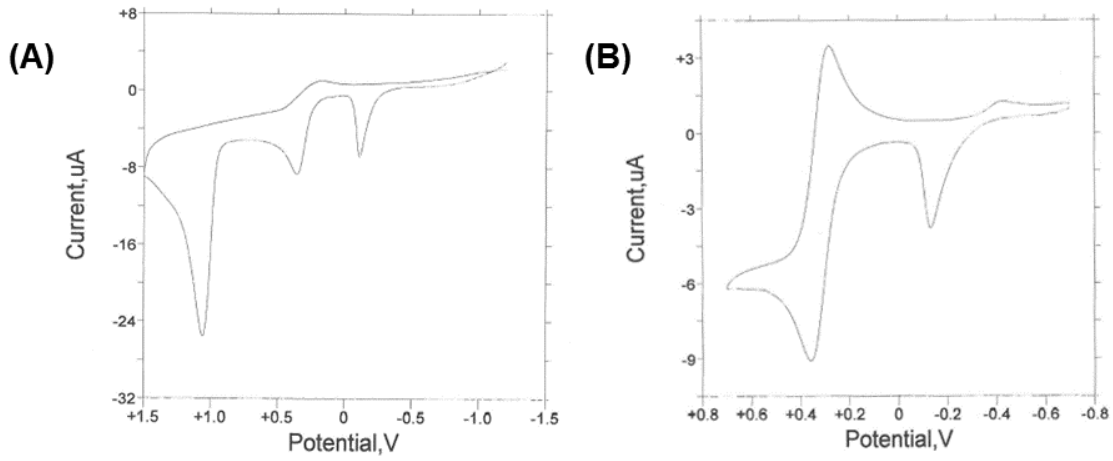

Figure 3.11: Voltammograms of **3.15** with the scanning potential range of -1.2 to 1.5 V (**A**) and -1.2 to 0.7 V (**B**).

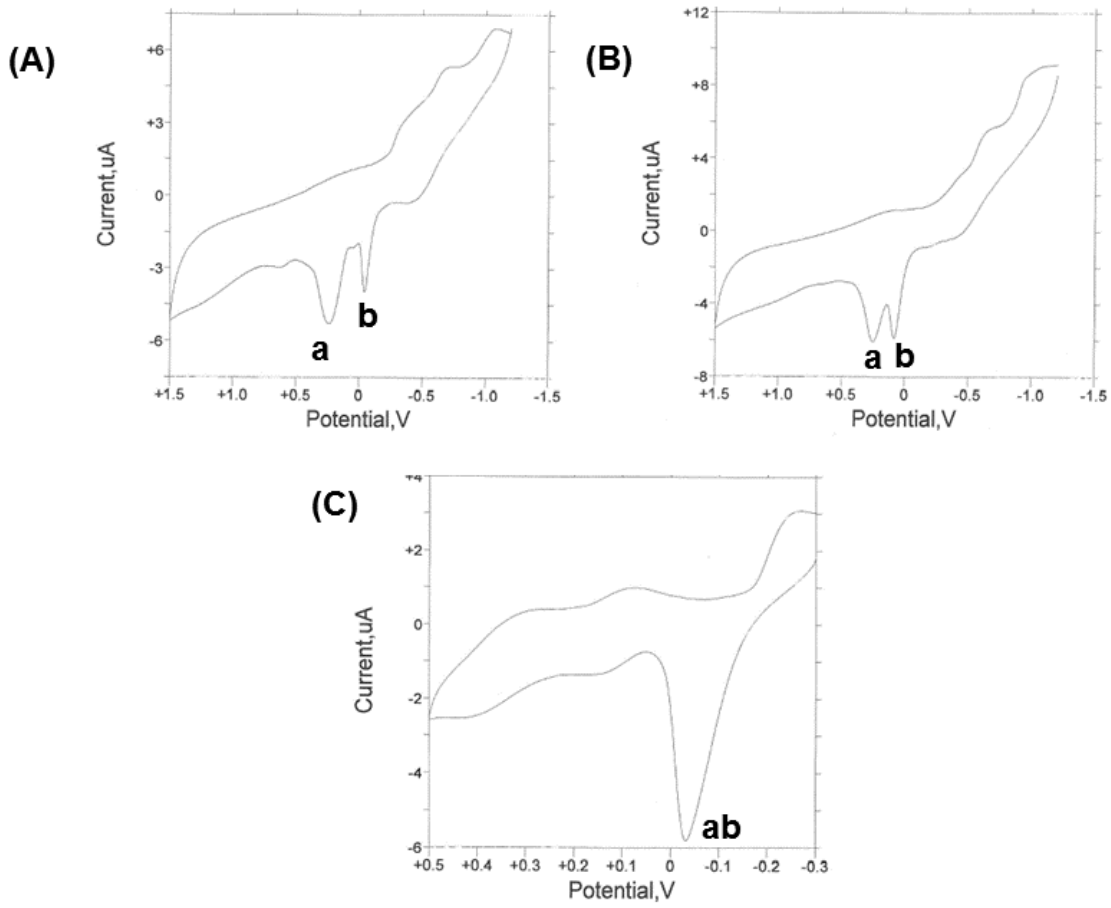

Figure 3.12: Voltammograms of **3.14** at 20 (**B**) and 40 (**C**) minute intervals from the initial sampling at **(A)**.

3.5 Summary

An alkylated PTA scaffold, **3.1**, was prepared, characterised and reacted with dimeric metal precursors, complexes **2.5-2.11** and **2.13-2.16**, to yield complexes **3.2-3.15**. Compounds were characterised using NMR (^{1}H, ^{13}C{^{1}H}, ^{31}P{^{1}H}, HSQC, COSY) and IR spectroscopies, elemental analysis, and high resolution electrospray ionisation (positive-ion and negative-ion modes) mass spectrometry. The spectroscopic and analytical data obtained for complexes **3.1-3.4** correspond well with the literature.[17] Complexes **3.5-3.15** are new compounds and their characterisation data are consistent with the proposed structures. Single crystals of **3.8** were analysed by X-ray diffraction, which further confirmed its molecular structure. Cyclic voltammetry studies revealed no reversible single-electron redox process for the Fc/Fc^{+} couple of complexes **3.13-3.15** when tested under the same conditions as the non-PTA analogues (**2.14-2.16**). This is in contrast to the non-PTA analogues (**2.14-2.16**) which were shown to have a reversible single-electron Fc/Fc^{+} wave. However, by limiting the scan range (from -1.5 V to +0.7 V), the voltammogram of complex **3.15** revealed a reversible single-electron Fc/Fc^{+} couple, with an i_{pa}/i_{pc} value close to unity.

3.6 References

1. S. Medici, M. Peana, V. M. Nurchi, J. I. Lachowicz, G. Crisponi and M. A. Zoroddu, *Coord. Chem. Rev.*, 2015, **284**, 329–350.
2. N. Muhammad and Z. Guo, *Curr. Opin. Chem. Biol.*, 2014, **19**, 144–153.
3. N. J. Wheate, S. Walker, G. E. Craig and R. Oun, *Dalton Trans.*, 2010, 8113–8127.
4. S. Dhar and S. J. Lippard, *Current Status and Mechanism of Action of Platinum-Based Anticancer Drugs*, Wiley-VCH Verlag GmbH and Co. KGaA, 2011, pp. 79–95.
5. A. Bergamo and G. Sava, *Dalton Trans.*, 2007, 1267–1272.
6. J. Rademaker-Lakhai, D. V. D. Bongard, D. Pluim, J. Beijnen and J. Schellens, *Clin. Cancer Res.*, 2004, **10**, 3717–3727.

7. S. Leijen, S. Burgers, P. Baas, D. Pluim, M. Tibben, E. van Werkhoven, E. Alessio, G. Sava, J. Beijnen and J. Schellens, *Invest. New Drugs*, 2015, **33**, 201–214.

8. C. Hartinger, S. Zorbas-Seifried, M. Jakupec, B. Kynast, H. Zorbas and B. Keppler, *J. Inorg. Biochem.*, 2006, **100**, 891–904.

9. R. Trondl, P. Heffeter, C. Kowol, M. Jakupec, W. Berger and B. Keppler, *Chem. Sci.*, 2014, **5**, 2925–2932.

10. C. Allardyce, P. Dyson, D. Ellis and S. Heath, *Chem. Commun.*, 2001, 1396–1397.

11. C. Scolaro, A. Bergamo, L. Brescacin, R. Delfino, M. Cocchietto, G. Laurenczy, T. Geldbach, G. Sava and P. Dyson, *J. Med. Chem.*, 2005, **48**, 4161–4171.

12. R. Pettinari, F. Marchetti, F. Condello, C. Pettinari, G. Lupidi, R. Scopelliti, S. Mukhopadhyay, T. Riedel and P. J. Dyson, *Organometallics*, 2014, **33**, 3709–3715.

13. A. Weiss, R. H. Berndsen, M. Dubois, C. Muller, R. Schibli, A. W. Griffioen, P. J. Dyson and P. Nowak-Sliwinska, *Chem. Sci.*, 2014, **5**, 4742–4748.

14. C. Scolaro, T. J. Geldbach, S. Rochat, A. Dorcier, C. Gossens, A. Bergamo, M. Cocchietto, I. Tavernelli, G. Sava, U. Rothlisberger and P. J. Dyson, *Organometallics*, 2006, **25**, 756–765.

15. S. Chatterjee, S. Kundu, A. Bhattacharyya, C. G. Hartinger and P. J. Dyson, *J. Biol. Inorg. Chem.*, 2008, **13**, 1149–1155.

16. C. Scolaro, A. B. Chaplin, C. G. Hartinger, A. Bergamo, M. Cocchietto, B. K. Keppler, G. Sava and P. J. Dyson, *Dalton Trans.*, 2007, 5065–5072.

17. A. R. Burgoyne, C. H. Kaschula, M. I. Parker and G. S. Smith, *Eur. J. Inorg. Chem.*, 2016, 1267–1273.

18. Z. Adhireksan, G. E. Davey, P. Campomanes, M. Groessl, C. M. Clavel, H. Yu, A. A. Nazarov, C. H. F. Yeo, W. H. Ang, P. Dröge, U. Rothlisberger, P. J. Dyson and C. A. Davey, *Nat. Commun.*, 2014, **5**, 3462–3474.

19. F. Caruso, M. Rossi, A. Benson, C. Opazo, D. Freedman, E. Monti, M. B. Gari-

boldi, J. Shaulky, F. Marchetti, R. Pettinari and C. Pettinari, *J. Med. Chem.*, 2012, **55**, 1072–1081.

20. R. Pettinari, F. Marchetti, C. Pettinari, F. Condello, A. Petrini, R. Scopelliti, T. Riedel and P. J. Dyson, *Dalton Trans.*, 2015, **44**, 20523–20531.

21. M. Erlandsson, V. R. Landaeta, L. Gonsalvi, M. Peruzzini, A. D. Phillips, P. J. Dyson and G. Laurenczy, *Eur. J. Inorg. Chem.*, 2008, 620–627.

22. W. Nkoana, D. Nyoni, P. Chellan, T. Stringer, D. Taylor, P. J. Smith, A. T. Hutton and G. S. Smith, *J. Organomet. Chem.*, 2014, **752**, 67–75.

Chapter 4

Preliminary Cytotoxic Evaluation and Mechanistic Insights

4.1 Introduction

Platinum group metal complexes have shown in recent years to be more favourable to use over the current platinum-based complexes used in cancer treatments.[1–4] Platinum-based drugs often exhibit potent cytotoxicity against cancer cells, but also against non-cancerous cells.[5] Recently less toxic metals and ligands have been used as alternatives to the more toxic platinum complexes.[6,7] Finding the balance between highly cytotoxic behaviour in cancerous cells and lower toxicity in non-cancerous cells is imperative for future drug development. Since the discovery of RAPTA by Dyson and co-workers,[8] derivatives of these complexes have shown great promise because some analogues show increased activity compared to RAPTA.[9,10] The prototype RAPTA-C exhibited high IC_{50} values (> 200 μM) for the inhibition of glutathione-S-transferase (GST), an enzyme responsible for conferring resistance to anticancer drugs.[11] However, due to the low cytotoxicity of the complex against non-cancerous cells, the RAPTA-C moiety has been incorporated into active compounds.[10]

One of the drug targets extensively studied with respect to ruthenium complexes, is DNA. In addition to DNA, ruthenium complexes also interact with other biological materials.[12] Ruthenium protein interactions have been considered as a potential pathway

to the treatment of cancer.[13] Recent studies have suggested this binding is essential for the antimetastatic behaviour of ruthenium complexes.[14] Inhibition of proteins, such as cathepsin B, GSK-3 and Pim-1 have also been investigated and shown to follow this pathway.[15,16] A high concentration of these proteins are present in tumours, making them more favourable targets rather than DNA.[15] To assist in the binding of metals to these proteins, researchers have used functional ligands as a method to achieve this.[13,17]

In the preceding chapters, the synthesis of non-PTA and PTA complexes were reported. This chapter investigates the anticancer activity of these two families of complexes as the results could give insight into whether incorporation of the alkylated benzyl PTA ligand **3.1** is beneficial to enhance cytotoxicity.

4.2 Single Dose Pre-screening

To identify the most active complexes, all of the metal complexes synthesised in this study were pre-screened for cytotoxicity in the MCF7 carcinoma breast cancer cell line at a single-dose concentration of 20 μM. This concentration was chosen based on the National Cancer Institute (NCI, USA) criteria which regard compounds with $IC_{50} \leq 20$ μg/mL ($\simeq 18$ μM for the complex with the largest molecular mass synthesised) as having high inhibiting activity.[18] Cisplatin was used as the positive control in this study. To compare the cytotoxicity at the tested concentration, cell viability was determined using the MTT assay protocol.[19] MTT, 3-(4,5-dimethylthiazol-2-yl)-2,5-diphenyltetrazolium bromide (yellow solution), is a tetrazolium reagent that gets reduced to a formazan, 3-(4,5-dimethylthiazol-2-yl)-2,5-diphenylformazan (blue crystal) by dehydrogenases of live cells (Figure 4.1).[20] After solubilisation of the formazan, the concentration of living cells can be determined by measuring the absorbance at 550 nm.[20]

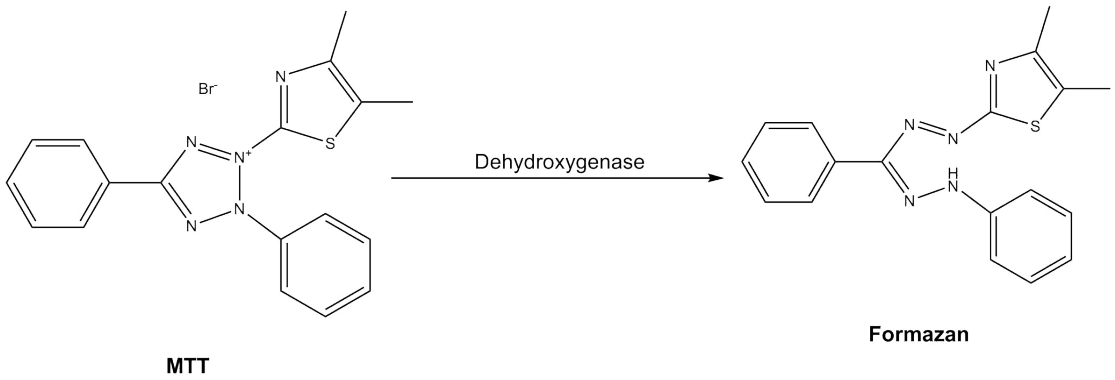

Figure 4.1: Conversion of MTT (3-(4,5-dimethylthiazol-2-yl)-2,5-diphenyltetrazolium bromide) to Formazan (3-(4,5-dimethylthiazol-2-yl)-2,5-diphenylformazan).

4.2.1 Cytotoxicity of Metal dimers and Precursors 2.5-2.16

The anticancer data obtained for complexes **2.5-2.16** are illustrated in Figure 4.2. In general, the ruthenium (**2.8**, **2.11** and **2.14**) and iridium complexes (**2.10** and **2.16**) showed greater activity than their rhodium (**2.9**, **2.12** and **2.15**) counterparts. With the exception of **2.12**, **2.14** and **2.15**, all of the complexes were found to be more active than the metal dimers (RuD, RhD and IrD). This provides evidence that the addition of the salicylaldimine group increases the cytotoxicity. Four complexes (**2.8**, **2.10**, **2.11** and **2.16**) displayed greater cytotoxicity than cisplatin at 20 μM against MCF7 cells, with the most active complex being **2.8**. In general, complexes bearing the trifluoromethane (**2.2**) and trimethylsilane (**2.3**) substructure were more active than complexes with the propyl (**2.1**) and ferrocenyl (**2.4**) salicylaldimine ligand. Compounds **2.2** and **2.3** both have higher ClogP values in comparison to **2.1** and **2.4** (Table 4.1), suggesting the cytotoxicity is linked to the degree of lipophilicity. Since complexes **2.8**, **2.10** and **2.11** showed promise in the pre-screen, these complexes were taken further to a multi-dose screen (see section **4.3**) to determine their IC_{50} values.

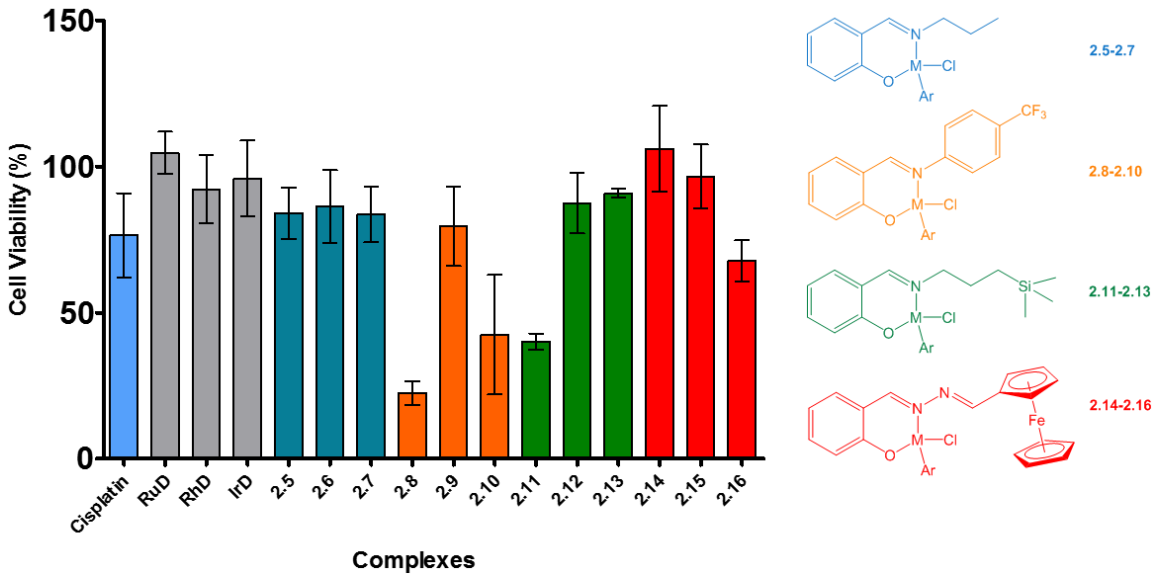

Figure 4.2: Cell viability was measured after MCF7 cells were treated with 20 μM of the non-PTA complexes **2.5-2.16** and the metal dimers RuD ([RuCl(μ-Cl)(*p*-cymene)]$_2$), RhD ([RhCl(μ-Cl)(Cp*)]$_2$) and IrD ([IrCl(μ-Cl)(Cp*)]$_2$) and determined using the MTT assay.

Table 4.1: Predicted values of ClogP[a]

Compound	ClogP
2.1	2.50
2.2	4.42
2.3	3.89
2.4	3.33[b]

[a] LogP values were calculated using MarvinSketch V5.9.4. [b] Predicted value using method described in Stringer *et. al.*[21]

4.2.2 Cytotoxicity of the PTA scaffold (3.1) and PTA complexes (3.1-3.15)

Compounds **3.1-3.4** showed little to no activity against MCF7 cells at the tested concentration. As these compounds are water soluble, a pre-screen of **3.1-3.4** was done in medium only (no DMSO was used to solubilise the compounds) with little change to

the data obtained when DMSO was used to solubilise the compound (Figure 4.3). This data shows that there is very little effect on the cell viability when DMSO was used in the assay. In order to compare the results of that obtained for compounds **2.5-2.16**, all of the biological studies for compounds **3.1-3.15** were performed using DMSO to solubilise the compounds. The data for complexes **3.1-3.15** are given in Figure 4.4. Complexes **3.2-3.15** were found to be less active than the non-PTA complexes at the same concentration (comparing the data in Figure 4.2 and Figure 4.4). These results strongly suggest that addition of the PTA moiety suppresses the activity. This may be due to the high solubility of these compounds in aqueous media which prevents the complex from passing through the cell membrane and preventing intracellular accumulation. As discussed in the previous section, the lipophilicity plays a key role in the activity of the complex. The lipophilicity of the PTA complexes are much lower than the preceding complexes due to the addition of **3.1**, which has a ClogP value of -0.99. Although not as active as their non-PTA counterparts, complexes **3.7** and **3.13** are comparable in activity to cisplatin at the tested concentration, but did not show comparable activity to **2.8**, **2.10** and **2.11** and therefore were not evaluated in the multi-dose screen.

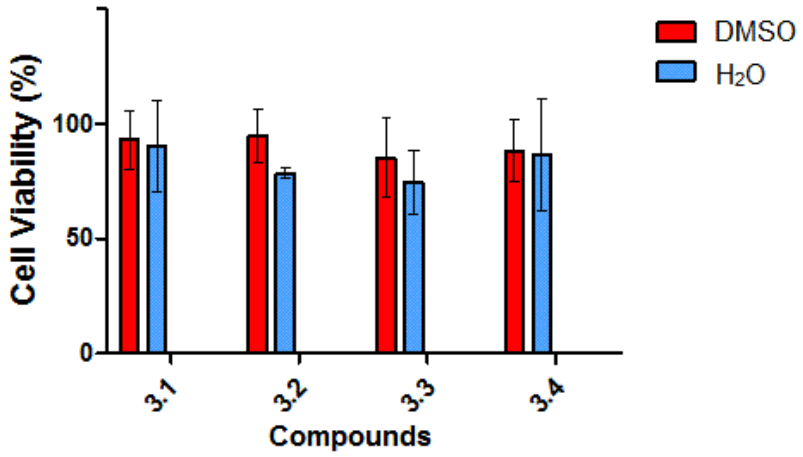

Figure 4.3: Comparison of the effect on MCF7 cell viability of 20 μM of complexes **3.1-3.4** dissolved in either DMSO or H_2O determined using the MTT assay.

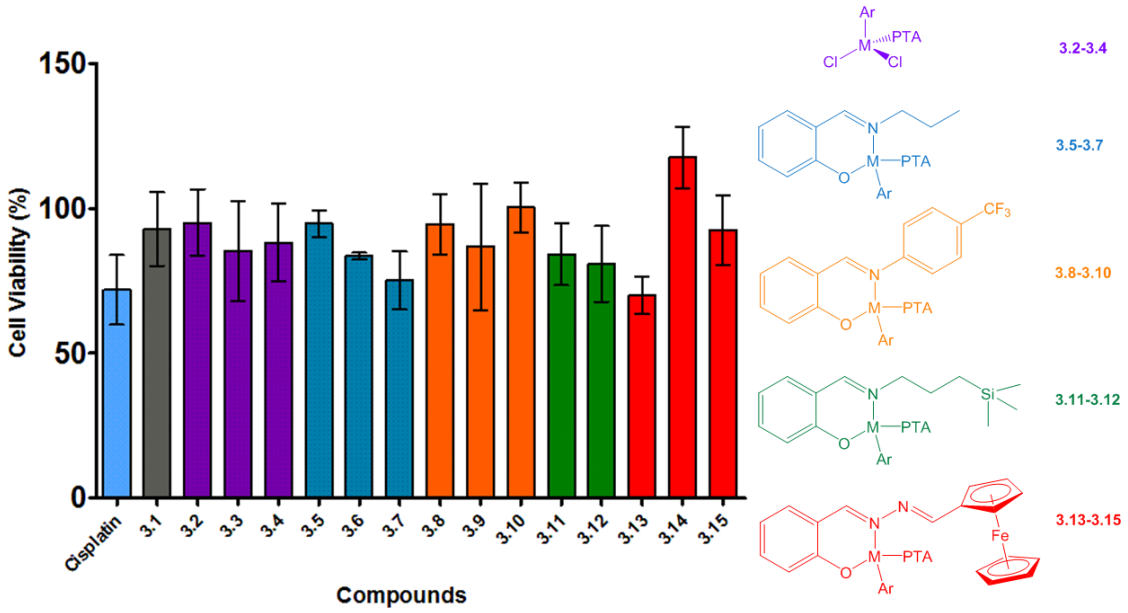

Figure 4.4: Cell viability of MCF7 cells obtained after treatment with PTA complexes **3.1**-**3.15** at 20 μM drug concentration.

4.3 Multi-dose screen of 2.8, 2.10, and 2.11

To determine the IC_{50} values of compounds **2.8**, **2.10** and **2.11** in MCF7 breast cancer cells, a multi-dose screen was conducted at 5, 10, 15, 20 and 25 μM concentrations. The experiments were performed on three different occasions in quadruplicate and the dose response curves and IC_{50} values are represented in Figure 4.5 and Table 4.2, respectively. As observed in the pre-screen, **2.8** was the most active complex, with an IC_{50} value of 16.83 μM. Changing from the ruthenium *p*-cymene (**2.8**) to iridium Cp* (**2.10**) moiety results in an IC_{50} of 20.75 μM. This suggests that the metal fragment plays an important role in the cytotoxicity exhibited in MCF7 cells. In changing the ligand from trifluoromethane (**2.8**) to trimethylsilane (**2.11**) in the ruthenium complexes, a slight drop in cytotoxicity was also observed (16.83 to 19.48 μM, respectively). The increase in cytotoxicity observed for **2.8** is consistent with reports that fluorine containing compounds show great promise as anticancer agents.[22] Compound **2.8** bears the ligand with the greatest ClogP value (**2.2**, see Table 4.1), which could suggest greater accumulation in the cells and therefore more interaction with intracellular targets. To evaluate their selectivity, the compounds were also tested against non-cancerous Chi-

nese hamster ovarian (CHO) cells. Complexes **2.10** and **2.11** showed lower toxicity in the CHO cells than in the MCF7 cell line, with IC_{50} values above 80 μM observed, which is considered to be inactive.[18] Complex **2.8** was found to be more active in the CHO cells (IC_{50} = 5.67 μM) than in the MCF7 cells (IC_{50} = 16.83 μM). Calculating the selectivity index (SI) of these complexes can give insight into which cell line the complex has greater selectivity to inhibit growth. The selectivity index shows that complex **2.8** has a greater selectivity for non-tumorous cells (SI = 0.34). This suggests that complex **2.8** may not be a suitable candidate for further testing as a potential anticancer drug. Larger selectivity indices were obtained for complexes **2.10** and **2.11** (SI > 4), suggesting that these complexes may be more selective towards cancerous cells and maybe be potential candidates for further testing.

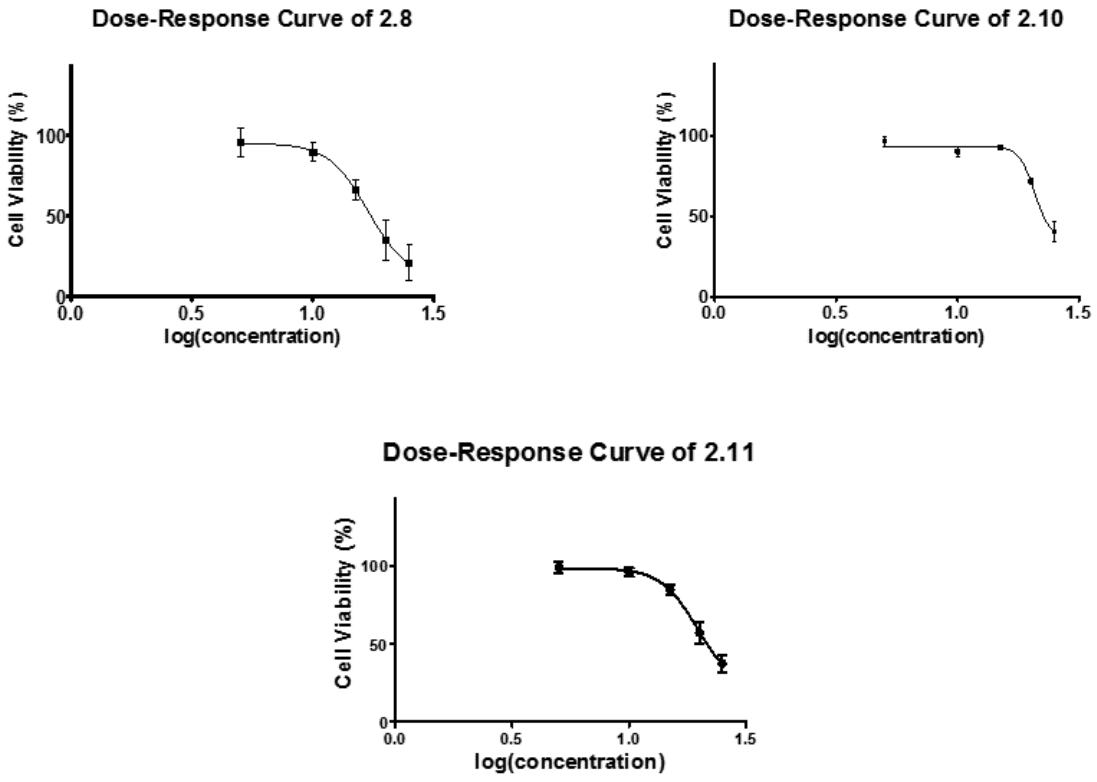

Figure 4.5: Dose-response curves of cell viability obtained by MTT assays for MCF7 cells treated with complexes **2.8**, **2.10** and **2.11**.

Table 4.2: IC_{50} values (with standard error (SE)) and selectivity indices (SI) of **2.8**, **2.10** and **2.11** against the MCF7 breast cancer cell line and the Chinese hamster ovarian (CHO) cell line.

Complex	**MCF7 (IC_{50}±SE, μM)**	**CHO (IC_{50}±SE, μM)**	**SI**[a]
2.8	16.83 ± 1.17	5.67 ± 0.59	0.34
2.10	20.75 ± 1.32	95.71 ± 6.05	4.61
2.11	19.48 ± 1.25	84.00 ± 17.70	4.31

[a]Selectivity Index: IC_{50}-CHO/IC_{50}-MCF7.

4.4 Stability and Insight into the Mechanism of Action

Determining the stability of compounds in blood and aqueous media is important for identifying potential drug candidates.[23] The stability of all biologically active compounds should be investigated in order to elucidate the reason for their activity. In some cases the candidate breaks down (depending on the environment) resulting in the formation of an active complex. In other cases the compound remains intact.[24] Two of the most active complexes in the pre-screen (**2.8** and **2.10**) were monitored using ^{1}H NMR spectroscopy in DMSO-d_6 for 48 hours at 37 °C (MTT assay temperature). To gain insight into the possible species found in media and serum, compounds were monitored in a mixture of 1:1 v/v % DMSO-d_6:H_2O and 150 mM NaCl(aq) in DMSO-d_6 (1:1 v/v % DMSO:H_2O) under the same conditions.[25] The reason for monitoring the effect of having NaCl present at high concentrations is to minimise any hydrolysis from occurring. As the most active complex against both the MCF7 and CHO cell lines was **2.8**, its interaction with guanosine 5′-monophosphate disodium salt hydrate (GMP), a RNA monomer, was monitored by ^{1}H NMR spectroscopy in a 1:1 v/v % DMSO-d_6:H_2O mixture.

4.4.1 Solvent Stability

The stability of complex **2.8** was investigated by ^{1}H NMR spectroscopy in DMSO-d_6 to simulate the chemical environment prior to cell viability studies. The ^{1}H NMR spectrum shows after 24 hours, the formation of a new species (0 to 24 hrs, Figure 4.6). Signals for the salicylaldimine group (signals 8-11 and 13, Figure 4.6) are observed to double up, evidence that a new species had formed. After 24 hours, the imine resonance of **2.8** (6, Figure 4.6) was observed as two signals. No significant change from 24 to 48 hours was observed, suggesting the formation of the new species had reached equilibrium with **2.8** within 24 hours. In contrast to the ruthenium case, **2.10** showed greater stability in DMSO-d_6 under these conditions. The stacked ^{1}H NMR spectra of **2.10** in DMSO-d_6 at 24 hour intervals are shown in Figure 4.7. No additional signals were observed within the 48 hour testing period (Figure 4.6). Integration of the signals after 48 hours in DMSO for **2.10** (Figure 4.7) is consistent with the reported data in Chapters 2 and 6 (i.e. no decomposition observed).

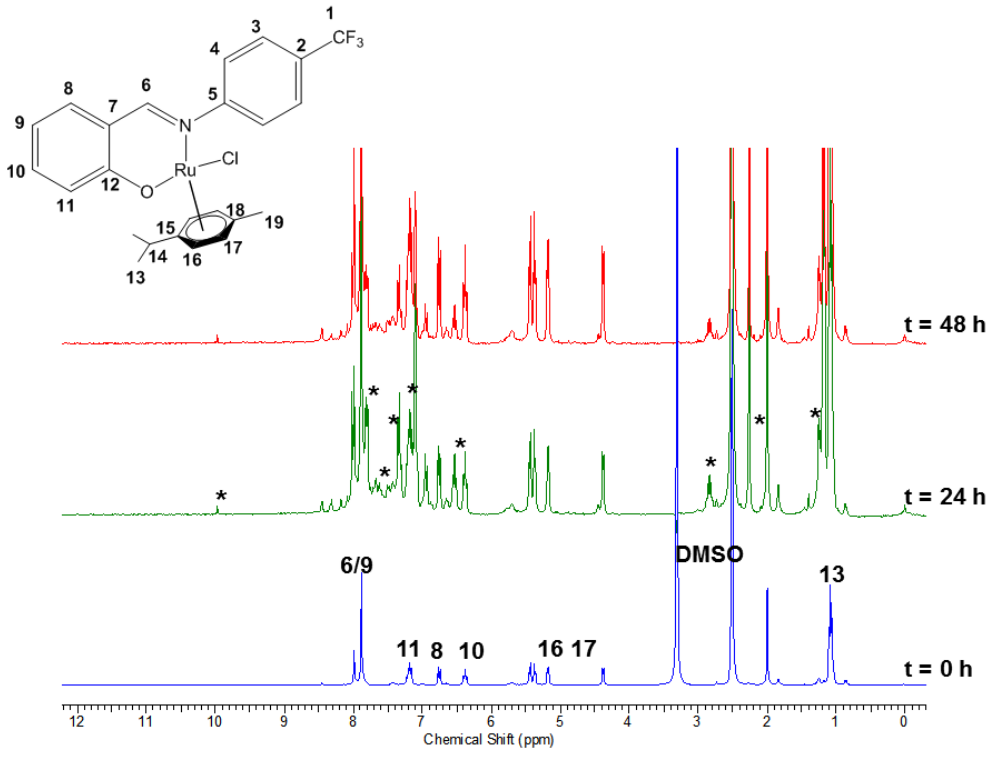

Figure 4.6: ^{1}H NMR spectra comparison of **2.8** over a 48 hour period in DMSO-d_6 sampling taken at 24 hour intervals. Signals labelled with an $*$ are from the new species formed during the experiment.

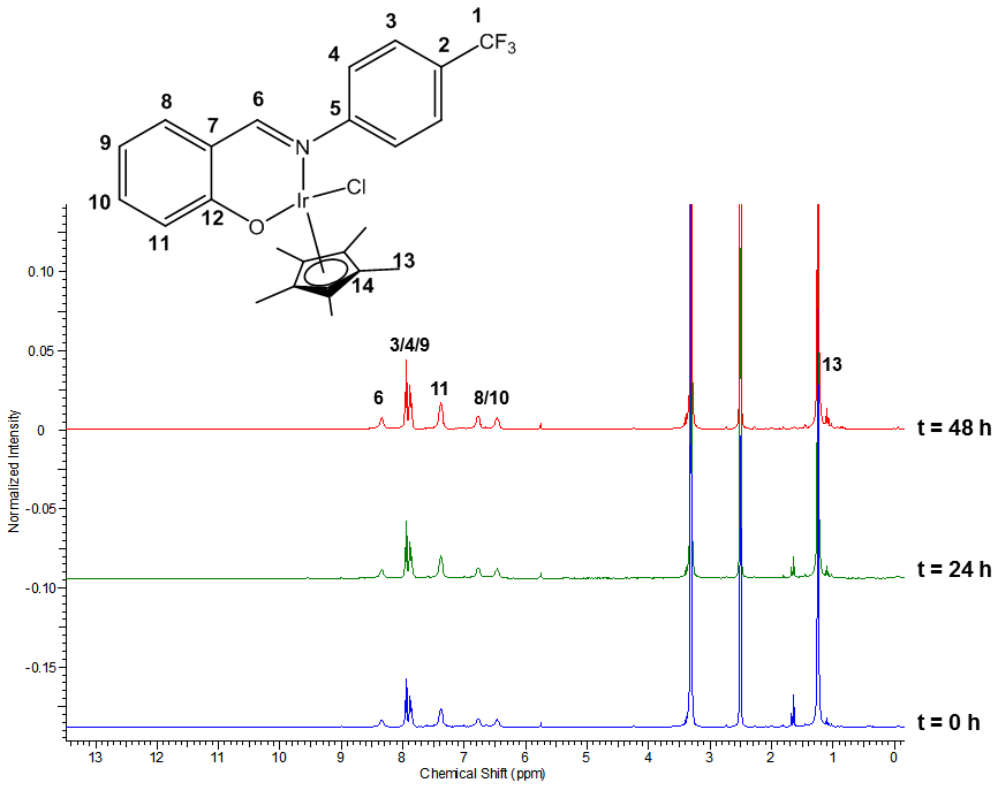

Figure 4.7: ^{1}H NMR spectra comparison of **2.10** over a 48 hour period in DMSO-d_6 sampling taken at 24 hour intervals.

The results obtained in this study suggests that the ruthenium complex (**2.8**) undergoes solvation and the resulting complex might be responsible for the cytotoxicity observed in the MTT assay. Contrast to this, the iridium complex (**2.10**) does not undergo solvation (remains intact) which suggest that this complex is possibly generating the cytotoxicity observed.

4.4.2 Aqueous Stability

The behaviour of the afore-mentioned complexes were also studied in partial aqueous solutions to mimic biological conditions. NaCl was used to mimic the salt concentration outside of cells in the body.[25] Complex **2.8** was analysed for its aqueous stability. A shift in the imine resonance was observed when both a high concentration of H_2O and NaCl is present (signal 6, Figure 4.8), suggesting there is a change in the species present in solution. Doubling of the aromatic and imine signals (3-11, Figure 4.8) are not observed in the aqueous-media spectra (signals 3-11 of [C] and [D], Figure 4.8),

suggesting the presence of a single species in solution. A downfield shift, as well as a change in the splitting pattern of the *p*-cymene proton resonances (following 13 from A to D, Figure 4.8), is observed which strongly suggests substitution of the labile Cl ligand with DMSO-d_6 or H_2O, as these are high in concentration. Since the biological assay medium contains a range of salts and is mainly constituted of H_2O, there is a high likelihood that the active complex is different to the complex that is initially isolated.

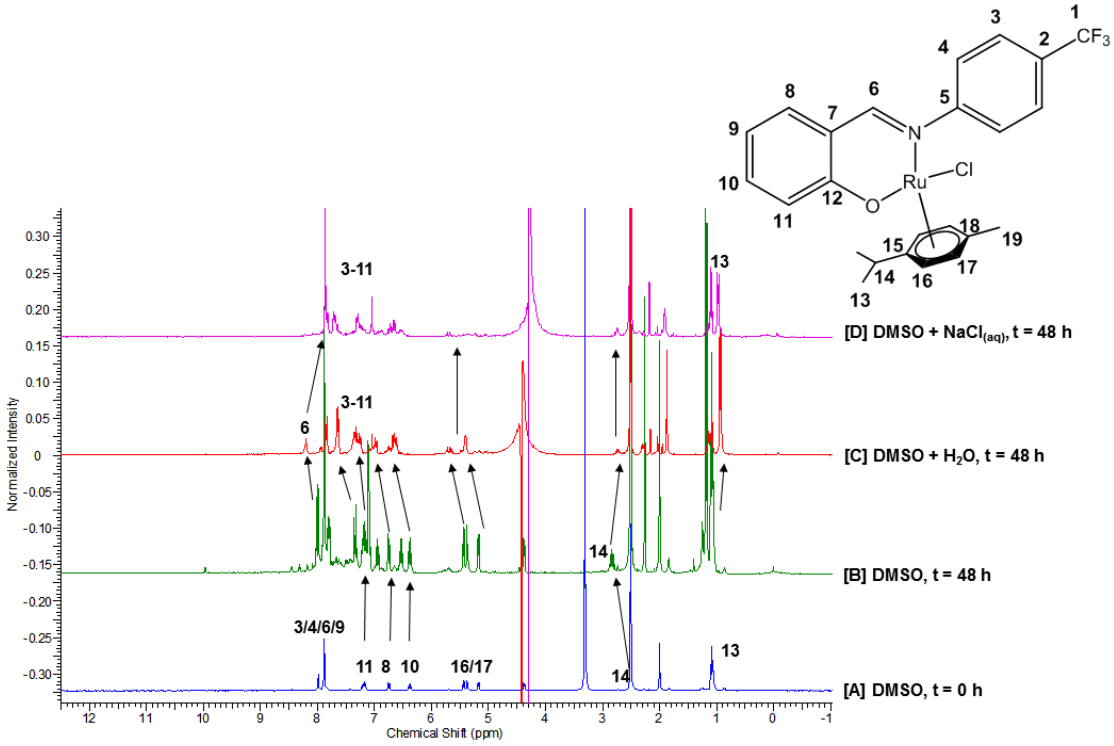

Figure 4.8: ^{1}H NMR spectra comparison of **2.8** at 0 and 48 hours after sample preparation in DMSO-d_6.

Complex **2.10**, though stable in DMSO, was found to form a new species in the different mixtures of DMSO and H_2O. Cleavage of the imine bond was observed when high concentrations of H_2O were present, supported by the appearance of the C**H**O signal in the ^{1}H NMR spectra [C] and [D] (Figure 4.9). The Cp* signal was observed at 1.25 and 1.18 ppm for the DMSO-d_6:H_2O and 150 mM NaCl(aq) samples, respectively, which differs from the DMSO-d_6 sample at 1.23 ppm (signal 13, [B], Figure 4.9). A doublet is observed for the Cp* (signal 13*, Figure 4.9) suggesting that the active species may not be the complex isolated initially.

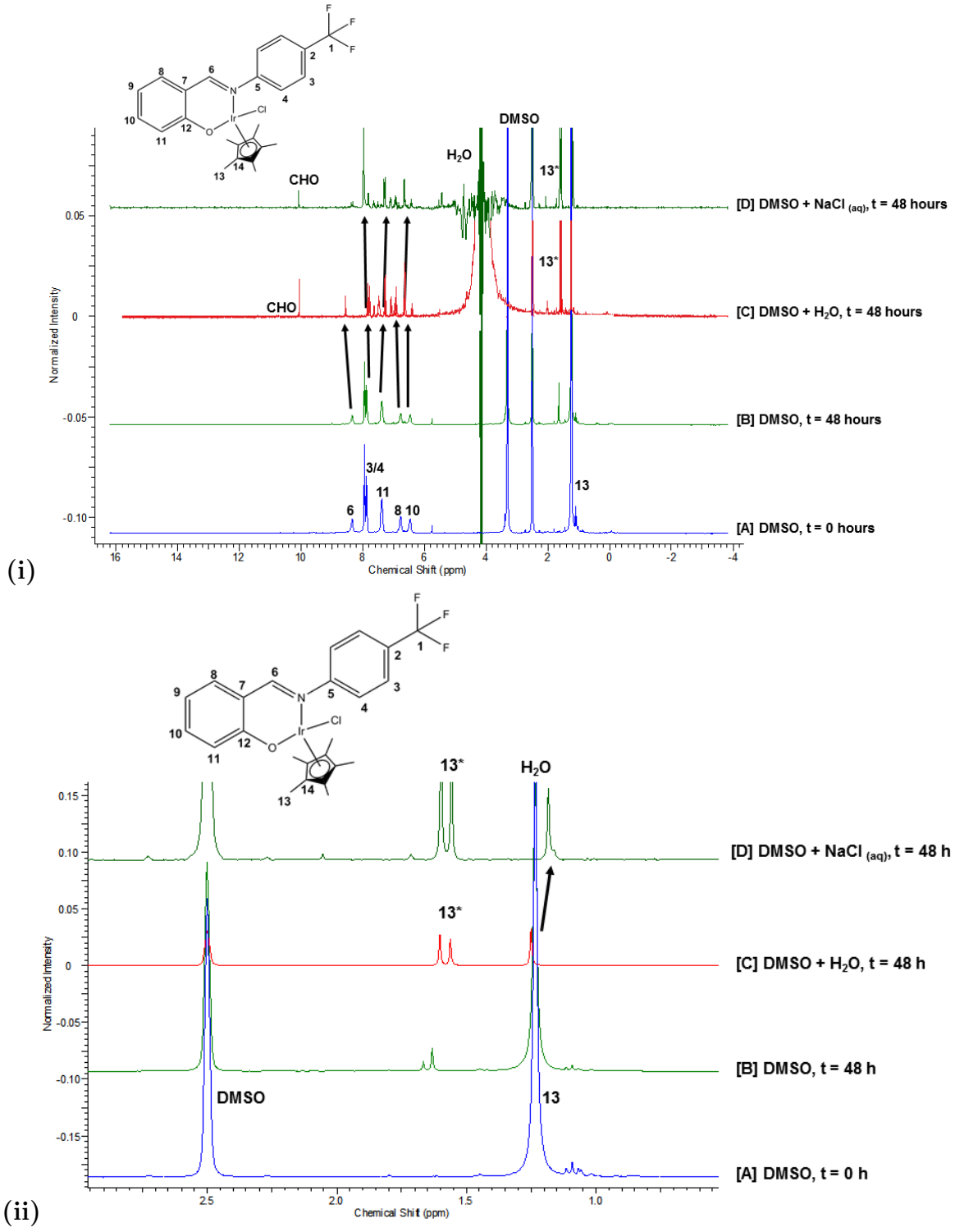

Figure 4.9: **(i)** ^{1}H NMR spectra comparison of **2.10** at 0 and 48 hours after sample preparation in DMSO-d_6 mixtures. **(ii)** Expanded region of **(i)** between 0.0-3.0 ppm.

4.4.3 Binding Study: 5′-GMP with 2.8

Guanosine 5′-monophosphate disodium (5′-GMP) is a simplistic model used to study possible nucleotide interaction of complexes. Complex **2.8**, the most active complex, was reacted with 5′-GMP in a DMSO-d_6:H_2O mixture, at 37 °C over 48 hours, to understand the interactions with RNA/DNA. Free GMP was studied under the same conditions and was observed to have no change from the initial ^{1}H NMR spectrum.

Ruthenium complexes have been reported to bind to single stranded DNA via nitrogen donor atoms from guanosine, in particular the N7 atom.[9,12,26] Complex **2.8** was analysed for its GMP binding affinity using ^{1}H NMR spectroscopy. A distinctive shift in the proton signals of the arene coordinated to the metal centre (signals 13, 14 and 19, Figure 4.10), indicating a change in the metal centre environment. The aqua product of the complex observed in the aqueous stability study (Figure 4.8) was observed in the **2.8**-GMP mixture, however this product is minor (see signals 6 and 13 in Figure 4.10). A shift of the proton resonance at 8.0 ppm (**a**, Figure 4.10) strongly supports the coordination of the complex at the N-7 atom. This result is consistent with the reported shift in the 5′-GMP proton signals for ruthenium-GMP products.[9] This suggests the reason why **2.8** is very active against both cell lines tested, as this mechanism would not be specific to cancerous cells only. The binding of **2.8** and GMP, and the aqua species formed suggests that an aqua species is formed before the nucleotide binds.[9] A similar mechanism is observed for cisplatin[5], which could explain the high levels of toxicity towards healthy cells.

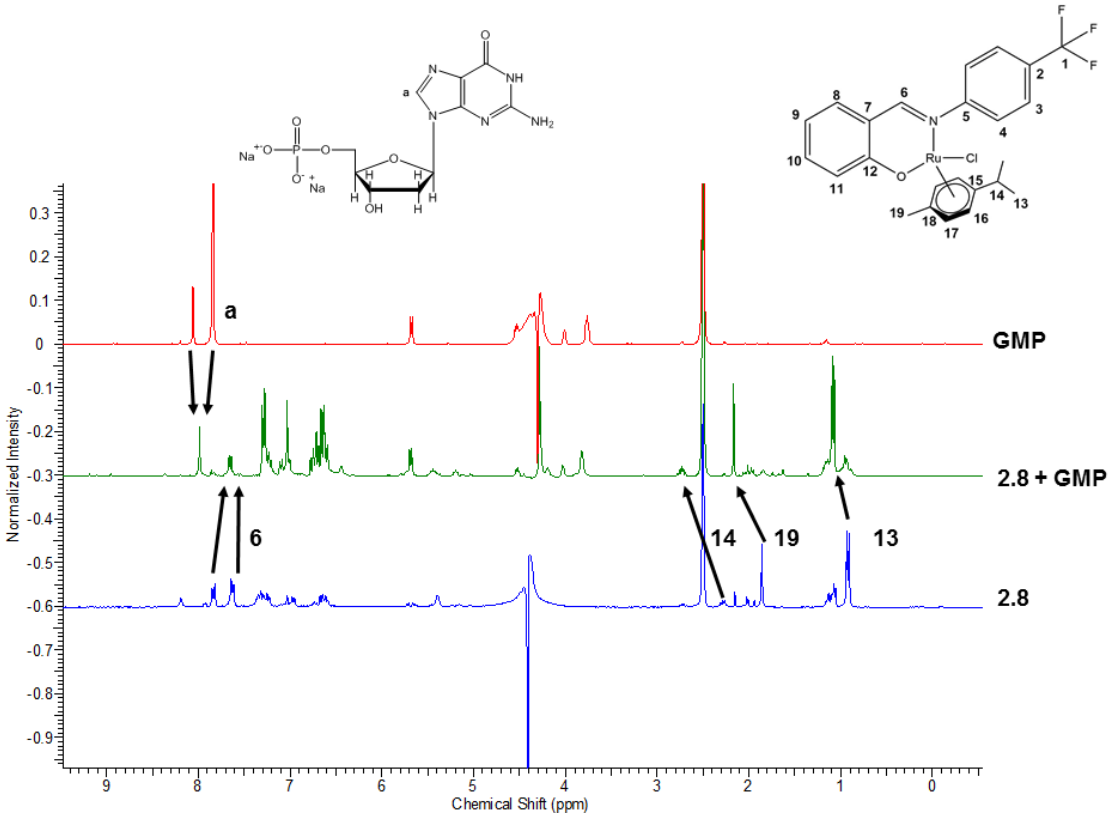

Figure 4.10: ^{1}H NMR spectra comparison of **2.8** and GMP after 48 hours in DMSO:H_2O mixtures.

4.5 Summary

The cytotoxicity of compounds **2.5**-**2.16**, **3.1**-**3.15**, as well as the dimeric metal precursors were evaluated against the MCF7 breast carcinoma cell line. Complexes **2.8**, **2.10** and **2.11** exhibited the highest activity in this cell line, with IC_{50} values of 16.83, 20.75 and 19.48 μM observed, respectively. The activity of these complexes can be linked to the lipophilicity of their ligands. The greater the ClogP value of the ligand of the complex, the greater the cytotoxicity observed. The most active complexes were also evaluated against the Chinese hamster ovarian (CHO) cell line as a representative of normal, healthy cells. Complex **2.8** was highly active against the CHO cells (IC_{50} = 5.67 μM), while the other two complexes (**2.10** and **2.11**) displayed lower toxicity (IC_{50} > 80 μM).

A possible mechanism of action for **2.8** and **2.10** was investigated using ^{1}H NMR spec-

troscopy in DMSO-d_6, DMSO:H_2O and NaCl(aq). Doubling of signals in the spectrum of complex **2.8** suggested low stability in DMSO-d_6, however complex **2.10** was found to be stable. Aqua and DMSO species of **2.8** and **2.10** were observed after 48 hours in DMSO-d_6:H_2O. Complex **2.8** showed evidence of binding to 5′-GMP, suggesting a possible mechanism of action similar to cisplatin and a reason for the cytotoxic behaviour against healthy cells.

4.6 References

1. E. Lukevics, D. Zaruma, J. Ashaks, I. Shestakova, I. Domracheva, V. Bridane and E. Yashchenko, *Chem. Heterocycl. Compd.*, 2009, **45**, 182–187.
2. S. Adhikari, N. R. Palepu, D. Sutradhar, S. L. Shepherd, R. M. Phillips, W. Kaminsky, A. K. Chandra and M. R. Kollipara, *J. Organomet. Chem.*, 2016, **820**, 70–81.
3. J. M. Cross, N. Gallagher, J. H. Gill, M. Jain, A. W. McNeillis, K. L. Rockley, F. H. Tscherny, N. J. Wirszycz, D. S. Yufit and J. W. Walton, *Dalton Trans.*, 2016, **45**, 12807–12813.
4. E. Alessio, *Eur. J. Inorg. Chem.*, 2016, doi: 10.1002/ejic.201600986.
5. J. Reedijk, *Eur. J. Inorg. Chem.*, 2009, 1303–1312.
6. K. D. Mjos and C. Orvig, *Chem. Rev.*, 2014, **114**, 4540–4563.
7. B. Desoize, *Anticancer Res.*, 2004, **24**, 1529–1544.
8. C. Scolaro, A. Bergamo, L. Brescacin, R. Delfino, M. Cocchietto, G. Laurenczy, T. Geldbach, G. Sava and P. Dyson, *J. Med. Chem.*, 2005, **48**, 4161–4171.
9. A. R. Burgoyne, C. H. Kaschula, M. I. Parker and G. S. Smith, *Eur. J. Inorg. Chem.*, 2016, 1267–1273.
10. K. J. Kilpin and P. J. Dyson, *Chem. Sci.*, 2013, **4**, 1410–1419.
11. D. M. Townsend and K. D. Tew, *Oncogene*, 2003, **22**, 7369–7375.
12. C. Scolaro, A. B. Chaplin, C. G. Hartinger, A. Bergamo, M. Cocchietto, B. K. Keppler, G. Sava and P. J. Dyson, *Dalton Trans.*, 2007, 5065–5072.

13. M. V. Babak, S. M. Meier, K. V. M. Huber, J. Reynisson, A. A. Legin, M. A. Jakupec, A. Roller, A. Stukalov, M. Gridling, K. L. Bennett, J. Colinge, W. Berger, P. J. Dyson, G. Superti-Furga, B. K. Keppler and C. G. Hartinger, *Chem. Sci.*, 2015, **6**, 2449–2456.

14. B. Wu, M. S. Ong, M. Groessl, Z. Adhireksan, C. G. Hartinger, P. J. Dyson and C. A. Davey, *Chem. Eur. J.*, 2011, **17**, 3562–3566.

15. A. Casini, C. Gabbiani, F. Sorrentino, M. P. Rigobello, A. Bindoli, T. J. Geldbach, A. Marrone, N. Re, C. G. Hartinger, P. J. Dyson and L. Messori, *J. Med. Chem.*, 2008, **51**, 6773–6781.

16. N. Pagano, J. Maksimoska, H. Bregman, D. S. Williams, R. D. Webster, F. Xue and E. Meggers, *Org. Biomol. Chem.*, 2007, **5**, 1218–1227.

17. Y. Q. Tan, P. J. Dyson and W. H. Ang, *Organometallics*, 2011, **30**, 5965–5971.

18. T. Srisawat, P. Chumkaew, W. Heed-Chim, Y. Sukpondma and K. Kanokwiroon, *Trop. J. Pharm. Res.*, 2013, **12**, 71–76.

19. T. Mosmann, *J. Immunol. Methods*, 1983, **65**, 55–63.

20. G. Abate, A. Aseffa, A. Selassie, S. Goshu, B. Fekade, D. WoldeMeskal and H. Miörner, *J. Clin. Microbiol.*, 2004, **42**, 871–873.

21. T. Stringer, D. Taylor, C. de Kock, H. Guzgay, A. Au, S. H. An, B. Sanchez, R. O'Connor, N. Patel, K. M. Land, P. J. Smith, D. T. Hendricks, T. J. Egan and G. S. Smith, *Eur. J. Med. Chem.*, 2013, **69**, 90–98.

22. C. Isanbor and D. O'Hagan, *J. Fluorine Chem.*, 2006, **127**, 303–319.

23. Y. G. Shin, J. L. Bolton and R. B. van Breemen, *Comb. Chem. High Throughput Screen.*, 2002, **5**, 59–64.

24. D. A. Seleci, M. Seleci, A. Jochums, J.-G. Walter, F. Stahl and T. Scheper, *RSC Adv.*, 2016, **6**, 87910–87918.

25. D. S. Prough and A. Bidani, *Anesthesiology*, 1999, **90**, 1247–1249.

26. A. Dorcier, P. J. Dyson, C. Gossens, U. Rothlisberger, R. Scopelliti and I. Tavernelli, *Organometallics*, 2005, **24**, 2114–2123.

Chapter 5

Conclusion and Future Prospects

5.1 Overall Summary and Conclusions

In this study various salicylaldimine complexes of ruthenium, rhodium and iridium have been synthesised and fully characterised using spectroscopic and analytical techniques such as 1D (^{1}H, ^{13}C{^{1}H}, ^{31}P{^{1}H}) and 2D (COSY, HSQC) NMR spectroscopy, IR spectroscopy and mass spectrometry. Most of the complexes that are reported here have been synthesised for the first time to the best of our knowledge.

In order to afford the complexes, four salicylaldimine ligands (**2.1**-**2.4**) were prepared via a Schiff-base condensation reaction from commercially available reagents. Characterisation of these ligands revealed that the proposed compounds were obtained. These ligands were isolated in high yields. The salicylaldimine ligands were then complexed using [RuCl(μ-Cl)(*p*-cymene)]$_2$, [RhCl(μ-Cl)(Cp*)]$_2$ or [IrCl(μ-Cl)(Cp*)]$_2$ via a bridge-splitting reaction, after deprotonation of the ligand using a suitable base, to yield a series of neutral salicylaldimine PGM complexes (**2.5**-**2.16**). Complexes **2.8**-**2.13** are new and have been fully characterised. The spectroscopic and analytical data revealed that the ligand coordinates to the metal in a *(N,O)*-bidentate fashion. For complexes **2.5**-**2.16** an upfield shift in the imine proton resonance in the ^{1}H NMR spectra from ligand to complex is observed, as well as a downfield shift of the **C**-O-M carbon resonance in the ^{13}C{^{1}H} NMR spectra. A shift of the imine stretching vibration to lower wavenumber further confirmed the *(N,O)*-bidentate coordination mode. Complexation

was further confirmed by the molecular structures obtained for **2.8**-**2.10** using X-ray diffraction. A pseudo-tetrahedral geometry was observed about the metal centre for these complexes, indicative of a piano-stool structure.

Once the neutral complexes had been synthesised, a series of PTA-containing complexes were prepared. Reaction of $[RuCl(\mu\text{-}Cl)(p\text{-cymene})]_2$, $[RhCl(\mu\text{-}Cl)(Cp^*)]_2$, $[IrCl(\mu\text{-}Cl)(Cp^*)]_2$, **2.5**-**2.11** and **2.13**-**2.16** with an alkylated PTA scaffold (**3.1**) afforded complexes **3.2**-**3.15**. Complexes **3.2**-**3.7** and **3.11**-**3.13** were isolated as chloride salts and were observed to be hygroscopic. Complexes **3.8**-**3.10**, **3.14** and **3.15** were isolated as PF_6 salts, since decomposition of the chloride analogues of these complexes was observed. Complexes **3.5**-**3.15** are new compounds and were fully characterised. A significant downfield shift of the phosphorus resonance of the PTA is observed upon coordination to the metal centre, suggesting the synthesis of the target complexes. The molecular structure of **3.8** was obtained and further confirmed the proposed structure. The molecular structure revealed that the phosphorus atom of the PTA scaffold coordinates to the metal centre, and substitutes the chlorido ligand (comparing **2.8** and **3.8**). The molecular structure also shows that the three-legged piano-stool geometry was retained upon complexation with **3.1**.

All of the complexes, as well as **3.1** and the dimeric metal precursors, were screened for potential anticancer activity in MCF7 breast cancer cells *in vitro*. The salicylaldimine complexes **2.8**, **2.10** and **2.11** exhibit enhanced activity in comparison to cisplatin at the 20 μM tested concentration. For multidose screening, IC_{50} values below 21 μM were observed. Compounds containing PTA (**3.1**-**3.15**) and the dimeric precursors did not display good activity at the tested concentration in comparison to cisplatin. Complexes **2.8**, **2.10** and **2.11** were also screened against Chinese hamster ovarian cells (CHO) to gauge selectivity. Complex **2.8** showed cytotoxicity in the CHO cells, suggesting that the complex was not very selective towards cancer cells (SI = 0.34), whereas **2.10** and **2.11** were more selective towards MCF7 (SI > 4). To understand the possible reason for the cytotoxicity, binding studies of **2.8** and a nucleotide, guanosine 5′-monophosphate disodium (5′-GMP) were conducted. Binding of the complex to the nucleotide was observed, suggesting a similar mechanism of action to cisplatin (i.e. it

interacts with the N7 atom of guanine, which is similar in structure to 5′-GMP).

5.2 Future Prospects

Based on our findings in this study, the following adjustments could be made to enhance the biological activity of the complexes reported here.

5.2.1 Further Mechanistic Insights

Compounds **2.8**, **2.10** and **2.11** exhibited good activity and a preliminary investigation into a possible mechanism of action was conducted. The activity observed for some compounds is promising, but certain modifications could be made to increase the potency as well as selectivity. Once promising compounds are afforded, we must understand their interactions with the biomolecules located inside the cells. Additional tests, such as Western-Blot analysis and DNA binding studies, can give additional information of the binding affinity to RNA or DNA. This would also give insight into how the complex interacts (e.g. π-π stacking, coordination) with nucleic acids. Additional studies (e.g. viscosity, UV absorption, DNA denaturing, protein binding) might also give further insights into the mechanism of action. Based on the data obtained from the tests, modification of either the ligand or metal could change or strengthen interactions with biomolecules. Screening against other cancer cell lines (e.g. A2780 and A2780cis, HEK, MDA-MB-231) would give additional information into the biological profile of these complexes, as well as the type of cancer cell lines most susceptible to the complexes.

5.2.2 Modifications to Enhance Activity

The metal appears to have a significant effect on the activity in this study. Most of the rhodium complexes tested exhibited very poor activity in comparison to the ruthenium and iridium complexes. Two of the three most active complexes have a ruthenium

centre; however, **2.8** had low selectivity towards cancerous cells. The iridium complex, **2.10**, exhibits enhanced activity as well as some selectivity towards cancerous cells. This suggests strongly that iridium(III) complexes should be researched in greater depth to determine whether this metal is more effective than others and could present a different approach towards the treatment of this disease.

Some ligand types are observed to show favourable effects on the biological activity of the complexes. Several ligands appear to increase the cellular uptake of the complex, which could allow for better interactions with biomolecules. It was observed in this study that an increase in the lipophilicity of the ligand yielded more potent anticancer activity, as observed with complexes containing **2.2** and **2.3**. Further increasing the lipophilicity by adding more fluorine groups or a fatty acid, might increase the activity. A balance between lipo- and hydrophilicity of the drug candidates is very important. The use of alkylated PTA derivatives did not result in an increase in the activity of the salicylaldimine complexes **2.5**-**2.16**. A less hydrophilic approach could be implemented to help find the optimal balance. A common technique is to use solvated complexes. Using DMSO or aqua ligands instead of chlorido ligands (as most chlorido groups usually get displaced to form aqua or solvated complexes) would aid in the solubility. This would help with the hydrophilic-lipophilic crossover, as well as in any mechanistic pathways. Figure 5.1 is a proposed structure that incorporates the suggested changes to the complexes exhibiting the most promising cytotoxic responses. It is suggested that the investigation of the synthesis and properties of such compounds would provide a promising avenue to extend this study for future research.

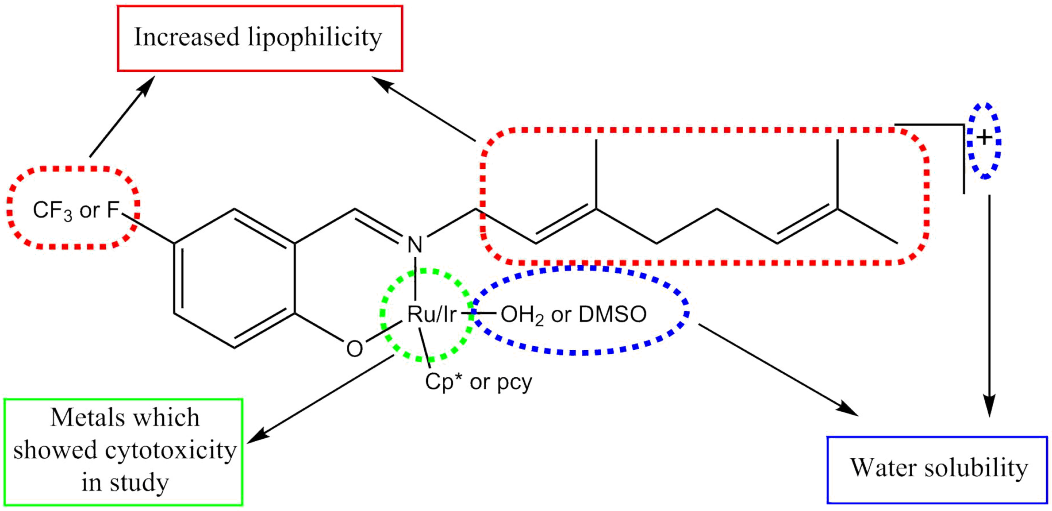

Figure 5.1: Proposed structure for modification to active complexes.

Chapter 6

Experimental

6.1 General Details

Reagents were purchased from Sigma-Aldrich or Merck and were used without further purification. Solvents were purchased from KIMIX and were dried using molecular sieves. Nuclear magnetic resonance (NMR) spectra were recorded on a Bruker Topspin GmbH (^{1}H at 400.22 MHz, ^{13}C$\{^{1}$H$\}$ at 100.65 MHz, ^{19}F$\{^{1}$H$\}$ at 376.58 MHz, ^{31}P$\{^{1}$H$\}$ at 162.01 MHz) or a Varian Mercury 300 (^{1}H at 300.08 MHz) spectrometer, with a Bruker Biospin GmbH casing and sample injector at 30 °C. Chemical shifts were reported using tetramethylsilane (TMS) as the internal standard. Infrared (IR) absorptions were measured on a Perkin-Elmer Spectrum One FT-IR spectrometer using attenuated total reflection (ATR) in the solid state. Elemental analysis was carried out using a Fissions EA 110 CHNS elemental analyser. Electron impact (EI) mass spectrometry was carried out on a JEOL GCmate II mass spectrometer (**2.1**-**2.7** and **2.14**-**2.16**). Electrospray ionisation (ESI) mass spectrometry was carried out on a Waters API Quattro instrument in the positive-ion (**2.8**-**2.13** and **3.1**-**3.15**) and negative-ion (**3.5**-**3.15**) modes. Melting points were determined using a Büchi melting point B-540 apparatus and are uncorrected. The dimeric precursors ([RuCl(μ-Cl)(*p*-cymene)]$_2$, [RhCl(μ-Cl)(Cp*)]$_2$ and [IrCl(μ-Cl)(Cp*)]$_2$) were synthesised using published methods.[1,2]

6.2 (*N,O*)-Salicylaldimine ligands (2.1-2.4)

6.2.1 Propylsalicylaldimine[3] (2.1)

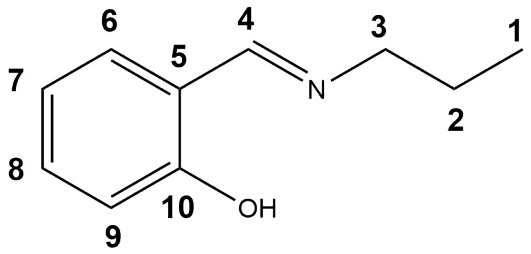

n-Propylamine (0.363 g, 6.14 mmol) and salicylaldehyde (0.690 g, 5.65 mmol) were added to a stirring solution of diethyl ether, and the resulting yellow solution was left to react for 18 hours. The ether mixture was washed with water (3 x 15 mL), the organic fraction collected and dried using anhydrous magnesium sulfate. The drying agent was removed by gravity filtration and the solvent removed under reduced pressure to yield the product (**2.1**) as a yellow oil. Yield: 0.845 g (91.6 %). **^{1}H NMR (400 MHz, $CDCl_3$) :** δ_H**(ppm)** = 1.00 (3H, t, ^3J = 7.4 Hz, H-1), 1.74 (2H, m, H-2), 3.56 (2H, td, ^3J = 6.8 Hz, ^4J = 1.2 Hz, H-3), 6.88 (1H, td, ^3J = 7.5 Hz, ^4J = 1.1 Hz, H-8), 6.97-6.99 (1H, m , H-6), 7.23-7.26 (1H, m, H-9), 7.28-7.31 (1H, m, H-7), 8.33 (1H, m, H-4), 13.66 (1H, s, OH). **^{13}C{^{1}H} NMR (100 MHz, $CDCl_3$) :** δ_C**(ppm)** = 11.59 (C-1), 23.99 (C-2), 61.16 (C-3), 116.95 (C-6), 118.27 (C-8), 118.77 (C-5), 131.01 (C-9), 131.92 (C-7), 161.37 (C-10), 164.46 (C-4). **IR (ATR):** ν_{max}**/cm^{-1}** = 1633 (C=N). **EI-MS** *m/z* 163.0042 (100%, $[M]^+$). **Analysis Calc. for $C_{10}H_{13}NO$**: C, 73.59; H, 8.03; N, 8.58. Found: C, 73.66; H, 8.03; N, 8.26.

6.2.2 *N*-(*p*-Trifluoromethyl)phenylsalicylaldimine[4] (2.2)

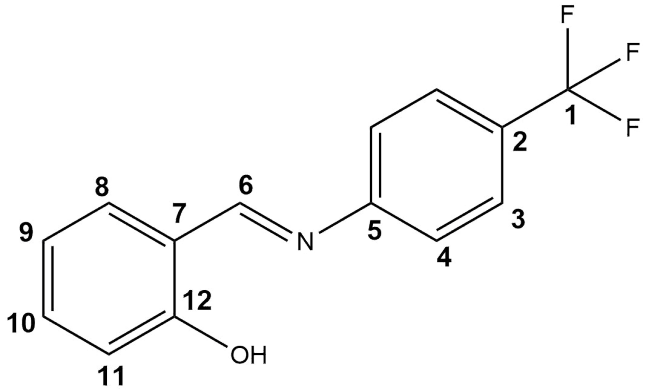

Salicylaldehyde (0.460 g, 3.77 mmol) and 4-(trifluoromethyl)aniline (0.614 g, 3.98 mmol) were added to diethyl ether (2 mL) and the resulting yellow suspension was left to react for 16 hours. The suspension was diluted with 20 mL *n*-pentane and the yellow solid (**2.2**) filtered. Yield: 0.920 g (92.1 %). **Melting Point:** 198-200 °C. **^{1}H NMR (400 MHz, $CDCl_3$):** δ_H **(ppm)** = 6.98 (1H, t, ^3J = 7.2 Hz, H-10), 7.05-7.07 (1H, m, H-8), 7.36 (2H, d, ^3J = 8.3 Hz, H-3), 7.42-7.45 (2H, m, H-9 and H-11), 7.77 (2H, d, ^3J = 8.3 Hz, H-4), 8.68 (1H, s, H-6), 12.80 (1H, br s, OH). **^{13}C{^{1}H} NMR (100 MHz, $CDCl_3$):** δ_C**(ppm)** = 117.44 (C-8), 118.93 (C-7), 119.33 (C-10), 121.46 (C-4), 124.89 (q, $^1J_{C-F}$ = 272.0 Hz, C-1), 126.64 (q, $^3J_{C-F}$ = 3.7 Hz, C-3), 128.74 (q, $^2J_{C-F}$ = 32.5 Hz, C-2), 132.68 (C-9), 133.90 (C-11), 151.70 (C-5), 161.25 (C-12), 164.48 (C-6). **^{19}F{^{1}H} NMR (376 MHz, $CDCl_3$):** δ_F**(ppm)** = -62.22 (s). **IR (ATR):** ν_{max}**/cm^{-1}** = 1623 (C=N). **EI-MS** *m/z* 265.007 (100%, $[M]^+$). **Analysis Calc. for $C_{14}H_{10}F_3NO$**: C, 63.40; H, 3.80; N, 5.28. Found: C, 63.05; H, 3.36; N, 5.05.

6.2.3 *N*-(3-Trimethylsilyl)propylsalicylaldimine (2.3)

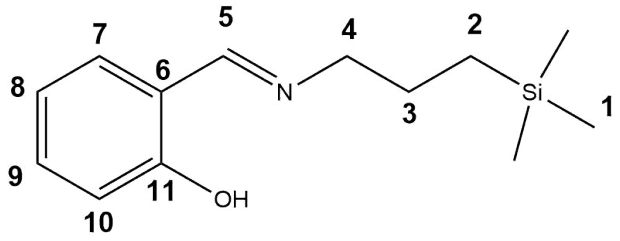

Salicylaldehyde (0.437 g, 3.58 mmol) and 3-aminopropyltrimethylsilane (0.548 g, 4.17 mmol) were stirred in diethyl ether under an inert atmosphere for 16 hours. The resulting yellow solution was then washed with water (3 x 15 mL) to remove the excess amine. The organic fraction was collected, dried using anhydrous magnesium sulfate and the solvent removed to yield a yellow oil after gravity filtration of the drying agent. The oil (**2.3**) was dried *in vacuo*. Yield: 0.783 g (93.2 %). **^{1}H NMR (400 MHz, $CDCl_3$):** δ_H**(ppm)** = 0.02 (9H, s, H-1), 0.53-0.59 (2H, m, H-2), 1.66-1.76 (2H, m, H-3), 3.60 (2H, t, ^{3}J = 7.4 Hz, H-4), 6.89 (1H, t, ^{3}J = 7.4 Hz, H-9), 6.99 (1H, d, ^{3}J = 8.3 Hz, H-7), 7.26-7.35 (2H, m, H-8 and H-10), 8.35 (1H, s, H-5), 13.70 (1H, s, OH). **^{13}C{^{1}H} NMR (100 MHz, $CDCl_3$):** δ_C**(ppm)** = -1.79 (C-1), 14.14 (C-2), 25.51 (C-3), 62.68 (C-4), 117.03 (C-7), 118.30 (C-9), 118.81 (C-6), 131.04 (C-10), 131.97 (C-8), 161.47 (C-11), 164.42 (C-5). **EI-MS** *m/z* 235.1259 (100%, $[M]^+$). **Analysis Calc. for $C_{13}H_{21}NOSi$**: C, 66.33; H, 8.99; N, 5.95. Found: C, 66.31; H, 9.20; N, 5.96.

6.2.4 Salicylaldehyde hydrazone (L1)

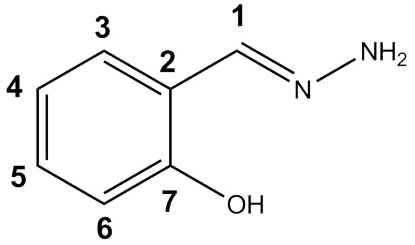

A solution of salicylaldehyde (3.68 g, 31.3 mmol) in ethanol (40 mL) was added to a stirring solution of hydrazine hydrate (3.0 mL) in ethanol (70 mL) over 65 minutes. The clear solution was stirred for an additional 5 minutes before being concentrated to 20 mL and cooled to aid the crystallisation of the product, **L1**. The white crystals were isolated by filtration and dried *in vacuo*. Yield: 1.47 g (34.5 %). **^{1}H NMR (400**

MHz, $CDCl_3$): δ_H **(ppm)** = 5.44 (2H, br s, NH_2), 6.86 (1H, t, ^3J = 7.5 Hz, H-5), 6.94 (1H, d, ^3J = 8.2 Hz, H-3), 7.09-7.11 (1H, m, H-6), 7.18-7.23 (1H, m, H-4), 7.87 (1H, s, H-1), 11.04 (1H, s, OH). **IR (ATR):** ν_{max}**/cm**$^{-1}$ = 1615 (C=N), 3383 (NH_2). **EI-MS** *m/z* 136.04 (100%, $[M]^+$). **Analysis Calc. for $C_7H_8N_2O$**: C, 61.75; H, 5.92; N, 20.58. Found: C, 61.65; H, 5.69; N, 20.56.

6.2.5 Ferrocenyl salicylaldimine[5] (2.4)

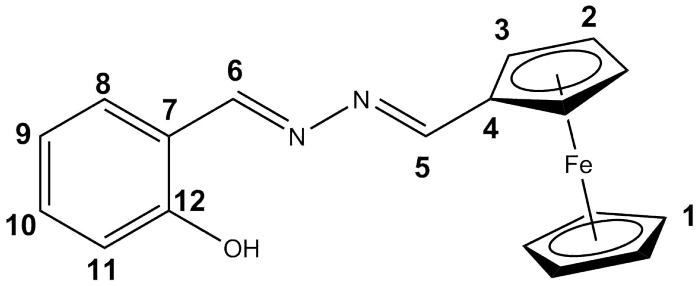

To a stirring solution of salicylaldehyde hydrazone, **L1** (0.677 g, 5.00 mmol) in methanol (30 mL), ferrocenecarboxaldehyde (1.07 g, 5.02 mmol) in methanol was added dropwise. The red solution was stirred for 16 hours at room temperature. The resulting red precipitate (**2.4**) was isolated by vacuum filtration, washed with cold methanol and dried *in vacuo*. Yield: 0.944 g (74.9%). **Melting Point:** 128-129 °C. **^{1}H NMR (300 MHz, $CDCl_3$):** δ_H **(ppm)** = 4.25 (5H, s, H-1), 4.51 (2H, br s, H-2), 4.74 (2H, br s, H-3), 6.94 (1H, t, ^3J = 7.4 Hz, H-10), 7.03 (1H, d, ^3J = 8.1 Hz, H-8), 7.30 – 7.38 (2H, m, H-11 and H-9), 8.54 (1H, s, H-5), 8.70 (1H, s, H-6), 11.84 (1H, s, OH). **^{13}C{^{1}H} NMR (100 MHz, $CDCl_3$):** δ_C**(ppm)** = 68.99 (C-2), 69.45 (C-1), 71.17 (C-4),71.51 (C-3), 116.86 (C-9), 117.97 (C-7), 119.38 (C-8), 132.00 (C-11), 132.31 (C-10), 159.54 (C-12), 162.55 (C-6), 163.75 (C-5). **IR (ATR):** ν_{max}**/cm**$^{-1}$ = 1586 (C=N), 1618 (C=N). **EI-MS** *m/z* 332.05 ($[M]^+$, 100%). **Analysis Calc. for $C_{18}H_{16}FeN_2O$**: C, 65.08; H, 4.86; N, 8.43. Found: C, 64.50; H, 4.85; N, 8.13.

6.3 (*N,O*)-salicylaldimine metal complexes (2.5-2.16)

6.3.1 General Synthesis

(i) Synthesis of 2.5-2.10 and 2.12

Compounds **2.1**, **2.2** or **2.3** and triethylamine were reacted in dichloromethane for 60 minutes. To the yellow solution, [RuCl(μ-Cl)(*p*-cymene)]$_2$, [RhCl(μ-Cl)(Cp*)]$_2$ or [IrCl(μ-Cl)(Cp*)]$_2$ was added and stirred for 18 hours. The solution was then washed with water (3 x 15 mL) in a separating funnel, and the organic fraction collected and dried using anhydrous magnesium sulfate. After removal of the drying agent by filtration, the solvent was removed and the residue taken up in a minimal amount of dichloromethane, to which diethyl ether was added to precipitate the desired complex.

(ii) Synthesis of 2.11 and 2.13

[RuCl(μ-Cl)(*p*-cymene)]$_2$ or [IrCl(μ-Cl)(Cp*)]$_2$ was added to a stirring solution of triethylamine and **2.3** in diethyl ether and was stirred for 18 hours at room temperature. The excess dimer and triethylammonium chloride that formed during the reaction were filtered off and a red or orange solution was obtained. The solvent was removed *in vacuo* and the residue washed with *n*-pentane to yield the desired complexes.

(iii) Synthesis of 2.14-2.16

Triethylamine and **2.4** were stirred in ethanol for 30 minutes. The resulting red mixture was diluted with ethanol (10 mL) before [RuCl(μ-Cl)(*p*-cymene)]$_2$, [RhCl(μ-Cl)(Cp*)]$_2$ or [IrCl(μ-Cl)(Cp*)]$_2$ was added to the reaction mixture and further stirred for 18 hours. The desired product precipitated and was isolated by vacuum filtration as a red or orange amorphous powder. The powder was washed with *n*-pentane (3 x 10 mL) and dried *in vacuo*.

6.3.1.1 Ruthenium propylsalicylaldimine complex[3] (2.5)

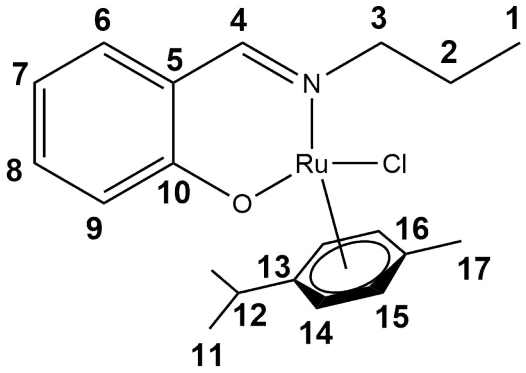

2.1 (0.0720 g, 0.441 mmol) and triethylamine (0.1 mL, 0.717 mmol) were reacted with [RuCl(μ-Cl)(p-cymene)]$_2$ (0.102 g, 0.167 mmol). Complex **2.5** was isolated as a brown powder. Yield: 0.0884 g (61.3 %). **Melting Point:** 189°C to dec. with melting. **^{1}H NMR (400 MHz, CDCl$_3$):** δ_H **(ppm)** = 1.03 (3H, t, ^3J = 7.4 Hz, H-1), 1.14 (3H, d, ^3J = 6.6 Hz, H-11), 1.24 (3H, d, ^3J = 6.6 Hz, H-11), 1.96-1.98 (1H, m, H-2), 1.99-2.07 (1H, m, H-2), 2.21 (3H, s, H-17), 2.78 (1H, sept, ^3J = 6.9 Hz, H-12), 3.99 (1H, m, H-3), 4.20 (1H, m, H-3), 5.04 (1H, m, H-15), 5.38 (1H, m, H-15), 5.40 (2H, m, H-14), 6.40 (1H, t, ^3J = 7.2 Hz, H-8), 6.90 (1H, m, H-6), 6.95 (1H, m, H-9), 7.15 (1H, m, H-7), 7.67 (1H, s, H-4). **^{13}C{^{1}H} NMR (100 MHz, CDCl$_3$) :** δ_C**(ppm)** = 11.56 (C-1), 18.52 (C-17), 21.67 (C-11), 22.68 (C-11), 24.36 (C-2), 30.51 (C-12), 71.07 (C-3), 80.24 (C-15), 81.90 (C-15), 83.75 (C-14), 97.37 (C-16), 101.60 (C-13), 114.01 (C-8), 119.31 (C-5), 122.30 (C-9), 134.28 (C-6), 134.49 (C-7), 163.47 (C-4), 165.04 (C-10). **IR (ATR):** ν_{max}**/cm^{-1}** = 1624 (C=N). **EI-MS** m/z 433.07 (100%, [M]$^+$). **Analysis Calc. for C$_{20}$H$_{26}$ClNORu**: C, 55.48; H, 6.05; N, 3.24. Found: C, 55.13; H, 6.25; N, 3.01.

6.3.1.2 Rhodium propylsalicylaldimine complex[6] (2.6)

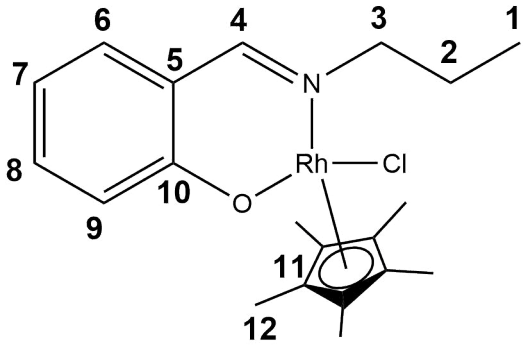

2.1 (0.0711 g, 0.436 mmol) and triethylamine (0.0726 g, 0.717 mmol) were reacted with [RhCl(μ-Cl)(Cp*)]$_2$ (0.100 g, 0.162 mmol). Complex **2.6** was isloated as a red powder. Yield: 0.0650 g (46.1 %). **Melting Point:** 216°C to dec. with melting. **^{1}H NMR (400 MHz, CDCl$_3$):** δ_H **(ppm)** = 0.98 (3H, t,^3J = 7.4 Hz, H-1), 1.55 (15H, s, H-12), 1.84-1.86 (1H, m, H-2), 2.09-2.17 (1H, m, H-2), 3.70-3.90 (1H, m, H-3), 3.90-4.15 (1H, m, H-3), 6.44 (1H, t, ^3J = 7.2 Hz, H-8), 6.94-6.96 (1H, m, H-6), 7.01 (1H, dd, ^3J = 7.8 Hz, ^4J = 1.8 Hz, H-9), 7.15-7.19 (1H, m, H-7), 7.80 (1H, m, H-4). **^{13}C{^{1}H} NMR (100 MHz, CDCl$_3$):** δ_C**(ppm)** = 8.69 (C-12), 11.53 (C-1), 23.90 (C-2), 65.63 (C-3), 92.75 (d, $^1J_{C-Rh}$ = 8.1 Hz, C-11), 114.10 (C-8), 121.93 (C-5), 123.88 (C-6), 133.79 (C-9), 134.02 (C-7), 162.47 (C-4), 166.76 (C-10). **IR (ATR):** ν_{max}**/cm^{-1}** = 1627 (C=N). **EI-MS** *m/z* 434.88 (60%, [M]$^+$). **Analysis Calc. for C$_{20}$H$_{27}$ClNORh**: C, 55.12; H, 6.25; N, 3.21. Found: C, 54.95; H, 6.09; N, 2.90.

6.3.1.3 Iridium propylsalicylaldimine complex[6] (2.7)

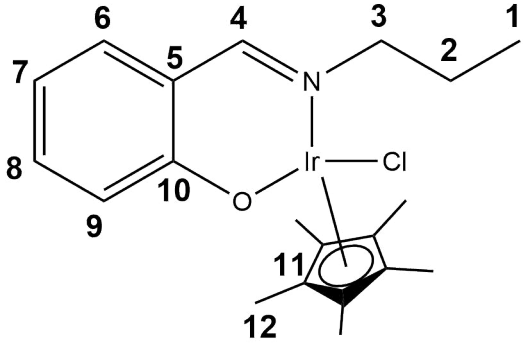

2.1 (0.0557 g, 0.341 mmol) and triethylamine (0.1 mL, 0.717 mmol) were reacted with [IrCl(μ-Cl)(Cp*)]$_2$ (0.0998 g, 0.125 mmol). Complex **2.7** was isolated as a yellow

powder. Yield: 0.0251 g (19.0 %). **Melting Point:** 209°C to dec. with melting. **^{1}H NMR (400 MHz, $CDCl_3$):** δ_H **(ppm)** = 0.99 (3H, t,^3J = 7.3 Hz, H-1), 1.52 (15H, s, H-12), 1.87-2.17 (2H, m, H-2), 3.85-4.09 (2H, m, H-3), 6.42 (1H, t, ^3J = 7.3 Hz, H-8), 6.88-6.90 (1H, m, H-6), 7.02 (1H, dd, ^3J = 7.7 Hz, ^4J = 1.8 Hz, H-9), 7.22-7.24 (1H, m, H-7), 7.75 (1H, s, H-4). **^{13}C{^{1}H} NMR (100 MHz, $CDCl_3$):** δ_C**(ppm)** = 8.85 (C-12), 11.44 (C-1), 23.98 (C-2), 68.39 (C-3), 84.70 (C-11), 114.84 (C-8), 121.88 (C-5), 122.77 (C-6), 133.17 (C-9), 134.06 (C-7), 159.82 (C-4), 165.22 (C-10). **IR (ATR):** ν_{max}**/cm^{-1}** = 1625 (C=N). **EI-MS** m/z 525.14 (95%, $[M]^+$). **Analysis Calc. $C_{20}H_{27}ClIrNO$**: C, 45.75; H, 5.18; N, 2.67. Found: C, 45.47; H, 5.05; N, 2.41.

6.3.1.4 Ruthenium trifluoro complex (2.8)

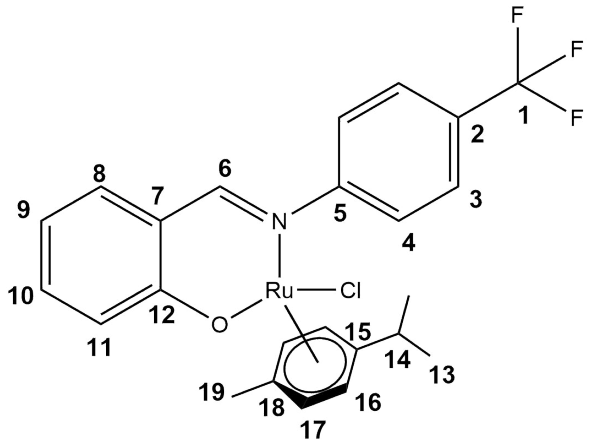

2.2 (0.0875 g, 0.330 mmol) and triethylamine (0.1 mL, 0.717 mmol) were reacted with [RuCl(μ-Cl)(p-cymene)]$_2$ (0.101 g, 0.164 mmol). Complex **2.8** was isolated as a brown powder. Yield: 0.0833 g (47.4%). **Melting Point:** 226°C to dec. with melting. **^{1}H NMR (400 MHz, $CDCl_3$):** δ_H **(ppm)** = 1.14 (3H, d, ^3J = 6.8 Hz, H-13), 1.19 (3H, d, ^3J = 6.8 Hz, H-13), 2.13 (3H, s, H-19), 2.64 (1H, sept, ^3J = 6.8 Hz, H-14), 4.25 (1H, d, ^3J = 5.4 Hz, H-17), 5.01 (1H, d, ^3J = 5.4 Hz, H-16), 5.28 (1H, d, ^3J = 6.4 Hz, H-16), 5.36 (1H, d, ^3J = 6.4 Hz, H-17), 6.42-6.44 (1H, m, H-10), 6.95 (1H, dd, ^3J = 7.8 Hz, ^4J = 1.8 Hz, H-11), 6.99-7.01 (1H, m, H-8), 7.22-7.27 (1H, m, H-9), 7.72-7.74 (3H, m, H-4 and H-6), 7.80-7.82 (2H, m, H-3). **^{13}C{^{1}H} NMR (100 MHz, $CDCl_3$):** δ_C**(ppm)** = 18.47 (C-19), 21.68 (C-13), 22.66 (C-13), 30.41 (C-14), 80.25 (C-16), 83.08 (C-17), 83.25 (C-17), 86.59 (C-16), 98.31 (C-15), 101.74 (C-18), 114.50 (C-10), 117.95

(C-7), 122.91 (C-8), 123.85 (q, $^{1}J_{C-F}$ = 270.1 Hz, C-1), 124.38 (C-4), 126.14 (q, $^{3}J_{C-F}$ = 2.9 Hz, C-3), 129.12 (q, $^{2}J_{C-F}$ = 30.0 Hz, C-2), 135.46 (C-11), 136.08 (C-9), 160.83 (C-5), 164.6 (C-6), 165.66 (C-12). **^{19}F{^{1}H} NMR (376 MHz, $CDCl_3$):** δ_F**(ppm)** = -62.21 (s). **IR (ATR):** ν_{max}**/cm^{-1}** = 1615 (C=N). **ESI-MS (HR)** *m/z* 238.1773 (100%, $[M+H+Na]^{2+}$ requires 238.2999). **Analysis Calc. for $C_{24}H_{23}ClF_3NORu$**: C, 53.88; H, 4.33; N, 2.62. Found: C, 53.55; H, 4.14; N, 2.10.

6.3.1.5 Rhodium trifluoro complex (2.9)

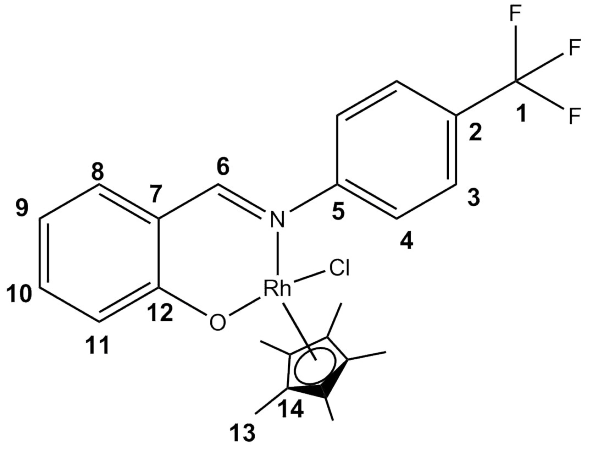

2.2 (0.0866 g, 0.327 mmol) and triethylamine (0.1 mL, 0.717 mmol) were reacted with $[RhCl(\mu\text{-}Cl)(Cp^*)]_2$ (0.101 g, 0.167 mmol). Complex **2.9** was isolated as an orange powder. Yield: 0.132 g (75.0 %). **Melting Point:** 241°C to dec. with melting. **^{1}H NMR (400 MHz, $CDCl_3$):** δ_H**(ppm)** = 1.35 (15H, s, H-13), 6.43-6.47 (1H, m, H-10), 7.01-7.07 (2H, m, H-8 and H-11), 7.24-7.28 (1H, m, H-9), 7.69 (2H, d, ^{3}J = 8.3 Hz, H-4), 7.94 (1H, s, H-6), 8.01 (2H, d, ^{3}J = 8.1 Hz, H-3). **^{13}C{^{1}H} NMR (100 MHz, $CDCl_3$):** δ_C**(ppm)** = 8.42 (C-13), 93.67 (d, J_{C-Rh} = 8.8 Hz, C-14), 114.33 (C-10), 119.21 (C-7), 123.96 (q, $^{1}J_{C-F}$ = 272.2 Hz, C-1), 124.35 (C-8), 125.22 (C-4), 125.83 (q, $^{3}J_{C-F}$ = 3.7 Hz, C-3), 128.90 (q, $^{2}J_{C-F}$ = 32.5 Hz, C-2), 135.51 (C-11), 135.81 (C-9), 157.15 (C-5), 165.10 (C-6), 166.80 (C-12). **^{19}F{^{1}H} NMR (376 MHz, $CDCl_3$):** δ_F**(ppm)** = -62.15 (s). **IR (ATR):** ν_{max}**/cm^{-1}** = 1603 (C=N). **ESI-MS (HR)** *m/z* 502.0861 (100%, $[M-Cl]^{+}$ requires 502.0865). **Analysis Calc. for $C_{24}H_{24}ClF_3NORh$**: C, 53.60; H, 4.50; N, 2.60. Found: C, 53.03; H, 4.31; N, 2.08.

6.3.1.6 Iridium trifluoro complex (2.10)

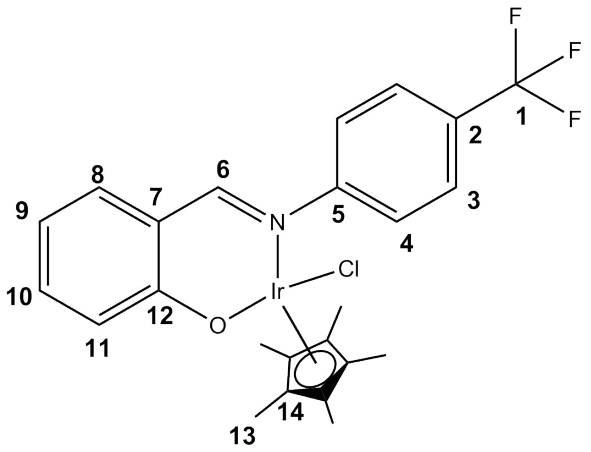

2.2 (0.0685 g, 0.258 mmol) and triethylamine (0.1 mL, 0.717 mmol) were reacted with [IrCl(μ-Cl)(Cp*)]$_2$ (0.0998 g, 0.125 mmol). Complex **2.10** was isolated as an orange powder. Yield: 0.108 g (69.0 %). **Melting Point:** 243°C to dec. with melting. **^{1}H NMR (400 MHz, CDCl$_3$):** δ_H **(ppm)** = 1.33 (15H, s, H-13), 6.46 (1H, t, ^3J = 7.2 Hz, H-10), 6.97 (1H, d, ^3J = 8.6 Hz, H-8), 7.11 (1H, d, ^3J = 7.6 Hz, H-11), 7.37 (1H, t, ^3J = 7.2 Hz, H-9), 7.67 (2H, d, ^3J = 8.1 Hz, H-4), 7.85 (2H, d, ^3J = 8.1 Hz, H-3), 8.01 (1H, s, H-6). **^{13}C{^{1}H} NMR (100 MHz, CDCl$_3$):** δ_C**(ppm)** = 8.43 (C-13), 85.81 (C-14), 115.21 (C-10), 120.09 (C-7), 123.53 (C-8), 123.80 (q, $^1J_{C-F}$ = 272.6 Hz, C-1), 125.45 (C-4), 125.57 (q, $^3J_{C-F}$ = 3.7 Hz, C-3), 129.77 (q, $^2J_{C-F}$ = 32.5 Hz, C-2), 134.65 (C-11), 135.77 (C-9), 159.12 (C-5), 161.41 (C-6), 164.34 (C-12). **^{19}F{^{1}H} NMR (376 MHz, CDCl$_3$):** δ_F**(ppm)** = -62.17 (s). **IR (ATR):** ν_{max}**/cm^{-1}** = 1615 (C=N). **ESI-MS (HR)** *m/z* 592.1528 (80%, [M-Cl]$^+$ requires 592.1439). **Analysis Calc. for C$_{24}$H$_{24}$ClF$_3$IrNO**: C, 45.97; H, 3.86; N, 2.23. Found: C, 45.63; H, 3.87; N, 1.75.

6.3.1.7 Ruthenium silane complex (2.11)

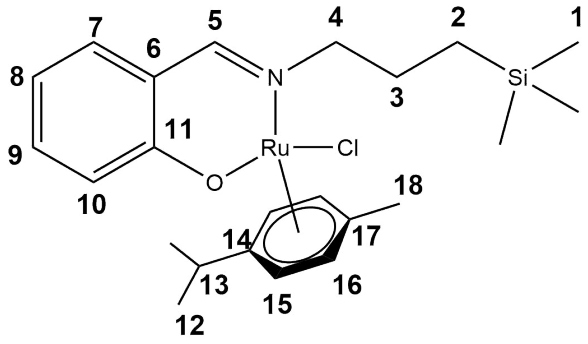

2.3 (0.0876 g, 0.372 mmol) and triethylamine (0.1 mL, 0.717 mmol) were reacted with [RuCl(μ-Cl)(p-cymene)]$_2$ (0.137 g, 0.224 mmol). Complex **2.11** was isolated as a dark brown crystalline powder. Yield: 0.0884 g (46.2%). **Melting Point:** 146°C to dec. with melting. **^{1}H NMR (400 MHz, CDCl$_3$):** δ_H **(ppm)** = 0.05 (9H, s, H-1), 0.44-0.54 (1H, m, H-2), 0.60-0.70 (1H, m, H-2), 1.15 (3H, d, ^3J = 6.9 Hz, H-12), 1.25 (3H, d, ^3J = 7.1 Hz, H-12), 1.84-1.96 (1H, m, H-3), 2.00-2.14 (1H, m, H-3), 2.22 (3H, s, H-18), 2.79 (1H, sept, ^3J = 7.0 Hz, H-13), 3.94-4.04 (1H, m, H-4), 4.20-4.29 (1H, m, H-4), 5.02 (1H, d, ^3J = 8.6 Hz, H-16), 5.39 (3H, m, H-15 and H-16), 6.38-6.42 (1H, m, H-9), 6.90-6.97 (2H, m, H-7 and H-10), 7.13-7.19 (1H, m, H-8), 7.67 (1H, s, H-5). **^{13}C{^{1}H} NMR (100 MHz, CDCl$_3$) :** δ_C**(ppm)** = -1.70 (C-1), 14.13 (C-2), 18.49 (C-18), 21.61 (C-12), 22.70 (C-12), 25.74 (C-3), 30.46 (C-13), 72.69 (C-4), 80.11 (C-16), 82.07 (C-16), 83.25 (C-15), 85.86 (C-15), 97.24 (C-17), 101.57 (C-14), 113.97 (C-9), 119.21 (C-6), 122.22 (C-7), 134.33 (C-8), 134.46 (C-10), 163.34 (C-5), 164.92 (C-11). **IR (ATR):** ν_{max}**/cm^{-1}** = 1618 (C=N). **ESI-MS (HR)** m/z 470.1460 (100%, [M-Cl]$^+$ requires 470.1459). **Analysis Calc. for C$_{23}$H$_{34}$ClNORuSi$\cdot_0 \cdot$ 6 H$_2$O**: C, 53.42; H, 6.89; N, 2.71. Found: C, 53.17; H, 6.81; N, 2.47.

6.3.1.8 Rhodium silane complex (2.12)

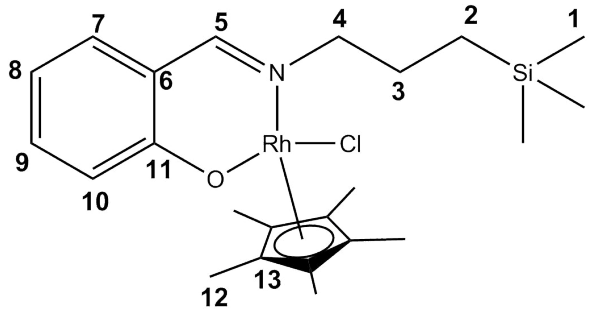

2.3 (0.0997 g, 0.423 mmol) and triethylamine (0.1 mL, 0.717 mmol) were reacted with [RhCl(μ-Cl)(Cp*)]$_2$ (0.126 g, 0.204 mmol). Complex (**2.12**) was isolated as a red powder. Yield: 0.101 g (48.8 %). **Melting Point:** 166°C to dec. with melting. **^{1}H NMR (400 MHz, CDCl$_3$):** δ_H **(ppm)** = -0.01 (9H, s, H-1), 0.48-0.52 (2H, m, H-2), 1.53 (15H, s, H-12), 1.68-1.71 (1H, m, H-3), 2.15-2.25 (1H, m, H-3), 3.80-4.03 (2H, m, H-4), 6.41-6.45 (1H, m, H-9), 6.92 (1H, d, ^3J = 8.4 Hz, H-7), 7.01 (1H, dd, ^3J = 7.7 Hz, ^4J = 1.7 Hz, H-10), 7.13-1.17 (1H, m , H-8), 7.78 (1H, s, H-5). **^{13}C{^{1}H} NMR (100 MHz, CDCl$_3$) :** δ_C**(ppm)** = -1.72 (C-1), 8.61 (C-12), 14.02 (C-2), 25.28 (C-3), 66.97 (C-4), 92.65 (d, $^1J_{C-Rh}$ = 8.1 Hz, C-13), 114.05 (C-9), 121.92 (C-6), 123.70 (C-7), 133.71 (C-8), 133.90 (C-10), 162.31 (C-5), 166.60 (C-11). **IR (ATR):** ν_{max}**/cm^{-1}** = 1621 (C=N). **ESI-MS (HR)** *m/z* 472.1551 (100%, [M-Cl]$^+$ requires 472.1543). **Analysis Calc. for C$_{23}$H$_{35}$ClNORhSi·0.2 Et$_2$O**: C, 54.68; H, 7.13; N, 2.68. Found: C, 55.32; H, 6.86; N, 2.39.

6.3.1.9 Iridium silane complex (2.13)

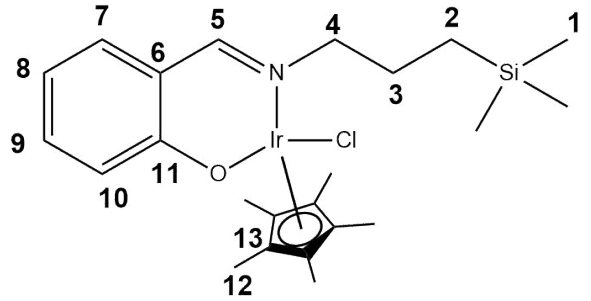

2.3 (0.0337 g, 0.143 mmol) and triethylamine (0.1 mL, 0.717 mmol) was reacted with [IrCl(μ-Cl)(Cp*)]$_2$ (0.0697 g, 0.0875 mmol). Complex **2.13** was isolated as a fine yellow powder. Yield: 0.0478 g (56.0 %). **Melting Point:** 158°C to dec. with melting. **^{1}H**

NMR (300 MHz, $CDCl_3$): δ_H**(ppm)** = 0.03 (9H, s, H-1), 0.51 (2H, br m, H-2), 1.56 (15H, s, H-12), 1.70-1.93 (1H, br m, H-3), 1.94-2.17 (1H, br m, H-3), 3.75-4.20 (2H, br m, H-4), 6.40-6.44 (1H, m, H-9), 6.87-6.90 (1H, m, H-7), 7.04 (1H, dd, ^3J = 7.7 Hz, ^4J = 1.8 Hz, H-10), 7.21-7.25 (1H, m, H-8), 7.75 (1H, s, H-5). **^{13}C{^{1}H} NMR (100 MHz, $CDCl_3$):** δ_C**(ppm)** = -1.70 (C-1), 8.83 (C-12), 14.03 (C-2), 25.45 (C-3), 69.86 (C-4), 84.64 (C-13), 114.79 (C-9), 121.88 (C-6), 122.71 (C-7), 133.15 (C-8), 134.00 (C-10), 159.72 (C-5), 165.19 (C-11). **IR (ATR):** ν_{max}**/cm^{-1}** = 1619 (C=N). **ESI-MS (HR)** *m/z* 562.2133 (100%, [M-Cl]$^+$) requires 562.2117. **Analysis Calc. for $C_{23}H_{35}ClIrNOSi\cdot$ 0.2 Et_2O**: C, 46.70; H, 6.09; N, 2.29. Found: C, 47.11; H, 5.86; N, 1.79.

6.3.1.10 Ruthenium ferrocenyl complex[5] (2.14)

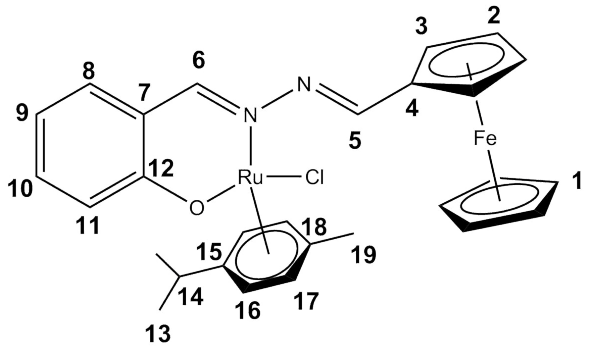

2.4 (0.280 g, 0.843 mmol) and triethylamine (0.120 mL, 0.840 mmol) were reacted with [RuCl(μ-Cl)(*p*-cymene)]$_2$ (0.254 g, 0.415 mmol). Complex **2.14** was isolated as a dark red powder. Yield: 0.380 g (75.1 %). **Melting Point:** 197°C to dec. with melting. **^{1}H NMR (400 MHz, $CDCl_3$):** δ_H**(ppm)** = 1.17 (3H, d, ^3J = 6.8 Hz, H-13), 1.22 (3H, d, ^3J = 7.0 Hz, H-13), 2.23 (3H, s, H-19), 2.83 (1H, sept, ^3J = 7.0 Hz, H-14), 4.29 (5H, s, H-1), 4.50 – 4.54 (2H, m, H-2 and H-3), 4.64 – 4.66 (1H, m, H-2), 4.77 – 4.78 (1H, m, H-3), 5.16 (1H, d, ^3J = 5.7 Hz, H-17), 5.43 (2H, br s, H-16), 5.48 (1H, d, ^3J = 5.8 Hz, H-17), 6.43 – 6.47 (1H, m, H-10), 6.97 (1H, dd, ^3J = 7.7 Hz, ^4J = 1.8 Hz, H-8), 7.01 (1H, d, ^3J = 8.4 Hz, H-11), 7.20 – 7.21 (1H, m, H-9), 7.80 (1H, s, H-6), 8.74 (1H, s, H-5). **^{13}C{^{1}H} NMR (100 MHz, $CDCl_3$):** δ_C**(ppm)** = 18.84 (C-19), 21.98 (C-13), 22.83 (C-13), 30.83 (C-14), 67.94 (C-3), 69.85 (C-1), 69.96 (C-2), 71.48 (C-2), 71.71 (C-3), 76.64 (C-4), 81.33 (C-17), 82.20 (C-17), 83.54 (C-16), 84.19 (C-16), 98.00 (C-18), 103.03 (C-15), 114.68 (C-9), 117.92 (C-7), 122.98 (C-8), 134.15 (C-11), 134.64

(C-10), 155.41 (C-6), 163.03 (C-5), 166.13 (C-12). **IR (ATR):** ν_{max}**/cm**$^{-1}$ = 1600 (C=N). **EI-MS** *m/z* 602.04 ([M]$^+$, 10%). **Analysis Calc. for $C_{28}H_{29}ClFeN_2ORu$**: C, 55.87; H, 4.86; N, 4.65. Found: C, 55.90; H, 5.00; N, 4.37.

6.3.1.11 Rhodium ferrocenyl complex[5] (2.15)

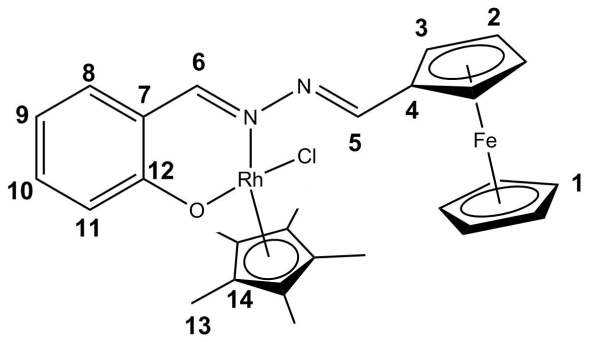

2.4 (0.221 g, 0.665 mmol) and triethylamine (0.1 mL, 0.717 mmol) was reacted with [RhCl(μ-Cl)(Cp*)]$_2$ (0.201 g, 0.325 mmol). Complex **2.15** was isolated as a dark red powder. Yield: 0.110 g (27.9 %). **Melting Point:** 152°C to dec. with melting. **^{1}H NMR (400 MHz, $CDCl_3$):** δ_H **(ppm)** = 1.54 (15H, s, H-13), 4.31 (5H, s, H-1), 4.47 – 4.49 (1H, m, H-2), 4.51 – 4.52 (1H, m, H-3), 4.56 – 4.58 (1H, m, H-2), 4.83 – 4.85 (1H, m, H-3), 6.49 – 6.53 (1H, m, H-10), 7.01 (1H, d, ^3J = 8.4 Hz, H-8), 7.11 (1H, dd, ^3J = 7.8 Hz, ^4J = 1.8 Hz, H-11), 7.20 – 7.25 (1H, m, H-9), 8.31 (1H, s, H-6), 9.24 (1H, s, H-5). **^{13}C{^{1}H} NMR (100 MHz, $CDCl_3$):** δ_C**(ppm)** = 9.07 (C-13), 66.44 (C-3), 70.06 (C-1), 71.29 (C-2), 71.34 (C-2), 71.79 (C-3), 76.55 (C-4), 93.59 (d, $^1J_{C-Rh}$ = 8.1 Hz, C-14), 115.04 (C-9), 120.04 (C-7), 124.13 (C-11), 134.43 (C-8), 134.69 (C-10), 160.35 (C-6), 165.71 (C-5), 167.73 (C-12). **IR (ATR):** ν_{max}**/cm**$^{-1}$ = 1611 (C=N). **EI-MS** *m/z* 604.04 ([M]$^+$, 10%). **Analysis Calc. for $C_{28}H_{30}ClFeN_2ORh$**: C, 55.61; H, 5.00; N, 4.63. Found: C, 55.68; H, 5.53; N, 4.47.

6.3.1.12 Iridium ferrocenyl complex[5] (2.16)

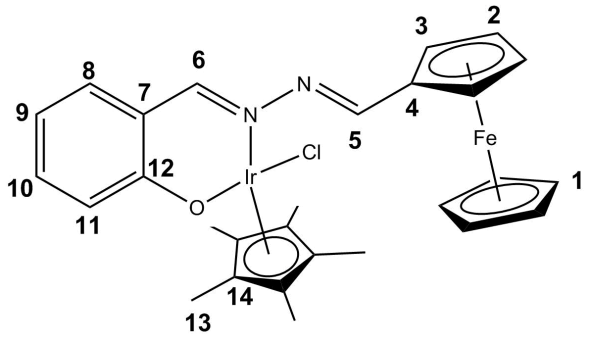

2.4 (0.172 g, 0.519 mmol) and triethylamine (0.1 mL, 0.717 mmol) was reacted with $[IrCl(\mu\text{-}Cl)(Cp^*)]_2$ (0.200 g, 0.251 mmol). Complex **2.16** was isolated as an orange powder. Yield: 0.102 g (29.1 %). **Melting Point:** 200°C to dec. with melting. **^{1}H NMR (400 MHz, $CDCl_3$):** δ_H **(ppm)** = 1.54 (15H, s, H-13), 4.31 (5H, s, H-1), 4.47 – 4.49 (1H, m, H-2), 4.51 – 4.52 (1H, m, H-3), 4.56 – 4.58 (1H, m, H-2), 4.83 – 4.85 (1H, m, H-3), 6.49 – 6.53 (1H, m, H-10), 7.01 (1H, d, ^3J = 8.4 Hz, H-8), 7.11 (1H, dd, ^3J = 7.8 Hz, ^4J = 1.8 Hz, H-11), 7.20 – 7.25 (1H, m, H-9), 8.31 (1H, s, H-6), 9.24 (1H, s, H-5). **^{13}C{^{1}H} NMR (100 MHz, $CDCl_3$):** δ_C**(ppm)** = 9.27 (C-13), 66.70 (C-3), 70.07 (C-1), 71.34 (C-2), 71.40 (C-2), 71.86 (C-3), 76.12 (C-4), 85.55 (C-14), 115.88 (C-9), 120.58 (C-7), 123.08 (C-11), 133.73 (C-8), 134.65 (C-10), 157.42 (C-6), 166.45 (C-12), 166.90 (C-5). **IR (ATR):** ν_{max}**/cm^{-1}** = 1594 (C=N), 1618 (C=N). **EI-MS** *m/z* 694.15 ($[M]^+$, 20%). **Analysis Calc. for $C_{28}H_{30}ClFeIrN_2O$**: C, 48.45; H, 4.36; N, 4.04. Found: C, 48.61; H, 4.41; N, 3.88.

6.4 Alkylated benzyl PTA scaffold (3.1) and mono-cationic complexes (3.2-3.4)

6.4.1 Alkylated Benzyl PTA Scaffold[7] (3.1)

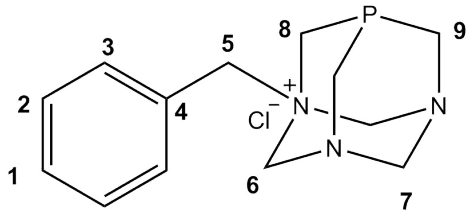

Under an inert atmosphere (Ar(g)), a solution of 1,3,5-triaza-7-phosphaadamantane (0.206 g,1.30 mmol) and benzyl chloride (0.220 g, 1.74 mmol) in THF (15 mL) was refluxed for 16 hours. A white precipitate was observed after this time, filtered and washed with cold THF (2 x 10 mL). The sample was then dried *in vacuo*. Compound **3.1** was isolated as a white solid. Yield: 0.367 g (98.8 %). **Melting Point:** 187-190 °C. $\mathbf{S_{293}}$**: (g/L ± SE, $\mathbf{H_2O}$)** = 22.0 ± 4.4. ^{1}**H NMR (400 MHz, $\mathbf{CD_3OD}$-d_4):** δ_H**(ppm)** = 3.82 - 3.99 (4H, m, H-9), 4.18 (2H, s, H-5), 4.30 (2H, d, ^{2}J = 4.0 Hz, H-8), 4.49 - 4.52 (1H, m, H-7), 4.61 - 4.65 (1H, m, H-7), AB spin system with A at 4.96 ppm and B at 5.10 ppm (4H, J_{AB} = 8.00 Hz, H-6), 7.54 - 7.57 (5H, m, H-1, H-2 and H-3). ^{13}**C{^{1}H} (100 MHz, $\mathbf{CD_3OD}$-d_4):** δ_C**(ppm)** = 47.62 (d, $^{1}J_{C-P}$ = 21.13 Hz, C-9), 54.26 (d, $^{1}J_{C-P}$ = 34.22 Hz, C-8), 67.29 (C-5), 71.49 (C-7), 81.14 (C-6), 126.87 (C-4), 130.59 (C-2), 131.98 (C-1), 134.24 (C-3). ^{31}**P{^{1}H} (162 MHz, $\mathbf{CD_3OD}$-d_4):** δ_P**(ppm)** = -81.43 (s). **ESI-MS (HR)** ***m/z*** 248.1318 (100 %, [M-Cl]$^+$ requires 248.1317). **Analysis for $\mathbf{C_{13}H_{19}ClN_3P{\cdot}0.5H_2O}$:** C, 53.34; H, 6.89; N, 14.35. Found: C, 53.28; H, 6.93; N, 15.60.

6.4.2 General Synthesis

Synthesis of 3.2-3.4

A suspension of **3.1** and [RuCl(μ-Cl)(p-cymene)]$_2$, [RhCl(μ-Cl)(Cp*)]$_2$ or [IrCl(μ-Cl)(Cp*)]$_2$ in dichloromethane was left to stir for 4 hours under an inert atmosphere (Ar). The resulting suspension was filtered by gravity to remove excess **3.1**, the filtrate collected and the solvent removed. The crystalline residue was washed with a mixture

of dichloromethane:diethyl ether (5:95 *v/v* %) and the isolated complex was dried *in vacuo*.

6.4.2.1 Ruthenium dichlorido PTA complex[8] (3.2)

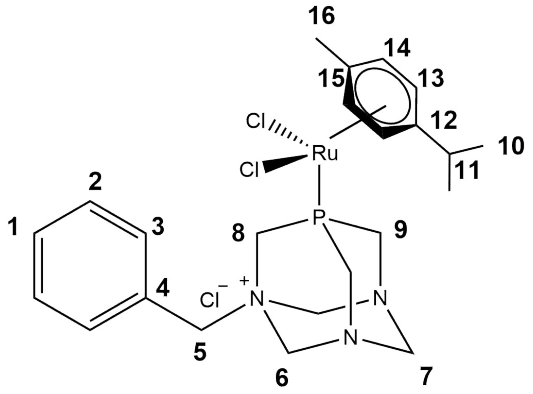

The alkylated benzyl PTA scaffold **3.1** (0.0474 g, 0.167 mmol) was reacted with [RuCl(μ-Cl)(*p*-cymene)]$_2$ (0.0523 g, 0.0854 mmol). Complex **3.2** was isolated as red crystalline flakes. Yield: 0.0691 g (68.6 %). **Melting Point:** 190°C– dec. with melting. $\mathbf{S_{293}}$**: (g/L ± SE, $\mathbf{H_2O}$)** = 12.2 ± 1.2. ^{1}**H NMR (400 MHz, $\mathbf{CDCl_3}$):** δ_H**(ppm)** = 1.22 (6H, d, ^3J = 6.8 Hz, H-10), 2.09 (3H, s, H-16), 2.79 (1H, sept, ^3J = 6.8 Hz, H-11), 4.18-4.21 (2H, m, H-9), 4.38 (2H, s, H-5), 4.44-4.47 (2H, m, H-9), 4.62 (2H, br s, H-8), 5.02-5.04 (2H, m, H-6), 5.27-5.31 (2H, m, H-7), 5.61-5.63 (2H, m, H-6), 5.95-6.05 (4H, m, H-13 and H-14), 7.49-7.61 (5H, m, H-1, H-2 and H-3). ^{13}**C{^{1}H} NMR (100 MHz, $\mathbf{CDCl_3}$):** δ_C**(ppm)** = 18.45 (C-16), 21.93 (C-10), 30.76 (C-11), 48.21 (d, $^1J_{C-P}$ = 20.5 Hz, C-9), 54.92 (d, $^3J_{C-P}$ = 10.1 Hz, C-7), 65.99 (C-8), 70.59 (d, $^3J_{C-P}$ = 3.2 Hz, C-5), 79.54 (C-6), 86.16 (d, $^2J_{C-P}$ = 5.9 Hz, C-14), 89.82 (d, $^2J_{C-P}$ = 4.4 Hz, C-13), 97.10 (C-15), 107.94 (C-12), 128.99 (C-4), 129.70 (C-2), 131.35 (C-1), 132.83 (C-3). ^{31}**P{^{1}H} NMR (162 MHz, $\mathbf{CDCl_3}$):** δ_P**(ppm)** = -20.07 (s). **ESI-MS (HR)** ***m/z*** 554.0833 (100 %, [M-Cl]$^+$ requires 554.0832). **Analysis Calc.** $\mathbf{C_{23}H_{33}Cl_3N_3PRu \cdot 2\,H_2O}$: C, 44.13; H, 5.96; N, 6.71. Found: C, 43.89; H, 5.77; N, 6.70.

6.4.2.2 Rhodium dichlorido PTA complex[8] (3.3)

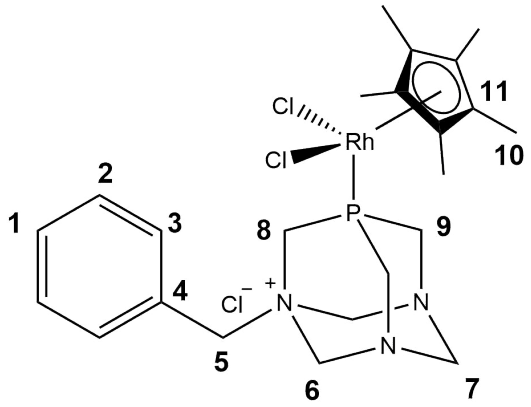

The alkylated benzyl PTA scaffold **3.1** (0.0707 g, 0.249 mmol) was reacted with [RhCl(μ-Cl)(Cp*)]$_2$ (0.0702 g, 0.114 mmol). Complex **3.3** was isolated as red crystalline flakes. Yield: 0.0781 g (58.0 %). **Melting Point:** 124°C– dec. with melting. **S_{293}: (g/L ± SE, H_2O)** =11.5 ± 5.7. **^{1}H NMR (400 MHz, $CDCl_3$):** δ_H**(ppm)** = 1.82 (15H, d, $^4J_{H-P}$ = 4.0 Hz, H-10), 4.26-4.28 (4H, m, H-9), 4.42 (1H, d, ^2J = 13.7 Hz, H-7), 4.57 (1H, d, ^2J = 14.1 Hz, H-7), 4.89-4.92 (2H, m, H-5), 5.03-5.05 (2H, d, $^1J_{H-P}$ = 2.6 Hz, H-8), 5.41-5.43 (4H, br m, H-6), 7.43-7.50 (3H, m, H-1 and H-2), 7.62 (2H, m, H-3). **^{13}C{^{1}H} NMR (100 MHz, $CDCl_3$):** δ_C**(ppm)** = 9.86 (C-10), 47.22 (d, $^1J_{C-P}$ = 16.1 Hz, C-9), 52.04 (d, $^1J_{C-P}$ = 9.5 Hz, C-8), 65.13 (C-5), 70.22 (C-7), 79.05 (C-6), 100.63 (d, $^1J_{C-Rh}$ = 3.7 Hz, C-11), 125.03 (C-4), 129.51 (C-2), 131.05 (C-1), 133.03 (C-3). **^{31}P{^{1}H} NMR (162 MHz, $CDCl_3$):** δ_P**(ppm)** = -24.16 (d, $^1J_{P-Rh}$ = 150.7 Hz). **ESI-MS (HR)** ***m/z*** 556.0906 (100 %, [M-Cl]$^+$ requires 556.0922). **Analysis Cal. for $C_{23}H_{34}Cl_3N_3PRh \cdot 2\,H_2O$**: C, 43.93; H, 6.09; N, 6.68. Found: C, 43.60; H, 6.05; N, 6.36.

6.4.2.3 Iridium dichlorido PTA complex[8] (3.4)

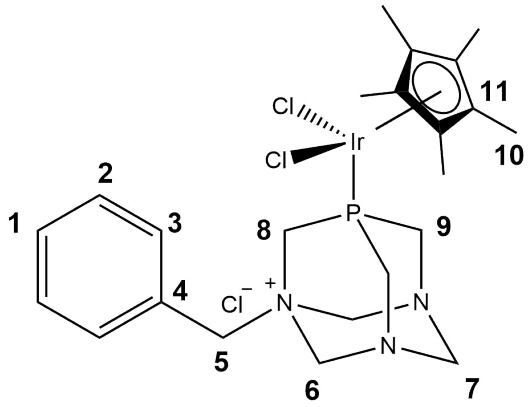

The alkylated benzyl PTA scaffold **3.1** (0.0604 g, 0.213 mmol) was reacted with [IrCl(μ-Cl)(Cp*)]$_2$ (0.0805 g, 0.101 mmol). Complex **3.4** was isolated as orange crystalline flakes. Yield: 0.0681 g (49.4 %). **Melting Point:** 176°C– dec. with melting. **S_{293}: (g/L ± SE, H_2O)** = 13.7 ± 3.4. **^{1}H NMR (400 MHz, $CDCl_3$):** δ_H**(ppm)** = 1.87 (15H, d, $^4J_{H-P}$ = 2.0 Hz, H-10), 4.23 (4H, m, H-9), 4.41 (1H, d, ^2J = 13.4 Hz, H-7), 4.68 (1H, d, ^2J = 13.4 Hz, H-7), 4.90-5.00 (4H, m , H-5 and H-8), 5.37 (2H, d, ^2J = 11.2 Hz, H-6), 5.54 (2H, d, ^2J = 11.5 Hz, H-6), 7.43-7.53 (3H, m, H-1 and H-2), 7.63 (2H, d, ^3J = 7.1 Hz, H-3). **^{13}C{^{1}H} NMR (100 MHz, $CDCl_3$):** δ_C**(ppm)** = 9.48 (C-10), 45.77 (d, $^1J_{C-P}$ = 23.5 Hz, C-9), 50.12 (d, $^1J_{C-P}$ = 19.1 Hz, C-8), 64.90 (C-5), 70.29 (d, $^3J_{C-P}$ = 5.9 Hz, C-7), 79.17 (C-6), 94.13 (d, $^2J_{C-P}$ = 2.2 Hz, C-11), 125.01 (C-4), 129.47 (C-2), 130.99 (C-1), 132.99 (C-3). **^{31}P{^{1}H} NMR (162 MHz, $CDCl_3$):** δ_P**(ppm)** = -51.26 (s). **ESI-MS (HR)** ***m/z*** 305.5901 (100%, [M-2Cl]$^{2+}$ requires 305.5904). **Analysis Calc. for $C_{23}H_{34}Cl_3IrN_3P \cdot (C_2H_5)_2O$**: C, 42.88; H, 5.87; N, 5.56. Found: C, 42.88; N, 6.02; N, 5.87.

6.5 (*N,O*)-Salicylaldimine metal PTA dicationic complexes (3.5-3.16)

6.5.1 General Synthesis

(i) Synthesis of 3.5-3.7

A suspension of the alkylated benzyl PTA scaffold **3.1** and **2.5**, **2.6** or **2.7** in dichloromethane was left to stir for 24 hours under an inert atmosphere (Ar) at ambient temperature. The resulting suspension was filtered by gravity to remove excess **3.1**, the filtrate collected and the solvent removed. The resulting solid was washed with a mixture of dichloromethane:diethyl ether (5:95 *v/v* %) and the resulting amorphous powder dried *in vacuo*.

(ii) Synthesis of 3.8-3.10, 3.14 and 3.15

Under an inert atmosphere (Ar), silver hexafluorophosphate and **2.8**, **2.9**, **2.10**, **2.15** or **2.16** were stirred in acetone at -40 °C. The resulting solution was warmed to room temperature and stirred for an additional 60 minutes. The solution was then cooled to -40 °C and **3.1** added. The mixture was then warmed to room temperature. The suspension was stirred for an additional 30 minutes, the mixture filtered through Celite®, the filtrate collected and the solvent removed *in vacuo*. The residue was dried *in vacuo* to yield the proposed complex as an amorphous powder.

(iii) Synthesis of 3.11-3.13

A solution of **3.1** and **2.11**, **2.13** or **2.14** in dry ethanol (10 mL) was left to stir for 24 hours under an inert atmosphere (Ar). The solvent was removed to yield a red or orange residue. This residue was dissolved in a minimal amount of dichloromethane, filtered by gravity to remove excess **3.1** and the product precipitated using *n*-pentane. The resulting powder was filtered by vacuum filtration and dried *in vacuo*.

6.5.1.1 Ruthenium propylsalicylaldimine PTA complex (3.5)

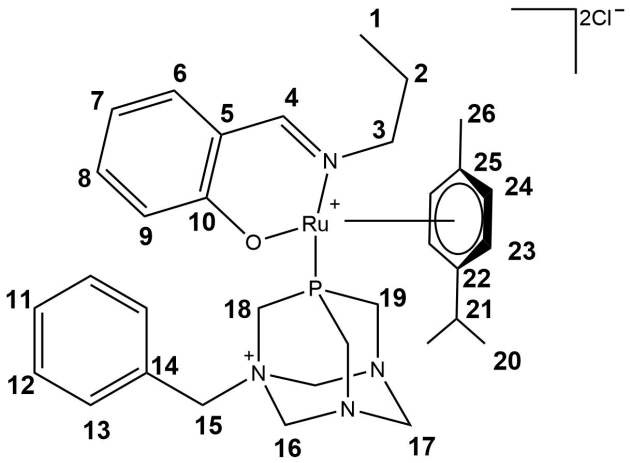

3.1 (0.0335 g, 0.118 mmol) was reacted with **2.5** (0.0496 g, 0.115 mmol). Complex **3.5** was isolated as a green powder. Yield: 0.0653 g (76.3 %). **Melting Point:** 164°C to dec. with melting. **^{1}H NMR (400 MHz, CD_3OD-d_4):** δ_H**(ppm)** = 1.11 (6H, m, H-1 and H-20), 1.28 (3H, d, ^3J = 7.0 Hz, H-20), 1.95-2.04 (2H, m, H-2), 2.17 (3H, s, H-26), 2.58 (1H, sept, ^3J = 7.0 Hz, H-21), 3.59-3.67 (1H, m, H-3), 3.89 (1H, m, H-19), 3.96-4.07 (1H, m, H-3), 4.21 (1H, m, H-19), 4.36-4.67 (7H, m, H-19 and H-18 and H-15 and H-17), 4.82-4.86 (1H, m, H-17), 5.04-5.07 (1H, m, H-16), 5.18-5.29 (3H, m, H-16), 5.71 (1H, d, ^3J = 5.9 Hz, H-23), 5.87 (1H, d, ^3J = 5.9 Hz, H-24), 6.39 (1H, d, ^3J = 5.9 Hz, H-24), 6.55-6.58 (1H, m, H-23), 6.63-6.67 (2H, m, H-6 and H-8), 7.22-7.26 (2H, m, H-9 and H-11), 7.37-7.45 (4H, m, H-12 and H-13), 7.51-7.60 (1H, m, H-7), 8.11 (1H, d, ^4J = 2.0 Hz, H-4). **^{13}C{^{1}H} NMR (100 MHz, CD_3OD-d_4):** δ_C**(ppm)** = 11.53 (C-1), 18.86 (C-26), 21.82 (C-20), 22.59 (C-20), 26.19 (C-2), 32.29 (C-21), 48.62 (C-19), 51.77 (d, $^1J_{C-P}$ = 11.7 Hz, C-18), 66.55 (C-15), 70.75 (d, $^3J_{C-P}$ = 5.9 Hz, C-17), 73.76 (C-3), 80.84 (d, $^3J_{C-P}$ = 2.9 Hz, C-16), 86.86 (C-23), 89.34 (C-25), 89.43 (C-24), 90.82 (C-23), 93.51 (C-24), 101.62 (C-22), 117.58 (C-8), 122.55 (C-5), 123.48 (C-6), 130.02 (C-14), 130.71 (C-12), 132.07 (C-11), 134.07 (C-13), 136.74 (C-9), 136.99 (C-7), 164.25 (C-10), 169.13 (C-4). **^{31}P{^{1}H} NMR (162 MHz, CD_3OD-d_4):** δ_P**(ppm)** = -13.77 (s). **IR (ATR):** ν_{max}**/cm^{-1}** = 1598 (C=N). **ESI-MS (HR)** ***m/z*** 681.2059 (15%, [M-Cl]$^+$ requires 681.2058). **Analysis Calc.** $\mathbf{C_{33}H_{45}Cl_2N_4OPRu \cdot 2\,H_2O}$: C, 52.66; H, 6.56; N, 7.44. Found: C, 52.15; H, 6.41; N, 7.86.

6.5.1.2 Rhodium propylsalicylaldimine PTA complex (3.6)

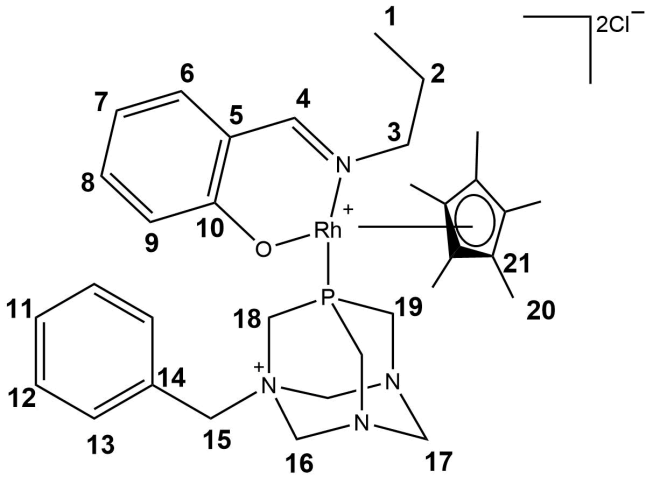

3.1 (0.0205 g, 0.0772 mmol) was reacted with **2.6** (0.0296 g, 0.0679 mmol). Compound **3.6** was isolated as a red powder. Yield: 0.0257 g (52.6 %). **Melting Point:** 87°C to dec. with melting. $\mathbf{S_{293}}$**: (g/L ± SE, $\mathbf{H_2O}$)** = 19.3 ± 3.1. ^{1}**H NMR (400 MHz, $\mathbf{CD_3OD}$-d_4):** δ_H **(ppm)** = 1.12 (3H, t, ^{3}J = 7.3 Hz, H-1), 1.72 (15H, d, $^{4}J_{H-P}$ = 3.9 Hz, H-20), 1.87-1.96 (1H, m, H-2), 1.98-2.09 (1H, m, H-2), 3.67-3.72 (1H, m, H-3), 3.85-3.93 (1H, m, H-3), 4.03-4.06 (1H, m, H-19), 4.15-4.19 (1H, m, H-19), 4.30-4.35 (2H, m, H-19), 4.44-4.59 (5H, m, H-15 and H-17 and H-18), 4.81-4.85 (1H, m, H-17), 5.06-5.09 (1H, m, H-16), 5.18-5.26 (3H, m, H-16), 6.69-6.74 (2H, m, H-6 and H-8), 7.28-7.35 (2H, m, H-12), 7.40 (4H, m, H-9 and H-11 and H-13), 7.48-7.52 (1H, m, H-7), 8.26 (1H, s, H-4). ^{13}**C{^{1}H} NMR (100 MHz, $\mathbf{CD_3OD}$-d_4):** δ_C**(ppm)** = 9.68 (C-20), 11.54 (C-1), 25.39 (C-2), 46.85 (d, $^{1}J_{C-P}$ = 10.1 Hz, C-19), 48.08 (d, $^{1}J_{C-P}$ = 14.1 Hz, C-19), 50.64 (d, $^{1}J_{C-P}$ = 11.1 Hz, C-18), 66.52 (C-15), 69.10 (C-17), 70.79 (C-3), 80.97 (d, $^{3}J_{C-P}$ = 37.2 Hz, C-16), 102.57 (d, $^{1}J_{C-Rh}$ = 5.1 Hz, C-21), 117.92 (C-8), 118.93 (C-5), 125.04 (C-6), 126.12 (C-14), 130.69 (C-12), 132.18 (C-11), 134.05 (C-13), 137.00 (C-7 and C-9), 166.98 (C-10), 168.18 (C-4). ^{31}**P{^{1}H} NMR (162 MHz, $\mathbf{CD_3OD}$-d_4):** δ_P**(ppm)** = -22.67 (d, $^{1}J_{P-Rh}$ = 152.0 Hz). **IR (ATR):** ν_{max}**/cm^{-1}** = 1619 (C=N). **ESI-MS (HR)** ***m/z*** 683.2157 (10%, [M-Cl]$^{+}$ requires 683.2147).

6.5.1.3 Iridium propylsalicylaldimine PTA complex (3.7)

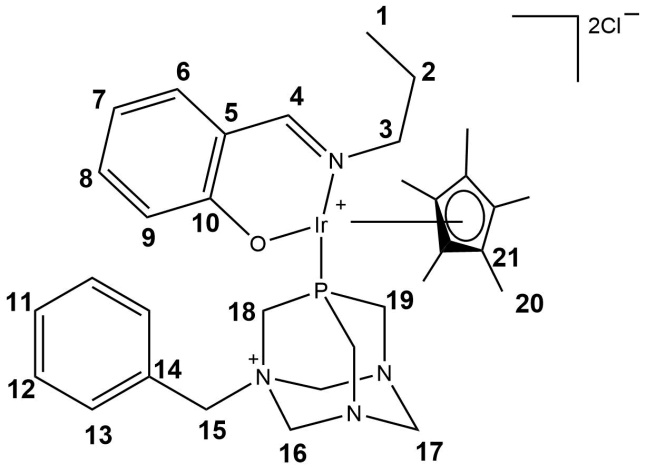

3.1 (0.0281 g, 0.0990 mmol) was reacted with **2.7** (0.0506 g, 0.0964 mmol). Complex **3.7** was isolated as a yellow powder. Yield: 0.0653 g (83.8%). **Melting Point:** 137°C to dec. with melting. $\mathbf{S_{293}}$**: (g/L, $\mathbf{H_2O}$)** = 33.4 ± 3.2. ^{1}**H NMR (400 MHz, $\mathbf{CD_3OD}$-d_4):** δ_H **(ppm)** = 1.09 (3H, t, ^{3}J = 7.3 Hz, H-1), 1.75-1.76 (15H, m, H-20), 1.93-1.99 (1H, m, H-2), 2.05-2.11 (1H, m, H-2), 3.72-3.80 (1H, m, H-3), 3.94-4.02 (1H, m, H-3), 4.08-4.18 (2H, m, H-19), 4.26-4.39 (2H, m, H-19), 4.43-4.48 (4H, m, H-15 and H-18), 4.60-4.63 (1H, m, H-17), 4.80-4.82 (1H, m, H-17), 5.06-5.09 (1H, m, H-16), 5.21-5.28 (3H, m, H-16), 6.70-6.76 (2H, m, H-6 and H-8), 7.37-7.43 (6H, m, H-9 and H-11 and H-12 and H-13), 7.50-7.53 (1H, m, H-7), 8.14 (1H, s, H-4). ^{13}**C{^{1}H} NMR (100 MHz, $\mathbf{CD_3OD}$-d_4):** δ_C**(ppm)** = 9.60 (C-20), 11.29 (C-1), 25.41 (C-2), 46.00 (d, $^{1}J_{C-P}$ = 20.1 Hz, C-19), 47.03 (d, $^{1}J_{C-P}$ = 17.6 Hz, C-18), 66.41 (C-15), 70.82 (C-17), 72.24 (C-3), 80.97 (C-16), 96.66 (C-21), 118.82 (C-8), 123.37 (C-5), 123.58 (C-6), 126.16 (C-14), 130.73 (C-12), 132.19 (C-11), 134.06 (C-13), 136.41 (C-9), 137.08 (C-7), 163.40 (C-10), 165.69 (C-4). ^{31}**P{^{1}H} NMR (162 MHz, $\mathbf{CD_3OD}$-d_4):** δ_P**(ppm)** = -42.69 (s). **IR (ATR):** ν_{max}**/cm^{-1}** = 1625 (C=N). **ESI-MS (HR)** ***m/z*** 773.2709 (55%, [M-Cl]$^{+}$ requires 773.2722). **Analysis Calc.** $\mathbf{C_{33}H_{46}Cl_2IrN_4OP \cdot 7\,H_2O}$: C, 42.39; H, 6.47; N, 5.99. Found: C, 42.81; H, 5.55; N, 5.78.

6.5.1.4 Ruthenium trifluorosalicylaldimine PTA complex (3.8)

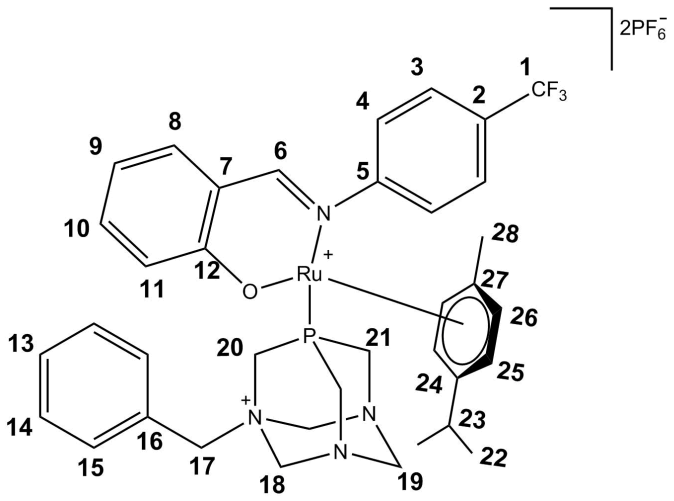

Silver hexafluorophosphate (0.0430 g, 0.169 mmol), **2.8** (0.0412 g, 0.0770 mmol) and **3.1** (0.0224 g, 0.0789 mmol) were reacted. Compound **3.8** was isolated as a green powder. Yield: 0.0351 g (43.9 %). **Melting Point:** 170°C to dec. with melting. **^{1}H NMR (400 MHz, CD_3OD-d_4):** δ_H**(ppm)** = 1.07 (3H, d, ^3J = 6.8 Hz, H-22), 1.16 (3H, d, ^3J = 7.1 Hz, H-22), 1.72 (3H, s, H-28), 2.25 (1H, sept, ^3J = 6.9 Hz, H-23), 3.71-3.75 (1H, m, H-21), 4.07-4.11 (1H, m, H-21), 4.17-4.22 (2H, m, H-21), 4.25-4.31 (2H, m, H-17), 4.42-4.50 (2H, m, H-20), 4.53-4.57(1H, m, H-19), 4.71-4.73 (1H, m, H-19), 4.82-4.85 (1H, m, H-18), 5.07-5.24 (3H, m, H-18), 5.45 (1H, d, ^3J = 5.4 Hz, H-26), 6.21 (1H, d, ^3J = 6.1 Hz, H-25), 6.32-6.35 (1H, m, H-25), 6.61-6.67 (2H, m, H-26 and H-10), 7.24-7.29 (2H, m, H-8 and H-11), 7.37-7.39 (2H, m, H-14), 7.45-7.52 (5H, m, H-3, H-13 and H-15), 7.56-7.60 (1H, m, H-9), 7.90-7.92 (2H, m, H-4), 8.14 (1H, d, ^4J = 2.2 Hz, H-6). **^{31}P{^{1}H} NMR (162 MHz, CD_3OD-d_4):** δ_P**(ppm)** = -144.3 (2P, sept, $^1J_{P-F}$ = 708.8 Hz,PF_6), -16.77 (1P, s, **P**$(CH_2N)_3$). **IR (ATR):** ν_{max}**/cm^{-1}** = 1600 (C=N). **ESI-MS (HR)** ***m/z*** 893.1887 (40%, [M-PF_6]$^+$ requires 893.1734). **Analysis Calc. $C_{37}H_{42}F_{15}N_4OP_3Ru$**: C, 42.82; H, 4.06; N, 5.40. Found: C, 42.29; H, 3.87; N, 5.20.

6.5.1.5 Rhodium trifluorosalicylaldimine PTA complex (3.9)

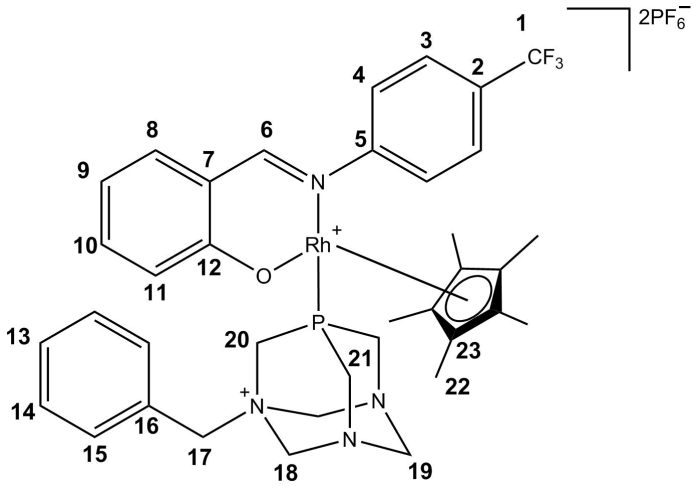

Silver hexafluorophosphate (0.0330 g, 0.130 mmol), **2.9** (0.0321 g, 0.0632 mmol) and **3.1** (0.0191 g, 0.0673 mmol) were reacted. Compound **3.9** was isolated as a red powder. Yield: 0.0114 g (17.3 %). **Melting Point:** 180°C to dec. with melting. **^{1}H NMR (400 MHz, CD_3OD-d_4):** δ_H**(ppm)** = 1.34-1.46 (15H, m, H-22), 3.99-4.07 (2H, m, H-21), 4.17-4.20 (1H, m, H-21), 4.27-4.28 (2H, m, H-17), 4.41-4.45 (1H, m, H-21), 4.53-4.57 (2H, m, H-20), 4.65-4.71 (1H, m, H-19), 4.82-4.91 (2H, m, H-18 and H-19), 4.99-5.02 (1H, m, H-18), 5.15-5.21 (2H, m, H-18), 6.73-6.76 (1H, m, H-10), 6.83-6.85 (1H, m, H-8), 7.32-7.34 (2H, m, H-14), 7.43-7.53 (7H, m, H-3, H-9, H-11, H-13 and H-15), 7.94-7.96 (2H, m, H-4), 8.50 (1H, s, H-6). **^{31}P{^{1}H} NMR (162 MHz, CD_3OD-d_4):** δ_P**(ppm)** = -144.42 (2P, sept, $^1J_{P-F}$ = 708.8 Hz, PF_6), -26.52 (1P, d, $^1J_{P-Rh}$ = 148.7 Hz, **P**$(CH_2N)_3$). **IR (ATR):** ν_{max}**/cm^{-1}** = 1599 (C=N). **ESI-MS (HR)** ***m/z*** 1040.1489 (20%, $[M]^+$ requires 1040.1465), 502.0871 (100%, $[M\text{-}2PF_6\text{-}C_{13}H_{19}N_3P]^+$ requires 502.0865). **Analysis Calc.** $\mathbf{C_{37}H_{43}F_{15}N_4OP_3Rh \cdot 4\,H_2O}$: C, 39.94; H, 4.62; N, 5.04. Found: C, 39.76; H, 4.45; N, 4.73.

6.5.1.6 Iridium trifluorosalicylaldimine PTA complex (3.10)

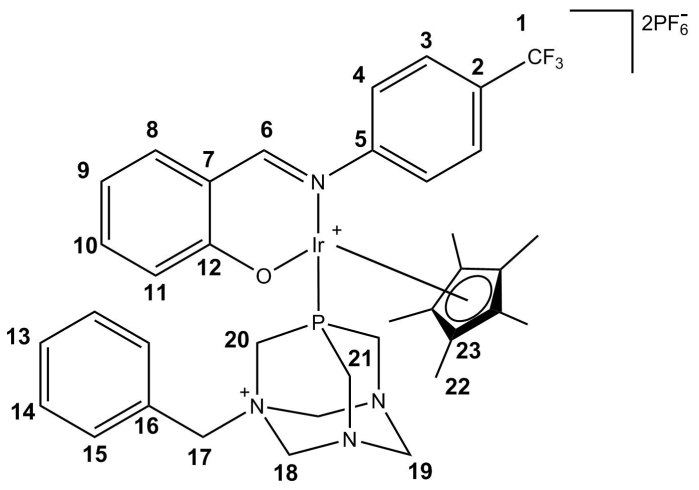

Silver hexafluorophosphate (0.0420 g, 0.165 mmol), **2.10** (0.0412 g, 0.0657 mmol) and **3.1** (0.0187 g, 0.0659 mmol) were reacted. Compound **3.10** was isolated as a yellow powder. Yield: 0.0221 g (19.6 %). **Melting Point:** 164°C– dec. with melting. **^{1}H NMR (400 MHz, CD_3OD-d_4):** δ_H**(ppm)** = 1.49 (15H, d, $^4J_{H-P}$ = 2.7 Hz, H-22), 4.05-4.12 (2H, m, H-21), 4.19-4.30 (2H, m, H-17), 4.39-4.50 (2H, m, H-21), 4.55-4.69 (2H, m, H-20), 4.86-4.95 (2H, m, H-19), 5.00-5.09 (2H, m, H-18), 5.19-5.25 (2H, m, H-18), 6.74-6.79 (1H, m, H-10), 6.86 (1H, d, ^3J = 8.2 Hz, H-8), 7.32-7.35 (2H, m, H-9 and H-11), 7.44-7.57 (7H, m, H-3, H-13, H-14 and H-15), 7.95 (2H, d, ^3J = 8.3 Hz, H-4), 8.47-8.48 (1H, m, H-6). **^{31}P{^{1}H} NMR (162 MHz, CD_3OD-d_4):** δ_P**(ppm)** = -144.41 (2P, sept, $^1J_{P-F}$ = 708.0 Hz, PF_6), -44.02 (1P, s, **P**$(CH_2N)_3$). **IR (ATR):** ν_{max}**/cm^{-1}** = 1602 (C=N). **ESI-MS (HR)** ***m/z*** 592.1453 (65%, [M-2PF_6-$C_{13}H_{19}N_3P$]$^+$ requires 592.1453). **Analysis Calc.** $\mathbf{C_{37}H_{43}F_{15}IrN_4OP_3 \cdot CH_2Cl_2}$: C, 36.64; H, 3.64; N, 4.50. Found: C, 35.95; H, 3.29; N, 5.01.

6.5.1.7 Ruthenium silane PTA complex (3.11)

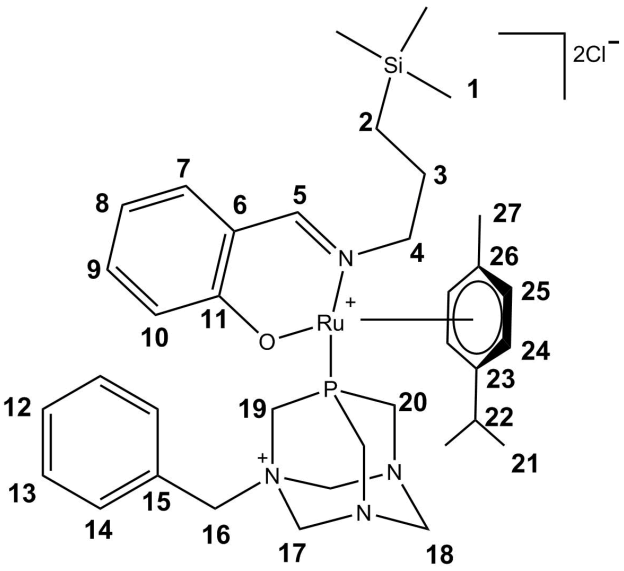

3.1 (0.0178 g, 0.0627 mmol) was reacted with **2.11** (0.0399 g, 0.0790 mmol). Complex **3.11** was isolated as a black powder. Yield: 0.0317 g (64.1 %). **Melting Point:** 119°C to dec. with melting. **^{1}H NMR (400 MHz, CD_3OD-d_4):** δ_H**(ppm)** = 0.13-0.15 (9H, m, H-1), 0.59-0.75 (2H, m, H-2), 1.13 (3H, d, ^3J = 7.0 Hz, H-21), 1.28 (3H, d, ^3J = 7.0 Hz, H-21), 1.98-2.04 (2H, m, H-3), 2.16 (3H, s, H-27), 2.57 (1H, sept, ^3J = 7.0 Hz, H-22), 3.52-3.61 (1H, m, H-4), 3.88-3.92 (1H, m, H-20), 4.03-4.10 (1H, m, H-4), 4.18-4.21 (1H, m, H-20), 4.32-4.45 (4H, m, H-16 and H-20), 4.52-4.67 (3H, m, H-18 and H-19), 4.81-4.83 (1H, m, H-18), 5.04-5.07 (1H, m, H-17), 5.17-5.25 (3H, m, H-17), 5.71 (1H, d, ^3J = 6.1 Hz, H-24), 5.83 (1H, d, ^3J = 5.6 Hz, H-25), 6.35 (1H, d, ^3J = 6.0 Hz, H-25), 6.50-6.53 (1H, m, H-24), 6.65-6.68 (2H, m, H-7 and H-9), 7.25-7.28 (2H, m, H-10 and H-12), 7.34-7.36 (2H, m, H-14), 7.41-7.44 (2H, m, H-13), 7.50-7.54 (1H, m, H-8), 8.08-8.11 (1H, m, H-5). **^{13}C{^{1}H} NMR (100 MHz, CD_3OD-d_4):** δ_C**(ppm)** = -1.48 (C-1), 14.71 (C-2), 18.87 (C-27), 21.89 (C-21), 22.56 (C-21), 27.51 (C-3), 32.27 (C-22), 48.61 (d, $^1J_{C-P}$ = 15.6 Hz, H-20), 50.27 (d, $^1J_{C-P}$ = 15.4 Hz, H-19), 51.72 (d, $^1J_{C-P}$ = 11.7 Hz, H-20), 66.75 (C-16), 70.87 (d, $^3J_{C-P}$ = 6.6 Hz, H-18), 75.04 (C-4), 80.95 (C-17), 86.93 (C-24), 89.26 (C-26), 89.36 (C-25), 93.51 (C-24), 101.82 (C-23), 117.65 (C-9), 120.71 (C-14), 122.70 (C-6), 123.53 (C-7), 126.11 (C-10), 130.74 (C-13), 132.10 (C-12), 134.10 (C-10), 136.74 (C-15), 137.02 (C-8), 164.38 (C-5), 169.13 (C-11). **^{31}P{^{1}H} NMR (162 MHz, CD_3OD-d_4):** δ_P**(ppm)** = -13.29 (s). **IR (ATR):** ν_{max}**/cm^{-1}** = 1601 (C=N). **ESI-MS (HR)** ***m/z*** 735.2667 (75%,

[M-2Cl+OH]$^+$ requires 735.2792). **Analysis Calc. $C_{36}H_{53}Cl_2N_4OPRuSi \cdot 2\,H_2O$**: C, 52.42; H, 6.97; N, 6.79. Found: C, 52.74; H, 6.44; N, 7.31.

6.5.1.8 Iridium silane PTA complex (3.12)

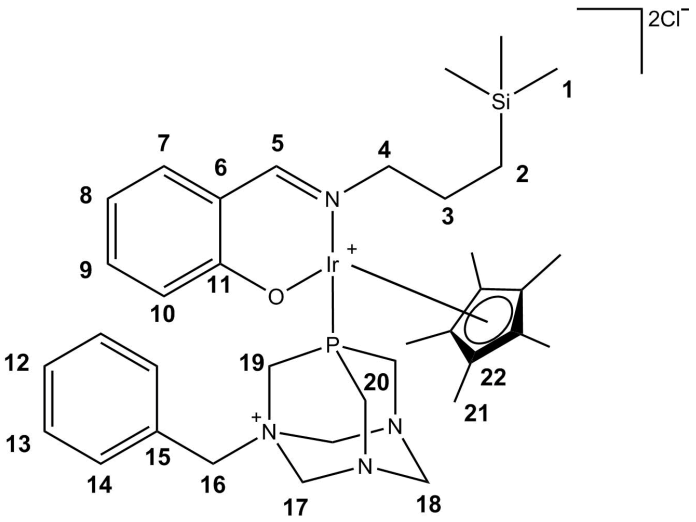

3.1 (0.0201 g, 0.0708 mmol) was reacted with **2.13** (0.0278 g, 0.0465 mmol). Complex **3.12** was isolated as an orange powder. Yield: 0.0173 g (42.2 %). **Melting Point:** 79 – 84 °C. **S_{293}: (g/L ± SE, H_2O)** = 29.8 ± 2.7. **^{1}H NMR (400 MHz, CD_3OD-d_4):** δ_H**(ppm)** = 0.13 (9H, s, H-1), 0.57-0.65 (1H, m, H-2), 0.70-0.78 (1H, m, H-2), 1.75 (15H, d, $^4J_{H-P}$ = 2.6 Hz, H-21), 1.88-1.97 (1H, m, H-3), 2.13-2.22 (1H, m, H-3), 3.65-3.72 (1H, m, H-4), 4.16-4.22 (3H, m, H-4 and H-20), 4.29-4.33 (1H, m, H-20), 4.49-4.57 (5H, m, H-16 and H-19 and H-20), 4.62-4.65 (1H, m, H-18), 4.79-4.82 (1H, m, H-18), 5.05-5.08 (1H, m, H-17), 5.27-5.35 (3H, m, H-17), 6.71-6.75 (2H, m, H-7 and H-9), 7.35-7.43 (6H, m, H-8 and H-10 and H-13 and H-14), 7.46-7.51 (1H, m, H-12), 8.17 (1H, s, H-5). **^{13}C{^{1}H} NMR (100 MHz, CD_3OD-d_4):** δ_C**(ppm)** = -1.47 (C-1), 9.66 (C-21), 14.50 (C-2), 26.71 (C-3), 46.04 (d, $^1J_{C-P}$ = 19.8 Hz, C-19), 47.08 (d, $^1J_{C-P}$ = 18.3 Hz, C-20), 49.36 (d, $^1J_{C-P}$ = 18.3 Hz, C-20), 66.20 (C-16), 70.81 (d, $^3J_{C-P}$ = 6.6 Hz, C-18), 73.58 (C-4), 80.44 (d, $^3J_{C-P}$ = 4.4 Hz, C-17), 81.07 (d, $^3J_{C-P}$ = 4.4 Hz, C-17), 96.56 (d, $^2J_{C-P}$ = 2.9 Hz, C-22), 118.77 (C-9), 123.41 (C-6), 123.50 (C-7), 126.19 (C-15), 130.62 (C-13), 132.05 (C-14), 134.08 (C-12), 136.41 (C-10), 136.97 (C-8), 163.33 (C-11), 165.57 (C-5). **^{31}P{^{1}H} NMR (162 MHz, CD_3OD-d_4):** δ_P**(ppm)** = -42.27 (s). **IR (ATR):** ν_{max}**/cm^{-1}** = 1607 (C=N). **ESI-MS (HR)** ***m/z*** 845.3151 (100%, [M-Cl]$^+$ requires 845.3115). **Analysis Calc. $C_{36}H_{54}Cl_2IrN_4OPSi \cdot 3\,H_2O$**:

C, 46.24; H, 6.47; N, 5.99. Found: C, 46.18; H, 6.17; N, 5.93.

6.5.1.9 Ruthenium ferrocenyl PTA complex (3.13)

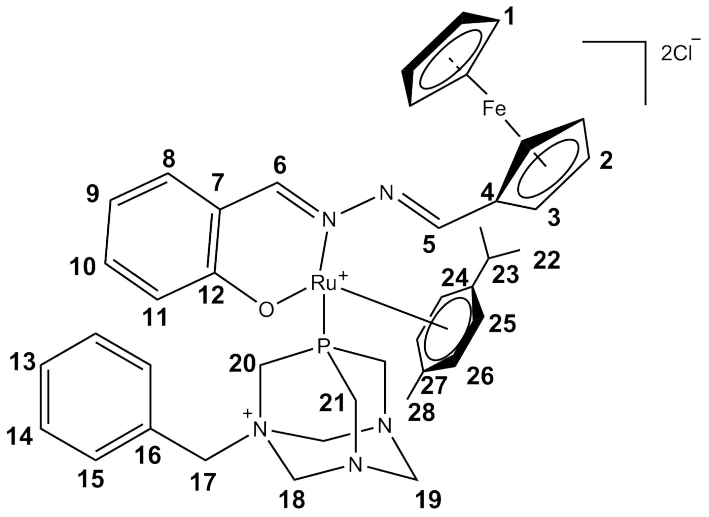

3.1 (0.0216 g, 0.0761 mmol) was reacted with **2.14** (0.0428 g, 0.0711 mmol). Complex **3.13** was isolated as a red powder. Yield: 0.0144 g (22.9 %). **^{1}H NMR (400 MHz, CD_3OD-d_4):** δ_H**(ppm)** = 1.12 (3H, d, ^3J = 6.8 Hz, H-22), 1.19 (3H, d, ^3J = 6.8 Hz, H-22), 2.00 (3H, s, H-28), 2.50 (1H, sept, ^3J = 6.8 Hz, H-23), 4.14-4.18 (2H, m, H-21), 4.26-4.42 (11H, m, H-1, H-17, H-20 and H-21), 4.57-4.60 (2H, m, H-2 and H-19), 4.68-4.70 (2H, m, H-3), 4.84-4.91 (2H, m, H-2 and H-19), 5.14-5.28 (4H, m, H-18), 5.80-5.83 (2H, m, H-25 and H-26), 6.31 (1H, d, ^3J = 5.9 Hz, H-25), 6.42 (1H, d, ^3J = 5.1 Hz, H-26), 6.71-6.77 (2H, m, H-8 and H-10), 7.32-7.38 (4H, m, H-9, H-11 and H-15), 7.42-7.46 (2H, t, ^3J = 7.5 Hz, H-14), 7.53-7.61 (1H, m, H-13), 7.93 (1H, d, ^3J = 2.0 Hz, H-6), 8.51 (1H, s, H-5). **^{13}C{^{1}H} NMR (100 MHz, CD_3OD-d_4):** δ_C**(ppm)** = 18.47 (C-28), 22.10 (C-22), 22.69 (C-22), 32.19 (C-23), 49.41 (d, $^1J_{C-P}$ = 23.1 Hz, C-21), 50.06 (d, $^1J_{C-P}$ = 16.1 Hz, C-20), 51.97 (d, $^1J_{C-P}$ = 11.0 Hz, C-21), 66.67 (C-17), 69.78 (C-2), 71.00 (C-1), 71.54 (C-19), 73.54 (C-3), 73.72 (C-3), 76.97 (C-4), 80.89 (m, C-18), 81.19 (C-18), 88.27 (C-25), 88.40 (C-26), 92.15 (C-26), 93.83 (C-25), 104.00 (C-27), 117.12 (C-24), 117.95 (C-10), 121.08 (C-7), 123.66 (C-8), 126.15 (C-16), 130.82 (C-14), 132.19 (C-13), 134.13 (C-15), 136.25 (C-11), 136.90 (C-9), 157.03 (C-6), 161.26 (C-5), 165.65 (C-12). **^{31}P{^{1}H} NMR (162 MHz, CD_3OD-d_4):** δ_P**(ppm)** = -11.94 (s). **IR (ATR):** ν_{max}**/cm^{-1}** = 1599 (C=N). **ESI-MS (HR)** ***m/z*** 567.0771 (40%, [M-Cl-$C_{13}H_{19}ClN_3P$]$^+$ requires 567.0673). **Anal-**

ysis Calc. $\mathbf{C_{41}H_{48}Cl_2FeN_5OPRu \cdot 4\,H_2O}$: C, 51.42; H, 5.89; N, 7.31. Found: C, 51.91; H, 5.75; N, 7.20.

6.5.1.10 Rhodium ferrocenylimine PTA complex (3.14)

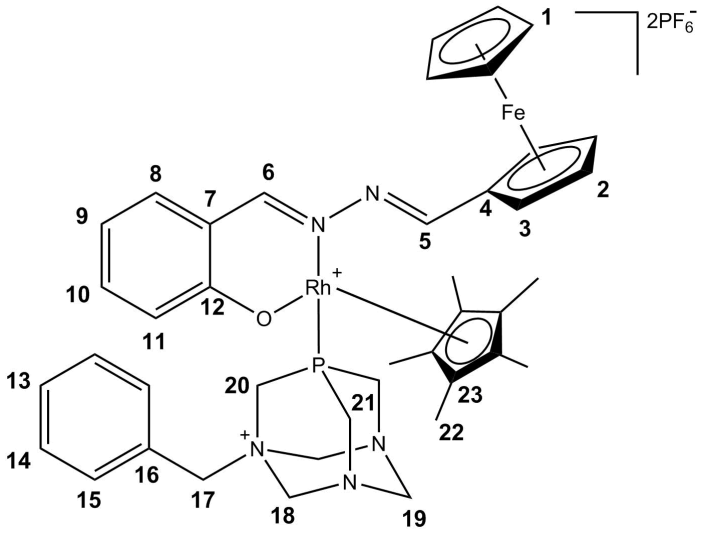

Silver hexafluorophosphate (0.0470 g, 0.185 mmol), **2.15** (0.0419 g, 0.0693 mmol) and **3.1** (0.0247 g, 0.0870 mmol) were reacted. Compound **3.14** was isolated as a red powder. Yield: 0.0194 g (25.3 %). **Melting Point:** 175°C to dec. with melting. **^{1}H NMR (400 MHz, CD_3OD-d_4):** δ_H**(ppm)** = 1.69 (15H, d, $^4J_{H-P}$ = 3.9 Hz, H-22), 3.89-3.94 (1H, m, H-21), 4.01-4.10 (3H, m, H-21), 4.21-4.23 (2H, m, H-17), 4.39 (5H, s, H-1), 4.55-4.59 (2H, m, H-20), 4.71-4.72 (2H, m, H-2), 4.77-4.79 (1H, m, H-19), 4.84-4.86 (2H, m, H-3), 4.92-5.01 (2H, m, H-18 and H-19), 5.13-5.21 (3H, m, H-18), 6.77-6.81 (1H, m, H-10), 6.86-6.90 (1H, m, H-8), 7.22-7.26 (1H, m, H-11), 7.40-7.46 (4H, m, H-14 and H-15), 7.50-7.56 (2H, m, H-9 and H-13), 8.31 (1H, s, H-5), 8.34 (1H, s, H-6). **^{31}P{^{1}H} NMR (162 MHz, CD_3OD-d_4) :** δ_P**(ppm)** = -144.43 (2P, sept, $^1J_{P-F}$ = 710.1 Hz, PF_6), -23.09 (1P, d, $^1J_{P-Rh}$ = 150.6 Hz, $\mathbf{P}(CH_2N)_3$). **IR (ATR):** ν_{max}**/cm^{-1}** = 1600 (C=N). **ESI-MS (HR)** ***m/z*** 569.0773 (100%, [M-2PF_6-$C_{13}H_{19}N_3P$]$^+$ requires 569.0757). **Analysis Calc.** $\mathbf{C_{41}H_{49}F_{12}FeN_5OP_3Rh \cdot 5\,H_2O}$: C, 41.12; H, 4.97; N, 5.85. Found: C, 41.02; H, 3.50; N, 5.84.

6.5.1.11 Iridium ferrocenylimine PTA complex (3.15)

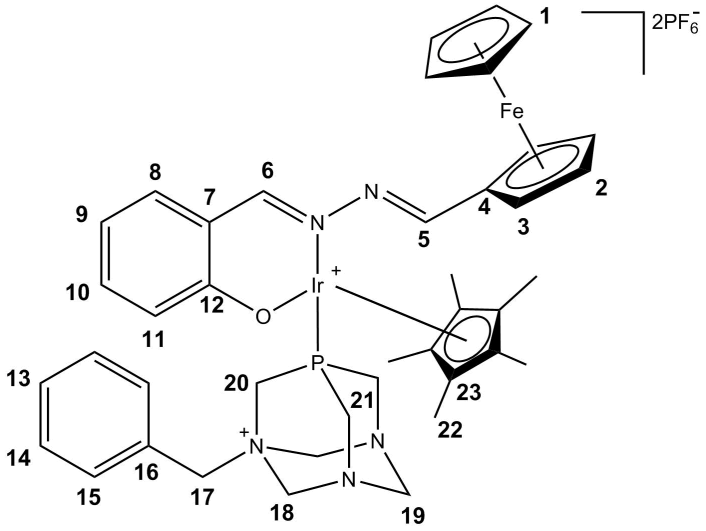

Silver hexafluorophosphate (0.0440 g, 0.173 mmol), **2.16** (0.0391 g, 0.0563 mmol) and **3.1** (0.0181 g, 0.0637 mmol) were reacted. Compound **3.15** was isolated as a red powder. Yield: 0.0243 g (36.1 %). **Melting Point:** 180°C– dec. with melting. **^{1}H NMR (400 MHz, CD_3OD-d_4):** δ_H**(ppm)** = 1.71 (15H, d, $^4J_{H-P}$ = 2.58 Hz, H-22), 3.98-4.11 (4H, m, H-17 and H-21), 4.18-4.26 (2H, m, H-21), 4.37 (5H, s, H-1), 4.52-4.59 (3H, m, H-19 and H-20), 4.69-4.70 (2H, m, H-2), 4.80-4.82 (2H, m, H-3), 4.86-4.90 (1H, m, H-19), 4.94-5.00 (2H, m, H-18), 5.12-5.22 (2H, m, H-18), 6.74-6.79 (1H, m, H-10), 6.82-6.85 (1H, m, H-8), 7.22-7.26 (1H, m, H-11), 7.37-7.54 (6H, m, H-9 and H-13 and H-14 and H-15), 8.31 (1H, s, H-5), 8.34 (1H, s, H-6). **^{31}P{^{1}H} NMR (162 MHz, CD_3OD-d_4):** δ_P**(ppm)** = -144.43 (2P, sept, $^1J_{P-F}$ = 710.1 Hz, PF_6), -42.36 (1P, s, **P**$(CH_2N)_3$). **IR (ATR):** ν_{max}**/cm^{-1}** = 1601 (C=N). **ESI-MS (HR)** ***m/z*** 659.1287 (40%, [M-2PF_6-$C_{13}H_{19}N_3P$]$^+$ requires 659.1331). **Analysis Calc. $C_{41}H_{49}F_{12}FeIrN_5OP_3 \cdot CH_2Cl_2$**: C, 39.36; H, 4.01; N, 5.46. Found: C, 39.00; H, 3.29; N, 5.91.

6.6 Single Crystal X-ray Analysis

Single crystal X-ray diffraction data were collected on a Bruker KAPPA APEX II DUO diffractometer using graphite-monochromated Mo-Kα radiation (λ = 0.71073 Å). The temperature was controlled using an Oxford Cryostream cooling system (Oxford Cryostat). Data scaling and absorption correction were performed using SAINT[9] and SADABS.[10] Structures were solved by direct methods using SHELXS-97[10] and refined by full-matrix least-squares methods based on F^2 using SHELXL-2014 with X-Seed[11,12] used as the graphical interface. X-Seed and POV-Ray were used to prepare molecular graphic images. The crystallographic data for complexes **2.8**-**2.10** and **3.8** are presented on Table 2.3 (page 47) and Table 3.3 (page 66), respectively. All crystals were isolated as red blocks from deuterated methanol in an NMR tube.

6.7 Cyclic Voltammetry Studies

Cyclic voltammetry studies were conducted using a Bioanalytical Systems Inc. BAS100W Electrochemical Analyser with a one-compartment, three electrode system comprising of a platinum disk working electrode, a platinum wire auxiliary electrode and a Ag/Ag^+ reference electrode (0.01 M $AgNO_3$ and 0.1 M [n-Bu_4N][ClO_4] in anhydrous acetronitrile). The reported E values (see Table 3.4) are with reference to this electrode. All measurements were made on anhydrous acetonitrile solutions which were 2-4 mM in sample and contained 0.1 M [n-Bu_4N][ClO_4] as background electrolyte, and performed at ambient temperature. IR compensation was employed for all measurements. Unless stated otherwise, the scan rate used was 100 mV/s. Under these conditions, the Fc/Fc^+ couple, which was used as a reference, had an $E_{1/2}$ value of +0.10 V and ΔE_p = 100 mV. All solutions were purged with argon and voltammograms were recorded under a blanket of argon. The platinum disk working electrode was polished between runs.

6.8 *In vitro* Cytotoxicity

Cells (MCF7) were seeded in a 96-well plate (5000 cells per well) and after 48 hours they were treated with vehicle (1.0 μM DMSO) or complexes **2.5**-**2.16** and **3.1**-**3.15** at 20 μM for 48 hours. Cell viability of these complexes was assessed using 3-(4,5-dimethylthiazol-2-yl)-2,5-diphenyltetrazolium bromide (MTT) assay, as described in the literature.[13] The absorbance at 550 nm was determined for each well using a spectrophotometer (RTQ2100C Microplate Reader, Ryto, China) and normalised to the RPMI medium absorbance. This experiment was performed three times in quadruplicate, and then the mean cell viability determined using GraphPad Prism version 5.0. For IC_{50} (concentration required for 50% viability) determination of **2.8**, **2.10** and **2.13**, cells were treated using concentrations of 5-25 μM on three occasions in quadruplicate. For the Chinese hamster ovarian (CHO) cells, 3000 cells per well were plated and tested at concentrations of 0.001, 0.01, 0.1, 1, 10 and 100 μg/mL.

6.9 Aqueous Stability and GMP Binding Study

The stability of complexes **2.8** and **2.10** was investigated by ^{1}H NMR experiments in which approximately 3.0 mg of the complex was dissolved in 0.5 mL DMSO-d_6, 0.5 mL of 50% H_2O in DMSO-d_6 (by volume) or 150 mM NaCl solution in 0.5 mL of 50% H_2O in DMSO-d_6 (by volume). The NMR samples were heated and maintained at 37 °C between sampling. ^{1}H NMR spectra were collected at 0, 24 and 48 hours after the initial sample preparation. Similarly, approximately 3.0 mg of sodium 5′-guanosine monophoshate was dissolved in 0.25 mL H_2O, and mixed with 3.0 mg of complex in 0.25 mL DMSO-d_6. The sample was monitored at 0, 24 and 48 hours after preparation while heated to 37 °C between NMR sampling.

6.10 References

1. M. A. Bennett, T.-N. Huang, T. W. Matheson, A. K. Smith, S. Ittel and W. Nickerson, in *16. (η^6-Hexamethylbenzene)Ruthenium Complexes*, John Wiley and Sons, Inc., 2007, pp. 74–78.

2. C. White, A. Yates, P. M. Maitlis and D. M. Heinekey, in *(η^5-Pentamethylcyclopentadienyl)Rhodium and -Iridium Compounds*, John Wiley and Sons, Inc., 2007, pp. 228–234.

3. P. Govender, A. K. Renfrew, C. M. Clavel, P. J. Dyson, B. Therrien and G. S. Smith, *Dalton Trans.*, 2011, **40**, 1158–1167.

4. L. Maqeda, B. C. Makhubela and G. S. Smith, *Polyhedron*, 2015, **91**, 128–135.

5. W. Nkoana, D. Nyoni, P. Chellan, T. Stringer, D. Taylor, P. J. Smith, A. T. Hutton and G. S. Smith, *J. Organomet. Chem.*, 2014, **752**, 67–75.

6. R. Payne, P. Govender, B. Therrien, C. M. Clavel, P. J. Dyson and G. S. Smith, *J. Organomet. Chem.*, 2013, **729**, 20–27.

7. F.-X. Legrand, F. Hapiot, S. Tilloy, A. Guerriero, M. Peruzzini, L. Gonsalvi and E. Monflier, *App. Cat. A: General*, 2009, **362**, 62 – 66.

8. A. R. Burgoyne, C. H. Kaschula, M. I. Parker and G. S. Smith, *Eur. J. Inorg. Chem.*, 2016, **2016**, 1267–1273.

9. *SAINT Version 7.60a, Bruker AXS Inc., Madison, WI, USA*, 2006.

10. *G. M. Sheldrick, SHELXS-97, SHELXL-2014 and SADABS version 2.05, University of Göttingen, Germany*, 2004.

11. L. J. Barbour, *J. Supramol. Chem*, 2001, **1**, 189–191.

12. J. L. Atwood and L. J. Barbour, *Cryst. Growth Des.*, 2003, **3**, 3.

13. J. Carmichael, W. G. DeGraff, A. F. Gazdar, J. D. Minna and J. B. Mitchell, *Cancer Res.*, 1987, **47**, 943–946.